


Summer 2006

Cellular Mechanism of Arglabin-Dimethylaminohydrochloride Cytotoxicity

Xiaofei Qin
Old Dominion University

Follow this and additional works at: https://digitalcommons.odu.edu/biomedicalsciences_etds

 Part of the [Cell Biology Commons](#)

Recommended Citation

Qin, Xiaofei. "Cellular Mechanism of Arglabin-Dimethylaminohydrochloride Cytotoxicity" (2006). Doctor of Philosophy (PhD), Dissertation, , Old Dominion University, DOI: 10.25777/b9ha-qz06
https://digitalcommons.odu.edu/biomedicalsciences_etds/75

This Dissertation is brought to you for free and open access by the College of Sciences at ODU Digital Commons. It has been accepted for inclusion in Theses and Dissertations in Biomedical Sciences by an authorized administrator of ODU Digital Commons. For more information, please contact digitalcommons@odu.edu.

CELLULAR MECHANISM OF ARGLABIN-
DIMETHYLAMINOHYDROCHLORIDE CYTOTOXICITY

by

Xiaofei Qin

M.D. August 1990, Capital Institute of Medicine, Beijing, P.R. China

A Dissertation Submitted to the Faculty of
Old Dominion University in Partial Fulfillment of the
Requirement for the Degree of

DOCTOR OF PHILOSOPHY

BIOMEDICAL SCIENCES

OLD DOMINION UNIVERSITY
AND
EASTERN VIRGINIA MEDICAL SCHOOL
August 2006

Approved by:

Christopher J. Osgood (Director)

Keith A. Carson (Member)

R. James Swanson (Member)

Lloyd Wolfenbarger, Jr. (Member)

ABSTRACT

CELLULAR MECHANISM OF ARGLABIN-DIMETHYLAMINOHYDROCHLORIDE CYTOTOXICITY

Xiaofei Qin

Old Dominion University and Eastern Virginia Medical School, 2006

Director: Dr. Christopher J. Osgood

Cancer is the second leading killer in the United States. Anticancer drug development is always based on the understanding of molecular and cellular mechanisms of carcinogenesis, as well as comprehensive knowledge of potential anticancer drugs. Arglabin-dimethylaminohydrochloride (arglabin-DMA) represents one of the new classes of anti-cancer agents that have shown promise in suppressing the growth of various tumor cells. However, the cellular mechanism of arglabin-DMA cytotoxic effects on tumor cells is still unclear. The current study was to determine the farnesyltransferase (FTase) inhibitory activity of arglabin-DMA and to investigate the effects of arglabin-DMA on three proteins: Ras, Rho and cyclin kinase inhibitor p21/WAF1/CIP1.

In vitro FTase assays were used to study the effect of arglabin-DMA on FTase activity. The FTase assay using expressed FTase showed that the 50% inhibition concentration of arglabin-DMA was 2.9 mM. The FTase assay using lysates of Ras/3T3 cells that had been incubated with arglabin-DMA showed that the highest FTase inhibition was 59% as compared to the no treatment control, and this inhibition plateaued when the arglabin-DMA concentration was 100 nM or higher. These results suggested that arglabin-DMA was transformed in cells and that the transformed arglabin-DMA inhibited FTase activity in Ras/3T3 cells. However, this inhibition was limited by the substrate availability in cells that may transform arglabin-DMA to an FTase inhibitor.

The study of the effects of arglabin-DMA on Ras protein, Rho protein, and cyclin kinase inhibitor p21/WAF1/CIP1 was performed using Ras/3T3 cells incubated with arglabin-DMA or FTI-277 (positive control) for 24 or 72 hours. Western blots and densitometry showed a decreased ratio of processed to unprocessed H-Ras protein in cell lysates incubated with 100 μ M of arglabin-DMA. Western blotting of active H-Ras protein from GTPase pull-down assays showed significant reduction of active H-Ras after incubation with 50 μ M of arglabin-DMA for 24 hours, or 1 μ M of arglabin-DMA for 72 hours. Only unprocessed RhoA was detected by Western blot after incubation with 10 μ M (or higher) arglabin-DMA or FTI-277. Western blots showed a trend of increased p21/WAF1/CIP1 production after 72 hours of incubation with arglabin-DMA and this increase was not found in the FTI-277 control.

This dissertation is dedicated to my grandmother, Xiuying Yao, a woman who does not know how to read and write but raised two doctors and two masters in her life, and to my son, Anthony Yan, who brought me the most precious moments.

ACKNOWLEDGMENTS

I want to express my deepest appreciation to my mentors, Dr. Lloyd Wolfinbarger and Dr. Christopher Osgood, for their kind and patient help on my academic growth and career development over last 10 years. Their tireless work not only have changed my life, but also prepared me for the future challenges and obstacles along my life and career. I also want to thank Dr. R. James Swanson and Dr. Keith A. Carson for their interesting lessons, which brought me to the fascinating world of human physiology and cell biology, and their guidance to my research and dissertation.

I will thank my colleagues and friends, Alyce Jones, Davorka Softic, Katrina Ruth, John Pace, and Sarah Gay, for their emotional support and critical comments over these years. I also want to thank my old friend Harriet Leach, a very strong woman who not only taught me English and culture in this country, but also offered her home for me to live for 3 years. I wish she would still be here to share the happy moments in my life. I am greatly thankful to my parents, Dr. Heng Wang and Qi Qin. Their dedication to work will always be my guide and motivation in my life. Finally, my thanks will go to my dearest husband, Dean Di Yan, for his support during all these good and bad years. For us, this is not just a dissertation; this is the life we have been through for last ten years.

TABLE OF CONTENTS

	Page
LIST OF FIGURES	ix
LIST OF TABLES	xii
INTRODUCTION	1
RAS PROTEINS AND ASSOCIATED SIGNAL TRANSDUCTION PATHWAY	1
RHO PROTEINS AND ASSOCIATED PATHWAY	4
CYCLIN KINASE INHIBITOR P21/WAF1/CIP1	6
PROTEIN FARNESYLTRANSFERASE AND PRENYLATION	6
FARNESYLTRANSFERASE INHIBITORS AND CURRENT MODELS FOR FTI MECHANISMS	9
ARGLABIN-DIMETHYLAMINOHYDROCHLORIDE	14
PURPOSE OF THIS STUDY	17
MATERIALS AND METHODS	20
ARGLABIN-DIMETHYLAMINOHYDROCHLORIDE	20
MOLECULAR MODELING	20
CULTURE OF H-RAS TRANSFORMED NIH-3T3 CELLS (RAS/3T3 CELLS)	21
<i>IN VITRO</i> CYTOTOXICITY ASSESSMENT OF ARGLABIN-DMA	23
FARNESYLTRANSFERASE EXPRESSION AND PURIFICATION	24
<i>IN VITRO</i> FTASE ASSAY USING FTASE EXPRESSED IN AN <i>E. COLI</i> EXPRESSION SYSTEM	28
CELL LYSATE PREPARATION	31
PROTEIN QUANTIFICATION	31
FTASE ASSAY USING FTASE PRODUCED IN H-RAS TRANSFORMED NIH/3T3 CELLS	32
GEL ELECTROPHORESIS	34
COOMASSIE BLUE STAINING	35
PROTEIN TRANSFER	35
IMMUNOPRECIPITATION	36
WESTERN BLOT	36
SMALL GTPASE PULL-DOWN ASSAY	37
DENSITOMETRY ANALYSES	39
STATISTICAL ANALYSES	39
RESULTS	40
<i>IN VITRO</i> CYTOTOXICITY OF ARGLABIN-DMA	40

	Page
THE EFFECT OF ARGLABIN-DMA ON FTASE ACTIVITY	42
THE EFFECT OF ARGLABIN-DMA ON RAS PROTEIN IN TRANSFORMED CELLS	68
THE EFFECTS OF ARGLABIN-DMA ON RHO PROTEIN IN TRANSFORMED CELLS.....	80
THE EFFECTS OF ARGLABIN-DMA ON P21/WAF1/CIP1 PROTEIN IN TRANSFORMED CELLS	87
DISCUSSION	91
SUMMARY	99
REFERENCES	100
APPENDICES	108
A. SUMMARY OF THE INTERMOLECULAR ENERGY BETWEEN FTASE AND VARIOUS LIGANDS	108
B. STATISTICAL EVALUATION OF THE BINDING AFFINITY BETWEEN FTASE AND VARIOUS LIGANDS	108
VITA	109

LIST OF FIGURES

Figure	Page
1. Ras Signal Transduction Pathway	3
2. Prenylation of Cellular Proteins.....	10
3. Structure of Farnesyltransferase	11
4. Schematic Diagram of Ras, RhoA, and p21/WAF1/CIP1 Proteins in Relation to Cell Cycle.....	15
5. Structure of Arglabin-dimethylamino (Arglabin-DMA)	16
6. Affinity Docking.....	22
7. Plasmid Map of pMAL	26
8. Plasmid Map of pGEX.....	27
9. Standard Curve of FTase Assay.....	30
10. Standard Curve for BCA Assay.....	33
11. Confluent Ras/3T3 Cells and NIH/3T3 Cells in Culture	43
12. Growth of Ras/3T3 Cells in Suspension.....	44
13. Growth Curves of Ras/3T3 Cells and NIH/3T3 Cells	45
14. Dose-response Curves of NIH/3T3 Cells and Ras/3T3 Cells to Arglabin-DMA.....	46
15. Percentage Ras/3T3 Cell Growth Inhibition by Arglabin-DMA.....	47
16. Coomassie Blue Staining of Expressed and Purified FTase.....	52
17. Dose Response Curve of FPT Inhibitor II	54
18. Percentage of Inhibition of FTase Activity by FPT Inhibitor II	55
19. Dose Response Curve of FTase Inhibitor II	56
20. Percentage of Inhibition of FTase Activity by FTase Inhibitor II	57

Figure	Page
21. Dose Response Curve of Arglabin-DMA	58
22. Percentage of Inhibition of FTase Activity by Arglabin-DMA	59
23. Lineweaver-Burk Double Reciprocal Plots of FPT Inhibitor II	61
24. Lineweaver-Burk Double Reciprocal Plots of FTase Inhibitor II	62
25. Lineweaver-Burk Double Reciprocal Plots of Arglabin-DMA	63
26. Western Blot of FTase after 24-hour Incubation with Arglabin-DMA or FTI-277	65
27. Western Blot of FTase after 72-hour Incubation with Arglabin-DMA or FTI-277	66
28. Specific Activity of FTase after 2-hour Incubation with Arglabin-DMA.....	69
29. Percentage of FTase Inhibition after 2-hour Incubation with Arglabin-DMA.....	70
30. Percentage of FTase Inhibition after 1-day Incubation with Arglabin-DMA.....	71
31. Percentage of FTase Inhibition after 2-day Incubation with Arglabin-DMA.....	72
32. Western Blot of H-Ras after 24-hour Incubation with Arglabin-DMA or FTI-277	75
33. Western Blot of H-Ras after 72-hour Incubation with Arglabin-DMA or FTI-277	76
34. Western Blot of H-Ras Protein after Small GTPase Pull-down Assays.....	77
35. Western Blot of K-Ras after 24-hour Incubation with Arglabin-DMA or FTI-277	79
36. Western Blot of RhoA after 24-hour Incubation with Arglabin-DMA or FTI-277	83

Figure	Page
37. Western Blot of RhoA after 72-hour Incubation with Arglabin-DMA or FTI-277	84
38 Western Blot of RhoA Protein after GTPase Pull-down Assay	85
39. Western Blot of RhoB after 24-hour Incubation with Arglabin-DMA or FTI-277	86
40. Western Blot of p21/WAF1/CIP1 after 24-hour Incubation with Arglabin-DMA or FTI-277	89
41. Western Blot of p21/WAF1/CIP1 after 72-hour Incubation with Arglabin-DMA or FTI-277	90
42. Diagram of Active Ras, Rho, and p21/WAF1/CIP1 Protein Production Affected by Arglabin-DMA in Ras/3T3 Cells.....	98

LIST OF TABLES

Table	Page
1. List of Antibodies Used for Immunoprecipitation (IP) and Western Blot (WB)	38
2. Intermolecular Energy between FTase and Various Ligands	49

INTRODUCTION

RAS PROTEINS AND ASSOCIATED SIGNAL TRANSDUCTION PATHWAY

Ras genes encode a family of GTP-binding proteins (p21 Ras) known to play major roles in controlling cell growth and differentiation (55). Three genes encode four isoforms of Ras protein: H-Ras, N-Ras, Ki-Ras4A and Ki-Ras4B. Ki-Ras4A and Ki-Ras4B are splice variants of the same gene (61, 67). H-Ras mutations are primarily found in carcinomas of the bladder, kidney, and thyroid. N-Ras mutations are primarily found in myeloid and lymphoid disorders, liver carcinoma, and melanoma. Ki-Ras mutations predominate in colon and pancreatic carcinomas (61).

Cycling between the active GTP-bound form and inactive GDP-bound form, p21 Ras protein acts as a regulatory switch in cell signaling. In normal cell signaling, inactivation of p21 Ras protein occurs through hydrolysis of bound GTP to GDP by the protein's intrinsic GTPase activity coupled with strong stimulation by GTPase-activating protein (GAP) (47, 55). Both normal and oncogenic forms of Ras protein share similar GTP/GDP binding properties, however, they differ in their ability to hydrolyze bound GTP. The weak GTPase activity of normal Ras protein is reduced approximately tenfold further in the oncogenic Ras protein. Moreover, the oncogenic forms of Ras protein are insensitive to GAP which functions to accelerate the slow intrinsic rate of GTP hydrolysis by normal Ras protein. The most frequently detected alterations in oncogenes in both animal tumor model systems and in human cancers are mutations in the ras family of oncogenes, which includes single point mutations at codons 12, 13, 61, or 117, or by alteration of mRNA

The journal model is Molecular and Cellular Biology.

splicing. Specific mutations in the ras gene impair GTPase activity and response to GAP of p21 Ras protein, rendering it constitutively active and resulting in uncontrolled cell growth and morphologic transformation of normal cells.

The Ras system is a ubiquitous signal transduction pathway that is part of the signal transduction system for multiple tyrosine kinase receptors such as those for the epidermal growth factor (EGF), platelet-derived growth factor (PDGF), and fibroblast growth factor (FGF) (Fig. 1) (27, 55). When a ligand binds its receptor, receptor dimerization occurs, triggering an autophosphorylation event and an interaction with “adaptor” proteins called Grb2 and Sos. Grb2 complexes with the tyrosine kinase receptor and the Sos protein via the Src protein homology domains called SH2 and SH3, respectively. Grb2 SH3 domains bind to proline-rich sequences present in Sos, allowing recruitment of Sos to the plasma membrane where Ras is bound. Sos activates Ras, and this activation results in release of GDP and binding of GTP. The activated Ras complexes with Raf protein, and this binding can induce a conformational change in Raf that activates its kinase activity. Activated Raf then phosphorylates a second kinase called MEK (mitogen-activated protein kinase kinase or MAPKK). MEK phosphorylates and thereby activates a third kinase, MAP kinase (MAPK), which has among its substrates various transcription factors such as Jun/Fos (AP-1) that regulate gene expression (27, 55, 63). This “kinase cascade” is a crucial signaling pathway regulating growth and differentiation in many cell types (Fig. 1).

In order for Ras protein to transduce its normal or oncogenic signal, it must be anchored to cell membranes, which include plasma membrane, endoplasmic reticulum (ER) membrane, and Golgi membrane (16, 17, 51). This process is accomplished by

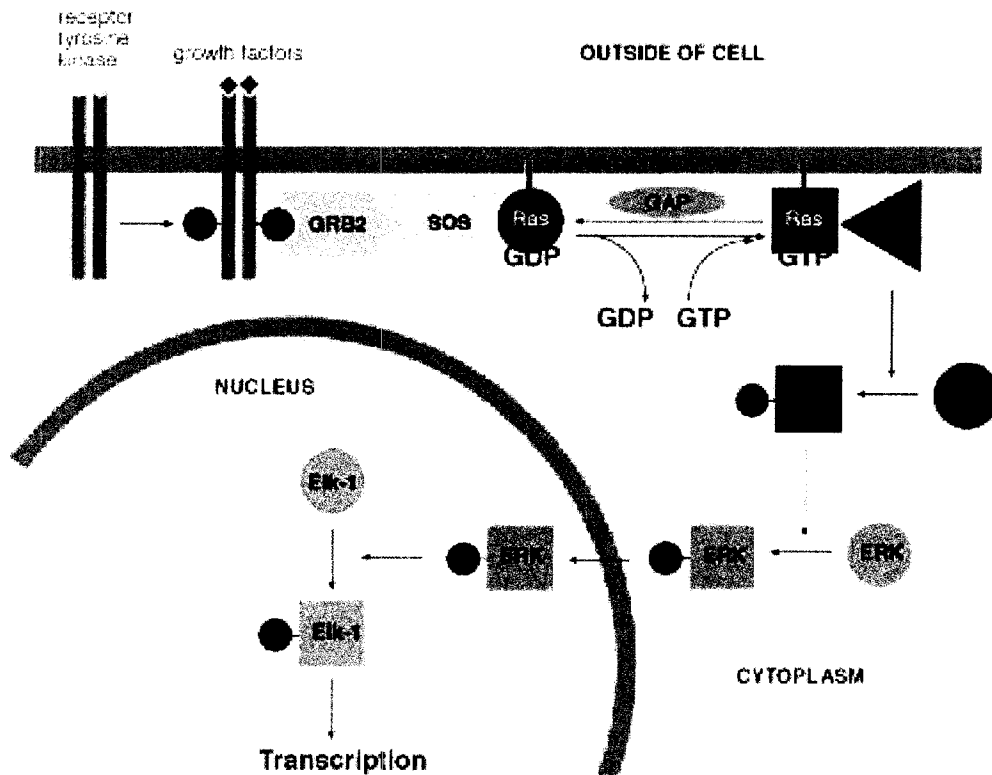


FIG. 1. Ras signal transduction pathway. Activated Ras protein (GTP-Ras) transfers signals through Raf, MEK, and MAP kinase protein, which then enter the nucleus and activate transcription factors of different genes (27, 55).

a series of post-translational modifications, including three steps: prenylation in the cytosol, protease digestion, and methylation. The prenylated product is a substrate for additional modifications: the terminal three amino acids are proteolyzed by enzymes to generate a new C terminus and the new C terminus is carboxymethylated on the ER by prenylcysteine carboxyl methyltransferase (pcCMT) (17, 42). N-Ras and H-Ras are further modified with palmitate moieties that are attached to one or two cysteines just upstream of the CAAX motif (17, 59). In the case of K-Ras, a polybasic sequence near the C terminus allows stable interaction with anionic phospholipids at the inner leaflet of the plasma membrane (2, 17). The first and rate-limiting step is prenylation that increases the hydrophobicity of Ras protein.

RHO PROTEINS AND ASSOCIATED PATHWAY

The Rho family of proteins in mammals comprises several members including RhoA, RhoB, RhoC, Rac1, Rac2, and Cdc42. Rho proteins transduce signals from plasma membrane receptors and control many cell functions requiring the assembly and organization of the actin cytoskeleton, such as those involved in cell polarity, motility, adhesion, cellular transformation, and apoptosis (5, 21, 36). The means by which prenylation affects interaction with membrane targets and/or regulatory proteins remain largely unknown.

Several features distinguish RhoB from other Rho proteins (24): first, its cellular localization in early endosomes and prelysosomal compartments is different from other members of the Rho protein family. Secondly, RhoB is an immediate early response gene that is induced by platelet-derived growth factor (PDGF), transforming growth factor- α

(TGF- α), the non-receptor tyrosine kinase v-Src, and ultraviolet irradiation in fibroblasts. Whether RhoB is also an immediate early response gene in human cancer cells is not known. Third, RhoB mRNA and protein levels turn over much more rapidly (half-lives of 20 and 120 minutes, respectively) (42) than other GTPases, which typically have half-lives on the order of 24 hours (5, 33). Therefore, although RhoA and RhoB share 90% amino acid sequence homology, their physiological functions are predicted to be distinct. The level of RhoB is maximal during the S phase of DNA synthesis and declines at S/G2-M transition. Finally, Rho proteins are singly geranylgeranylated with the exception of RhoB and RhoE. The latter two proteins can be either farnesylated or geranylgeranylated (4, 5).

RhoA is located primarily in the cytosol, with a small fraction being detected in the plasma membrane (17). A large number of GTPase activating proteins (GAPs) can stimulate the intrinsic GTPase activity of RhoA. RhoA regulates signal transduction pathways linking plasma membrane receptors to the assembly of focal adhesion and actin stress fibers. The nucleotide sequence of the rhoA gene predicts a protein of 193 amino acid residues. The molecular weight of RhoA is 21,769 daltons. The amino acid sequence of RhoA protein is 30% identical to H-Ras protein and differs from RhoB protein at the amino acid position 29. The protein contains four highly conserved regions required for binding guanine nucleotide and has a C-terminal CAAX box, -CLVL, which is the signal for post-translational modification (17). A geranylgeranyl group is present at the carboxy terminus after post-translational modification. CAAX boxes ending in leucine are substrates for geranylgeranylation but not farnesylation. Post-translationally modified RhoA, either GDP- or GTP-bound, will form a complex with Rho-GDI (GDP

dissociation inhibitor) and this complex is insensitive to GAP proteins. Inhibition of RhoA in SWISS 3T3 cells has been reported to block the cell cycle in G1 (72).

CYCLIN KINASE INHIBITOR P21/WAF1/CIP1

The tumor suppressor p53 transcriptionally activates a number of genes including the WAF1/CIP1 gene. The activation of WAF1/CIP1 by p53 appears to be key to the action of p53 as a tumor suppressor. The WAF1/CIP1 gene promoter contains a p53 response element. This gene encodes a 21-kD protein that binds cyclin dependent kinases (CDKs) and arrests cells in G1 or G2 phase of cell cycle (54, 62).

The 21-kD protein of the WAF1 gene is found in a complex involving cyclins, CDKs, and proliferating cell nuclear antigen (PCNA) in normal cells but not transformed cells and appears to be a universal inhibitor of CDK activity. One consequence of p21/WAF1 binding to and inhibiting CDKs is the prevention of CDK-dependent phosphorylation and subsequent inactivation of the retinoblastoma (Rb) protein that is essential for cell cycle progression (31). P21/WAF1 is, therefore, a potent and reversible inhibitor of cell cycle progression at both the G1 and G2 check points, presumably to allow sufficient time for DNA repair to be completed (26, 31).

PROTEIN FARNESYLTRANSFERASE AND PRENYLATION

Prenylation represents one of the most common lipid modifications of proteins. Some of the known substrates for prenylation include all p21 Ras proteins, nuclear lamin A and lamin B, transducin γ -subunit, Ras related Rho and Rac proteins, and γ -subunits of heterotrimeric G proteins (8, 23, 25, 28, 75). Protein prenylation involves C-terminal

addition of C15 (farnesyl) or C20 (geranylgeranyl) isoprenoids (Fig. 2). Both isoprenoids are intermediates in cholesterol biosynthesis. Protein prenylation reactions are carried out by one of three enzymes in the cell: farnesyltransferase (FT or FTase), geranylgeranyltransferase type I (GGT-I or GGTase-I), or geranylgeranyltransferase type II (GGT-II, GGTase-II or RabGGT). FT and GGT-I are related heterodimeric enzymes that share a common α -subunit. Prenylation at the carboxyl-terminal residues of proteins terminating with a CAAX sequence (where C is cysteine, A is an aliphatic acid and X is any amino acid) involves attachment of either farnesyl (C15) or geranylgeranyl (C20) isoprenoids, which can facilitate the integration of the protein into membranes (25). Farnesyltransferase prefers the C-terminal amino acid to be either serine or methionine for farnesylation, while leucine is the residue preferred by GGTase-I (19). Ki-Ras4A, Ki-Ras4B, N-Ras, and RhoB proteins can be either farnesylated or geranylgeranylated, whereas H-Ras proteins are singly farnesylated and RhoA proteins are singly geranylgeranylated (47, 60, 65, 67).

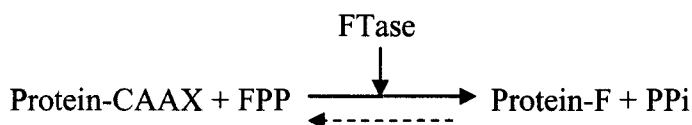
FTase is a heterodimer consisting of a 379-residue α -subunit (44-kD) and 437-residue zinc-containing β -subunit (48-kD) (20, 48, 49, 66). Both subunits are organized as α -helical secondary structures (Fig. 3). The α -subunit is composed of seven pairs of antiparallel α -helices folded into a crescent shaped structure. The β -subunit forms an unusual two layer α -helical barrel. The α -subunit is a right-handed superhelix based on seven copies of a helix-turn-helix repeat. The α -subunit of the human farnesyltransferase can be phosphorylated by type I TGF- β receptor, and the phosphorylation has been suggested to serve a regulatory purpose. The β -subunit is a α -helical barrel open at one end and plugged at the other by a turn in the chain at residues 398-402 near the C-

terminus. The active site containing Zn is located on the inside of the barrel near its upper end, where it is coordinated by the side chains of Asp297 β , Cys299 β , and His362 β . The other notable feature of the barrel is its hydrophobic interior surface: the hydrophobic character of the active site fits well with the hydrophobic nature of both farnesyl diphosphate and peptides such as CVIM.

Sequence differences between the rat and human FTase are on the surface of the enzyme away from the active-site Zn and in the interior of the barrel. This fact, together with the observation that the rat and human enzymes are closely related with 93% identity over 379 residues for the α -subunits and 97% identity over 437 residues for the β -subunits, suggests that the structure of the rat enzyme will be useful for drug design efforts.

The α -subunit contacts the β -subunit barrel around half its circumference at the upper open end of the barrel (66). This arrangement places several residues of the α -subunit near the active-site Zn. In particular, the side chains of Lys164 α and His201 α contribute to the formation of two anion binding sites 6.7Å and 7.5Å from the Zn. His248 β , Lys294 β , Lys353 β , Lys356 β , and Arg291 β also contribute to the formation of the two binding sites. The proximity of these sites to the active-site Zn as well as their highly charged character suggest that they represent part of the binding site for the diphosphate moiety of the substrate farnesyl diphosphate. The involvement of residues from both subunits is consistent with the observation that neither subunit alone is capable of binding FPP. Thus, both subunits would appear to have a role in binding and orienting the leaving group of FPP appropriately for catalysis.

The FTase reaction can be summarized as (22, 23):



FARNESYLTRANSFERASE INHIBITORS AND CURRENT MODELS OF FTI MECHANISMS

Three major groups of farnesyltransferase inhibitors (FTIs) have been developed (27, 73). The first group is molecules derived via peptidomimetic approaches, CAAX peptidomimetics, such as FTase inhibitor II (Calbiochem) and FTI 277 (Calbiochem). These compounds inhibit the isolated enzyme at nanomolar concentrations, but none of them have been developed further as clinically usable anticancer drugs. The second group is heterocyclic FTIs (R115777, SCH66336) that compete for the CAAX peptide binding site of FTase, not only inhibiting the isolated FTase at nanomolar concentrations, but also have demonstrated cytotoxic activity *in vitro* and *in vivo* in tumor cell lines with and without *ras* gene mutations (10). The third group is the FPP competitive compounds, such as FPT inhibitor II (CalBiochem) and FPT inhibitor III (Calbiochem), which inhibit the isolated enzyme FTase at nanomolar concentration and inhibit the growth of tumors produced by H-Ras transformed NIH/3T3 cells.

Ras plays a crucial role in cellular signal transduction pathways. The first and most critical post-translational modification of Ras is farnesylation catalyzed by the FTase. Consequently, inhibitors of FTase have been proposed as potential agents for treating cancers in which Ras plays a pivotal role (27, 40, 70, 71).

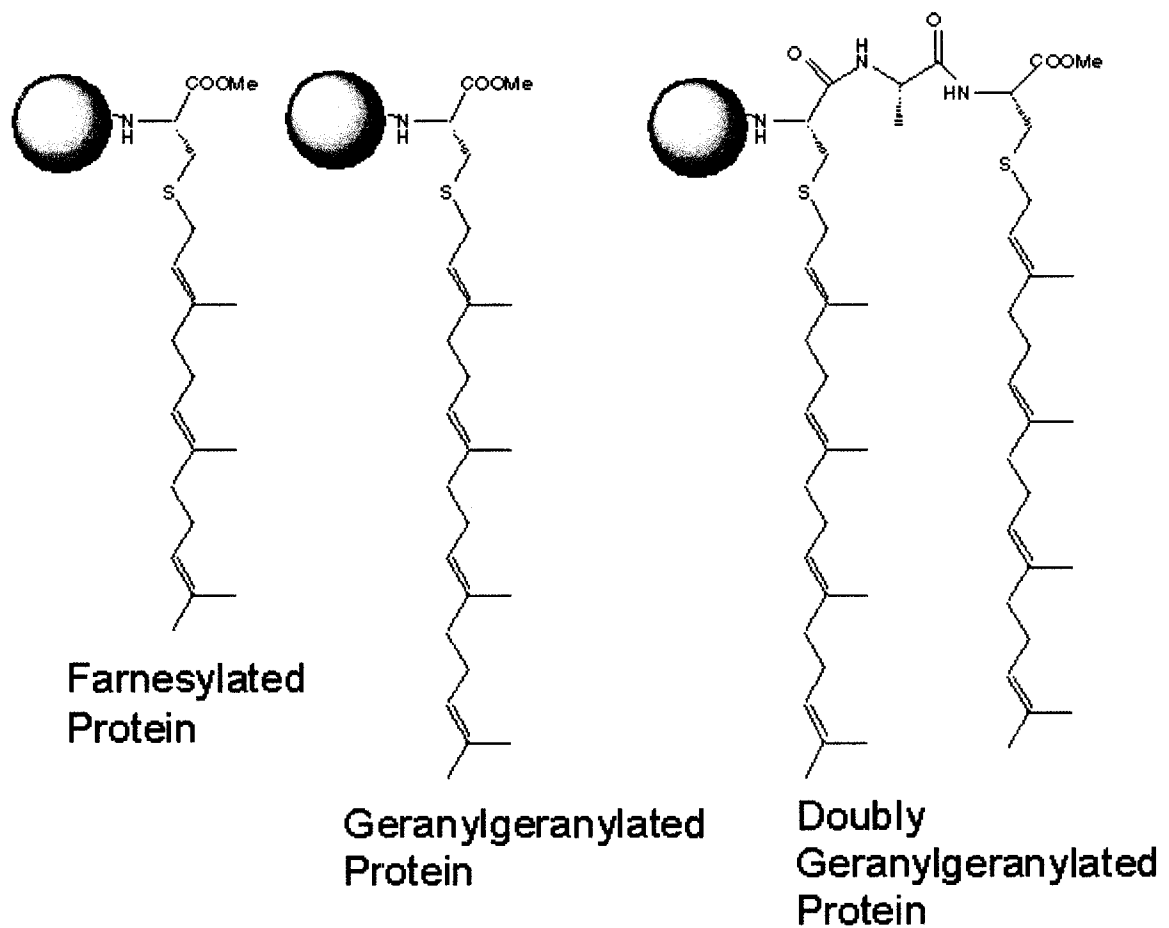


FIG. 2. Prenylation of cellular proteins. Some proteins such as H-Ras and Lamin B are modified with the 15-carbon farnesyl group, some such as RhoA contain the 20-carbon geranylgeranyl group, and some such as Rab proteins contain two geranylgeranyl groups. In all cases, the prenyl groups are at the C-terminus of the protein, and the α -carboxyl group is often methylated.

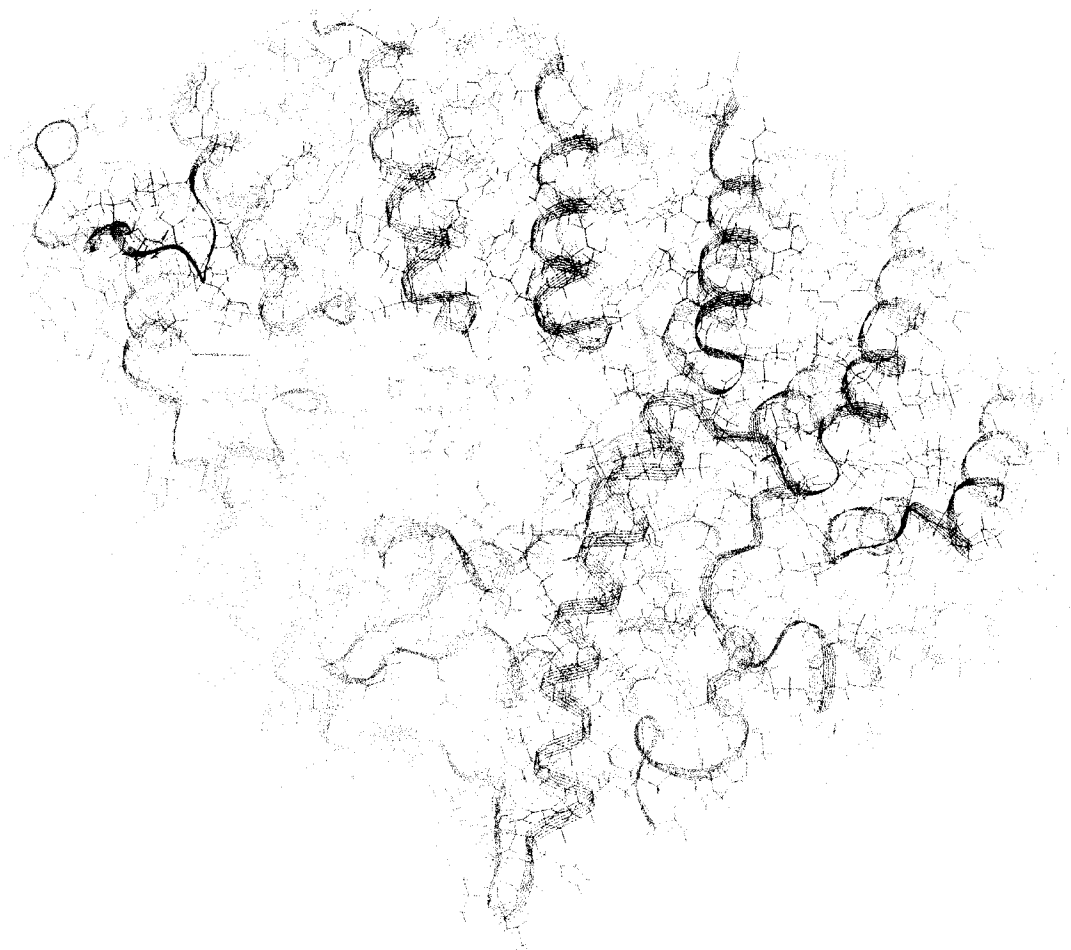


FIG. 3. Structure of farnesyltransferase. The X-ray diffraction structure of the FTase was obtained from the Brookhaven National Library Protein Data Bank. The α -subunit is composed of seven pairs of antiparallel α -helices folded into a crescent shaped structure (Top); the β -subunit forms an unusual two layer α -helical barrel (Bottom)

Although FTIs were originally developed as a Ras-targeted therapy, it currently appears that inhibition of Ras farnesylation cannot account for all of the actions of the compounds (27, 41, 42, 43). First, FTIs do not require the presence of the activated, mutant Ras protein to produce anti-tumor effects. In other words, the susceptibility of human tumor cell lines to FTIs is not correlated with Ras mutation status. Secondly, the Ki-ras4B isoform, the predominant isoform mutated in human cancers, can undergo geranylgeranylation catalyzed by GGT-I when cells are treated with FTIs (67, 76). Thus, tumors bearing the mutant Ki-ras4B isoform should be resistant to FTIs; however, some tumors bearing Ki-ras4B mutations are clearly responsive to FTI treatments. Thirdly, the relative lack of cytostatic effects of FTIs on normal cells is curious, because Ras is required for the proliferation of normal cells. Furthermore, the kinetics of phenotypic reversion induced by FTI treatment are in many cases simply too rapid to be explained by loss of Ras function through inhibition of its farnesylation. The reversion process occurs largely within 24 hours of cell treatment. FTIs only inhibit the production of newly synthesized Ras. The Ras protein is quite stable with a half-life of ~24 hours. Thus by the time reversion is complete, steady-state levels of farnesylated Ras are only reduced by approximately 50%. Finally, even though *in vivo* tumors seem to regress completely, cessation of FTI treatment leads to a rapid return of tumors. Tumor persistence would require continuous long-term FTI treatment that could increase the likelihood of side effects and drug resistance. Prendergast and his research team in the Wistar Institute suggested that cell growth inhibition by farnesyltransferase inhibitors is mediated by gain of geranylgeranylated RhoB (41, 42, 43, 56, 57).

RhoB has been implicated as an FTI target for several reasons (15): 1) RhoB is a

substrate for FTase, and FTIs inhibits its farnesylation resulting in decreased RhoB-F and increased RhoB-GG. Geranylgeranylated forms of RhoB (RhoB-GG) accumulate in drug-treated cells because of the action of geranylgeranyl transferase-I which is unaffected by FTI; 2) The short half-life of RhoB coincides better than that of Ras with regard to the kinetics of the reversal of transformation of FTI; 3) The cell cycle kinase inhibitor p21/WAF1/CIP1 is induced in cells and cell growth is inhibited when they are treated with FTIs; 4) The loss of RhoB-F and the gain of RhoB-GG associated with stress-fiber formation is compatible with anchorage-dependent growth, but not with anchorage-independent growth. For example, if Ras-transformed cells are cultured in suspension, where cell-cell but not cell-substratum attachment is possible, then FTIs induce massive apoptosis instead of reversion. Taken together, Chen's results (15) support the conclusion that alteration of RhoB prenylation is both necessary and sufficient to the FTI mechanism in malignant cells. Both RhoB-F and RhoB-GG induce apoptosis, inhibit oncogenic signaling, and suppress transformation *in vitro* and *in vivo* (15).

The Rho GTPases are essential for Ras-induced oncogenic transformation (7, 52, 62), and activated Rho acts synergistically with activated Raf in cell transformation. Raf, with activated serine/threonine kinase activity, sends positive signals down a kinase cascade (the mitogen-activated protein kinase pathway) and prompts cells to move through the G1 phase of the cell cycle towards S phase of cell cycle. Excessive signaling from Ras/Raf induces p21/WAF1/CIP1 and blocks entry into S phase. RhoA overcomes the cell-cycle block by suppressing expression of p21/WAF1/CIP1 (52, 62) (Fig. 4).

Although some evidence showed the involvement of RhoB in the anti-tumor activity

of FTIs (15, 42), direct evidence implicating RhoB in the mechanism of action of FTIs in human tumors is lacking. The roles of RhoB, RhoA, and p21/WAF1/CIP1 in cellular mechanism of FTI anticancer activity have not been determined.

ARGLABIN-DIETHYLAMINOHYDROCHLORIDE

The guaianolide arglabin, a sesquiterpene lactone extracted from *Artemisia myriantha*, is used in Chinese medicine for the treatment of menorrhagia and inflammatory diseases (13, 32, 35, 50). Arglabin is a registered anticancer compound in the Republic of Kazakhstan (1, 3, 9, 63). Over 200 patients with a variety of cancers have been treated with this compound and generated very promising results and few side effects. The water soluble dimethylaminohydrochloride derivative of arglabin (arglabin-DMA) was used in current anti-tumor treatments and in this study. The formula weight of arglabin-DMA is 327.85 daltons and the structure of arglabin-DMA is shown in Figure 5. According to previous research on sesquiterpene lactones (1, 3, 63), arglabin is derived from trans-farnesyl diphosphate by cyclization, rearrangements, and oxidation.

Shaikenov's studies showed that arglabin-DMA inhibits the incorporation of farnesylpyrophosphate into H-Ras protein by farnesyltransferase with the 50% inhibition concentration (IC₅₀) of 25 μ M (63, 64). The phosphorylated form of arglabin-DMA competitively inhibits the binding of farnesylpyrophosphate to farnesyltransferases according to their *in vitro* kinetic studies (63, 64). Their *in vitro* studies suggested that arglabin-DMA inhibited post-translational modification of Ras protein in cells. Arglabin-DMA inhibits anchorage-dependent proliferation of neuroblastoma (NB) cells with IC₅₀ of 10 μ g/ml (30.5 μ M) and inhibits anchorage-independent growth of NB and Kirsten

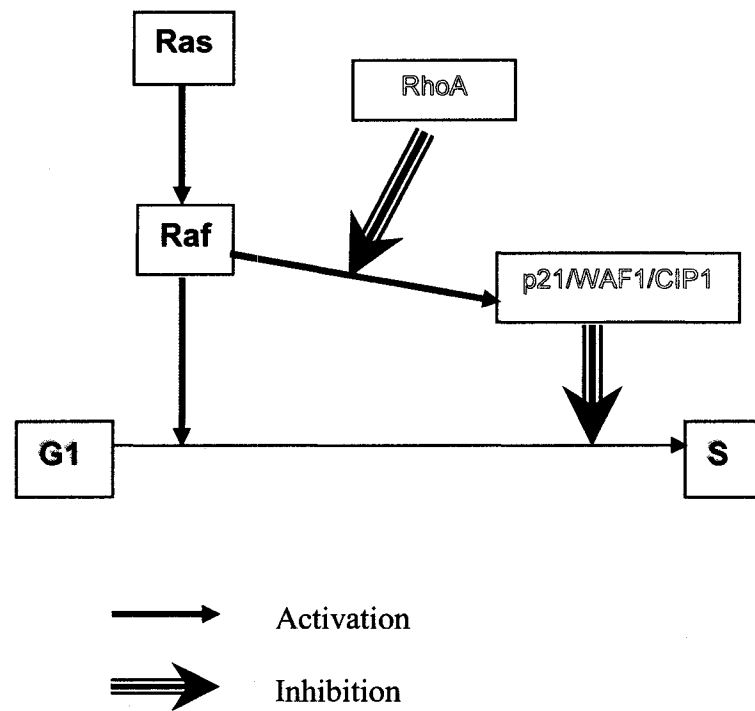


FIG. 4. Schematic diagram of Ras, RhoA, and p21/WAF1/CIP1 proteins in relation to the cell cycle (52, 62).

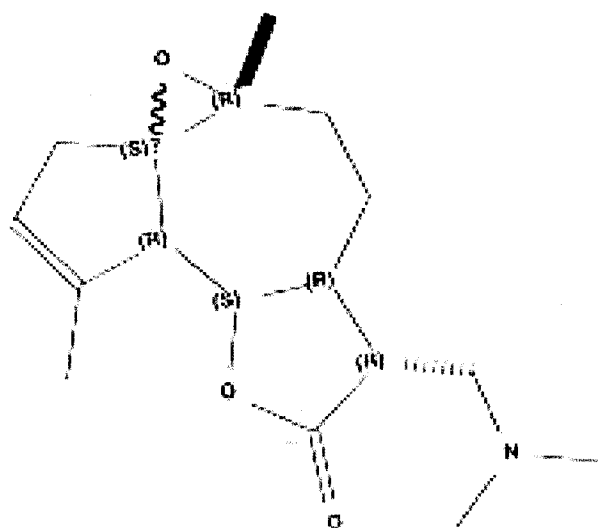


FIG. 5. Structure of arglabin-dimethylamino (arglabin-DMA).

MSV transformed normal kidney (KNRK) cells with the same IC₅₀ (64). Soft-agar colony formation assay of H-Ras transformed cells showed an IC₅₀ of 2 µg/ml (6.1 µM). The focus of Shaikenov's research was to determine whether arglabin-DMA is suitable for treatment of *ras* related malignancies.

PURPOSE OF THIS STUDY

The primary objective of this study was to better understand the cellular mechanism of arglabin-DMA cytotoxic effects on tumor cells. Two general hypotheses were examined in this study: (1) that arglabin-DMA inhibits protein farnesylation in Ras transformed cells, and (2) that the cytotoxic activity of arglabin-DMA on Ras transformed cells is primarily derived from farnesylation inhibition of Ras protein and/or Rho protein, and effects on cyclin kinase inhibitor p21/WAF1/CIP1. Three specific aims were addressed:

Determination of farnesyltransferase inhibitory activity of arglabin-DMA using farnesyltransferase expressed *in vitro* or produced in transformed cells.

Even though arglabin-DMA is a possible derivative of farnesylpyrophosphate (1, 3, 63), which is a substrate of farnesyltransferase, and has structural similarity with cellular polyprenols, direct evidence of arglabin-DMA as a farnesyltransferase inhibitor was lacking. The farnesyltransferase assay, using arglabin-DMA and farnesyltransferase expressed *in vitro*, has not been performed previously. One purpose of this study was therefore to determine whether *in vitro* farnesyltransferase activity was inhibited by arglabin-DMA.

Arglabin-DMA itself may not inhibit farnesyltransferase activity. However, a derivative of arglabin-DMA such as phosphorylated arglabin-DMA in cells may inhibit farnesyltransferase activity. Shaikenov's studies showed that arglabin-DMA was phosphorylated intracellularly and this complex competitively inhibited binding of farnesylpyrophosphate to farnesyltransferase, thus inhibiting farnesylation of Ras protein (63, 64). To further determine whether arglabin-DMA or its derivative inhibit farnesyltransferase activity in cells, investigation of farnesyltransferase activity of cell lysate generated from cells treated with arglabin-DMA was appropriate. The present study addressed the hypothesis that arglabin-DMA inhibits protein farnesylation in Ras transformed cells.

Determination of the inhibitory effects of arglabin-DMA on farnesylation of Ras proteins in transformed cells.

Currently, putative FTIs anticancer activity through their effects on oncoproteins is still speculative. FTIs were originally developed as a Ras-targeted therapy, since the most frequently detected alterations in oncogenes of human cancers are mutations in the *ras* family of oncogenes, and the most critical post-translational modification of Ras is farnesylation catalyzed by FTase (27, 45). H-Ras proteins are singly farnesylated and K-Ras protein can be either farnesylated or geranylgeranylated. The exact effects of arglabin-DMA on H-Ras and K-Ras proteins have not been elucidated. The present study investigated the effects of arglabin-DMA on H-Ras farnesylation and K-Ras prenylation.

Determination of the effects of arglabin-DMA on Rho protein prenylation and cyclin kinase inhibitor p21/WAF1/CIP1 production in transformed cells.

RhoB protein can be either farnesylated or geranylgeranylated through post-translational modification. If arglabin-DMA reduces farnesylation of RhoB by inhibiting farnesyltransferase activity, more translated RhoB protein is available for geranylgeranylation, thus more substrate (GGP) and enzymes (GGT-I/GGT-II) are utilized for RhoB geranylgeranylation. In addition, the half-life of RhoB is about 2 hours, while that of RhoA is about 24-31 hours, depending on cell type. The rate of RhoB production is much faster than RhoA. Thus, the total post-translational modification of RhoB might be kept at the same level. RhoA is singly geranylgeranylated. The availability of substrates (GGP) and enzymes (GGT-I/GGT-II) for geranylgeranylation can be limiting due to increased usage by RhoB protein. The reduction of geranylgeranylated RhoA may decrease the regulatory inhibition of cyclin kinase inhibitor p21/WAF1/CIP1 (Fig. 4). Thus, p21/WAF1/CIP1 protein could be expressed and inhibit transformed cells moving from G1 to S phase of cell cycle.

The effects of arglabin-DMA on prenylated RhoB protein, geranylgeranylated RhoA protein, and cyclin kinase inhibitor p21/WAF1/CIP1 were investigated. The present study addressed the hypothesis that the cytotoxic activity of arglabin-DMA on Ras transformed cells is primarily derived from farnesylation inhibition of Ras protein and/or Rho protein, and effects on cyclin kinase inhibitor p21/WAF1/CIP1.

MATERIALS AND METHODS

ARGLABIN-DIMETHYLAMINOHYDROCHLORIDE

Arglabin-dimethylaminohydrochloride (arglabin-DMA) was a gift from Dr. Shaikenov of NuOncology Labs, Inc. Arglabin-DMA is a water soluble form of arglabin [1(R), 10(S)-epoxy-5(S), 7(S)-guaia-3(4), 11(13)-dien-6, 12-olide], a sesquiterpene γ -lactone isolated from *Artemisia glabella* (64). The formula weight of arglabin-DMA is 327.85. The structure of arglabin-DMA is shown in Figure 4. Lyophilized arglabin-DMA was dissolved in isotonic saline to make various concentrations of arglabin-DMA used for the experiments reported here.

Other known FTIs were purchased from Calbiochem. FPP competitive compounds FPT inhibitor II (Calbiochem 344152) and FPT inhibitor III (Calbiochem 344154) are phosphonic acids. They are both potent and selective inhibitors of FTase ($IC_{50} = 75$ nM). They also inhibit Ras farnesylation in whole cells by 90% at 25 to 250 μ M. FTI-277 (Calbiochem 344555) and FTase inhibitor II (Calbiochem 344512) are CAAX peptidomimetics. They both selectively inhibit FTase with IC_{50} of 50 nM. FTI-277 inhibits H-Ras processing in whole cells with IC_{50} of 100nM. It is also highly effective and selective in disrupting constitutive H-Ras-specific activation of MAP kinase. Lyophilized FTIs were dissolved in isotonic saline to make various concentrations for the following experiments.

MOLECULAR MODELING

The farnesyltransferase X-ray diffraction structure consisting of atomic coordinates

of the binary complex of FTase and FPP was taken from the Brookhaven National Library Protein Data Bank (PDB). The substrate-binding site of the enzyme was prepared by removing the FPP molecule from the complex. The 3-D molecular structures of all ligands were drawn based on the 2-D structure diagram with the Insight II software purchased from Molecular Simulation Inc. (MSI) using a Silicon Graphics computer. The intermolecular energy of FTase and various ligands were measured using the Insight II docking program from MSI (Fig. 5). First, the stable docking models were searched while covering all possible binding modes and ligand confirmations. The top ten possible orientations of a ligand to dock to the active site of FTase were found, and then the intermolecular energies between the ligand and FTase were calculated. Intermolecular energies consisted of van der Waals, electrostatic, and hydrogen bond interactions (18, 30, 53). The ligands used for intermolecular energy calculation were FPT inhibitor II, FPT inhibitor III, FTI-277, FTase inhibitor II, FPP, arglabin-DMA, and phosphorylated arglabin-DMA.

CULTURE OF H-RAS TRANSFORMED NIH-3T3 CELLS (RAS/3T3 CELLS)

The Ras/3T3 cell line is a gift from Dr. Shaikenov of NuOncology Labs Inc. The control NIH/3T3 cell line (CRL-1658) was purchased from the American Type Culture Collection (ATCC) as a continuous cell line established from a NIH Swiss mouse embryo. Both cell lines were propagated in Dulbecco's Modified Eagle's Medium (DMEM) containing 10% fetal bovine serum (FBS) and 4 mM of L-glutamine at 37 ± 1 °C in a CO₂ incubator containing 5% CO₂ and 95% air.

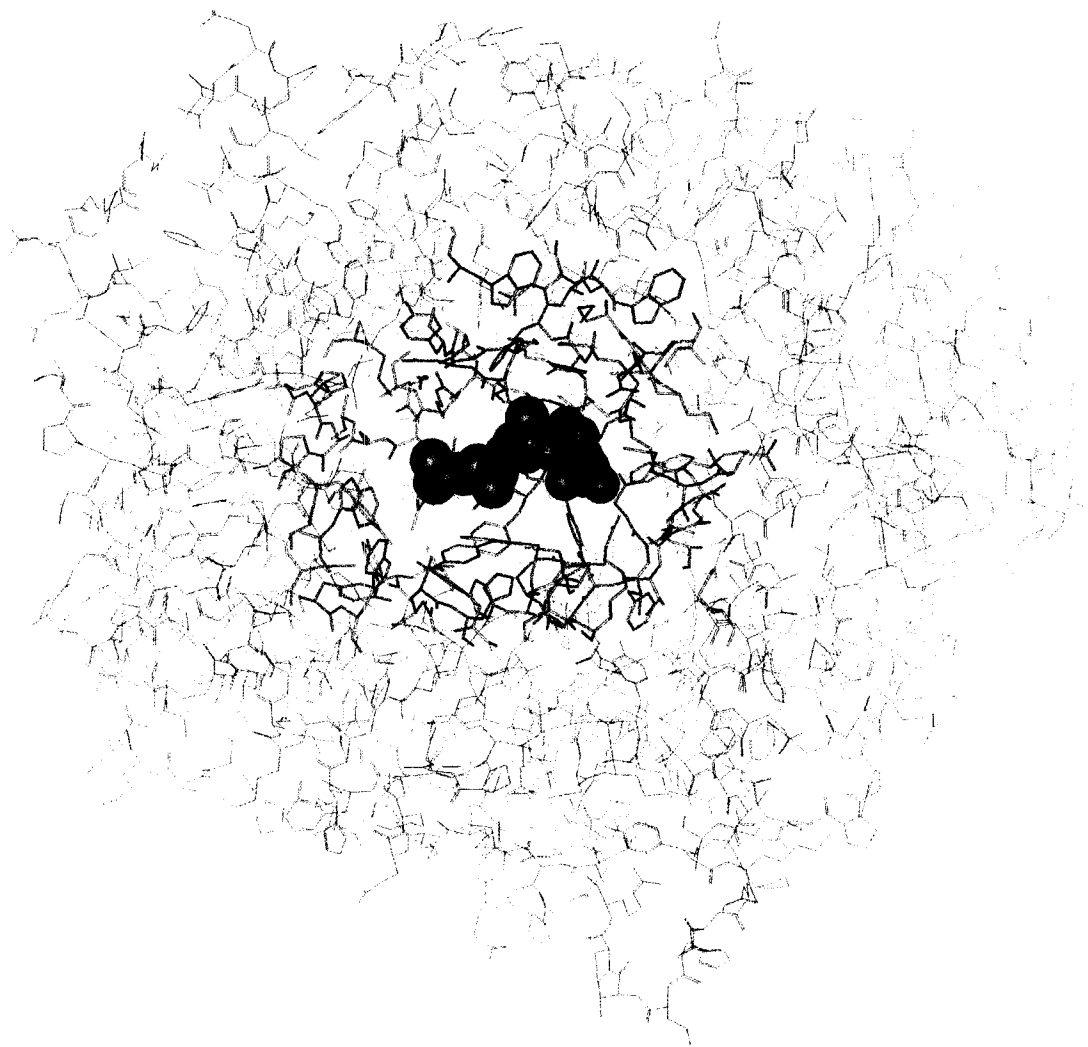


FIG. 6. Affinity docking. The intermolecular energy between farnesyl pyrophosphate (middle) and farnesyltransferase (peripheral) was calculated using an affinity docking program (Insight II from Molecular Simulations, Inc.). One frame of the docking process (interaction of FPP and active site of FTase) was captured in the figure.

Representative photos were taken using a digital camera (Olympus, DP11) attached to a phase contrast microscope (Olympus, CK40). Seven-day growth curves were generated for both cell lines. Cells were seeded at the same densities (5000 cells/cm²) on day 0, and viable cell numbers were counted each day for 7 days using the trypan blue exclusion method. Cell densities of both cell lines were calculated.

Suspension culture of Ras/3T3 cells was prepared by using poly (2-hydroxyethyl methacrylate) (poly-Hema or Poly-HEME) surface coated 6-well tissue culture plates (71). Each well was coated with 0.8 mL of 1.2% poly-HEME prepared in 95% of ethanol and allowed to air dry in a Class II laminar flow hood for 16-18 hours. Ras/3T3 cells were seeded in the coated plates at 20,000 cells per well density. The number of cells was counted each day for 6 days using the trypan blue exclusion method. Representative photos were taken using a digital camera attached to a phase contrast microscope.

IN VITRO CYTOTOXICITY ASSESSMENT OF ARGLABIN-DMA

In vitro cytotoxicity assays were performed using the MTT (3-[4,5-dimethylthiazol-2-yl]-2,5-diphenyl tetrazolium bromide) based *in vitro* toxicology assay kit from Sigma (Cat# TOX-1). Mitochondrial dehydrogenases of viable cells cleave the tetrazolium ring, yielding purple formazan crystals that are dissolved in acidified isopropanol. The resulting purple solution is spectrophotometrically measured. An increase or decrease in cell number results in a concomitant change in the amount of formazan formed, indicating the degree of cytotoxicity caused by the test material.

Ras/3T3 cells were seeded at 5000 cells per cm² in 96-well cell culture plates. After cells had grown to the mid-log phase, the cell culture media was replaced by various

concentrations of arglabin-DMA (0, 0.1, 1, 10, 25, 50, and 100 μM) made with complete cell culture media containing 10% FBS and 4 mM of L-glutamine. For controls, cell culture media containing 10% FBS and 4 mM of L-glutamine without arglabin-DMA was introduced to cells. The cells were incubated in a 37°C incubator containing 5% CO₂/95% air for 72 hours. A minimum of three replicates was used for each test group and control. After incubation, the media in each well was replaced by RPMI-1640 without phenol red (150 μl /well) and MTT solution (15 μl /well). The 96 well plates were incubated in a 37°C incubator containing 5% CO₂/95% air for 2 hours. Solubilization solution (150 μl /well) was added into each well after incubation to dissolve any formazan crystals formed in viable cells. The absorbency of the resulting solution was measured at a wavelength of 570 nm on a plate reader. The background absorbency was measured at a wavelength of 690 nm on a plate reader. The absorbency of viable cells was calculated by subtracting background absorbency from the absorbency of the resulting solution. The results were plotted on Excel worksheets and expressed as absorbency of the resulting solution generated from viable cells for each test group and control, or percentages of viable cells compared to the control. An increase or decrease in cell number resulted in a concomitant change in the amount of formazan formed, indicating the degree of cytotoxicity caused by the test material.

FARNESYLTRANSFERASE EXPRESSION AND PURIFICATION

Plasmid DNAs of human farnesyltransferase α and β subunits (gifts from Dr. Tomanoi of the University of California in Los Angeles) were used to express human FTase (Fig. 7 and Fig. 8). The construction of plasmid pMALc2-hFT α contained the

ampicillin resistance sequence and *malE*, which encodes maltose-binding protein (MBP). The plasmid pGEXhFT β construct conferred ampicillin resistance sequence and carried the glutathione S-transferase (GST) gene sequence. Both plasmid DNAs contained the same promoters for FTase and for induction by isopropyl-beta-D-thiogalactopyranoside (IPTG).

Plasmid DNAs for α and β subunits of FTase were co-transformed into DH5 α competent *Escherichia coli* (*E.coli*) cells by electroporation at 2.5 kV for 5 milliseconds. These *E.coli* cells were propagated and selected with a high concentration of ampicillin (200 μ g/mL). FT α and FT β gene transcription were induced with 1 mM IPTG at 37°C overnight. The cell pellets were resuspended in sonication buffer (1xPBS/1mM EDTA/1mM EGTA/ 0.1% Lubrol/ 0.1mM DTT) containing protease inhibitor cocktail (Sigma, P8849) and sonicated on ice. After centrifugation, the supernatants were purified with glutathione beads by mixing on a rocker at 4°C for 2 hours. The protein was eluted with elution buffer containing glutathione and concentrated using centrifugal filters (Amicon, Centricon YM-100, MWCO 100 kilodalton). Protein concentrations were determined using the bicinchoninic acid (BCA) assay. The relative protein size was confirmed with electrophoresis on SDS-polyacrylamide gel stained with coomassie blue. The enzyme activity of expressed FTase was determined by the subsequent *in vitro* FTase assay.

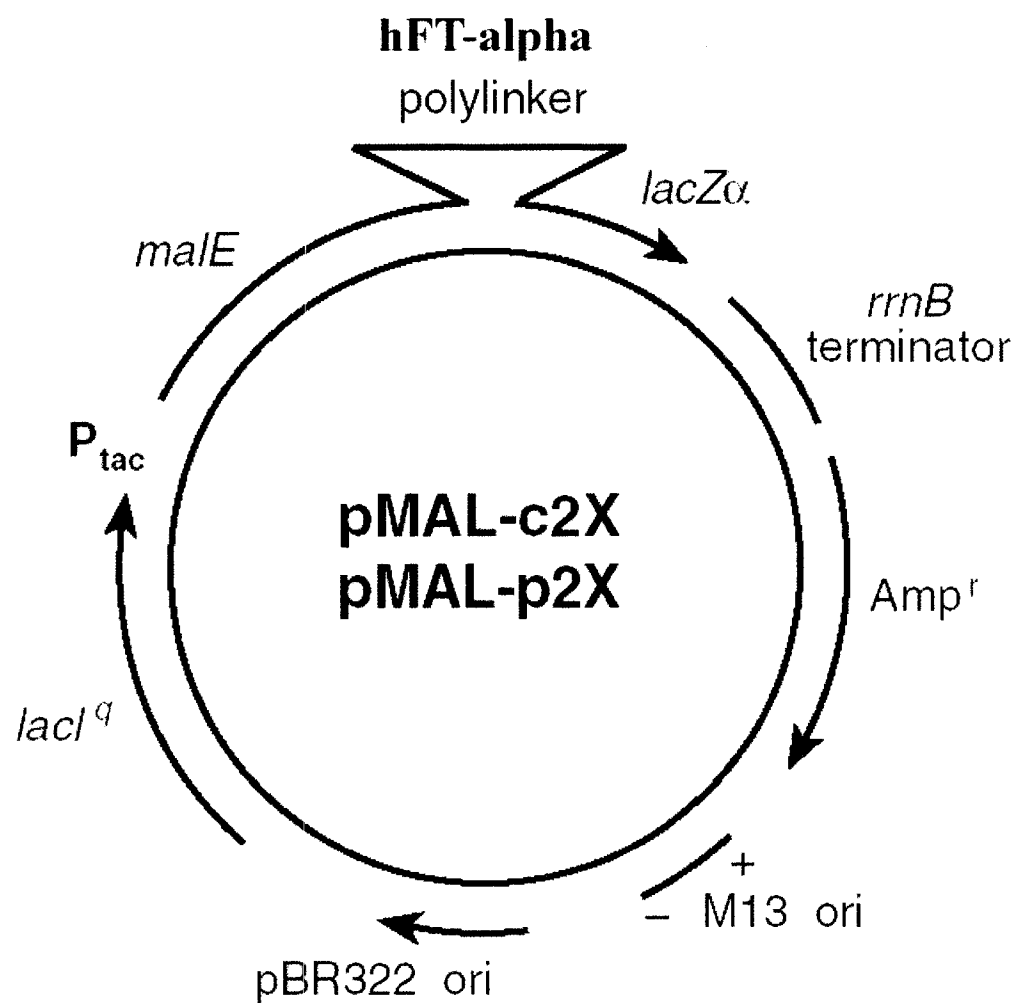


FIG. 7. Plasmid map of pMAL. The construction of plasmid pMALc2-hFT α contained the ampicillin resistance sequence and *malE* gene, which encodes maltose-binding protein (MBP).

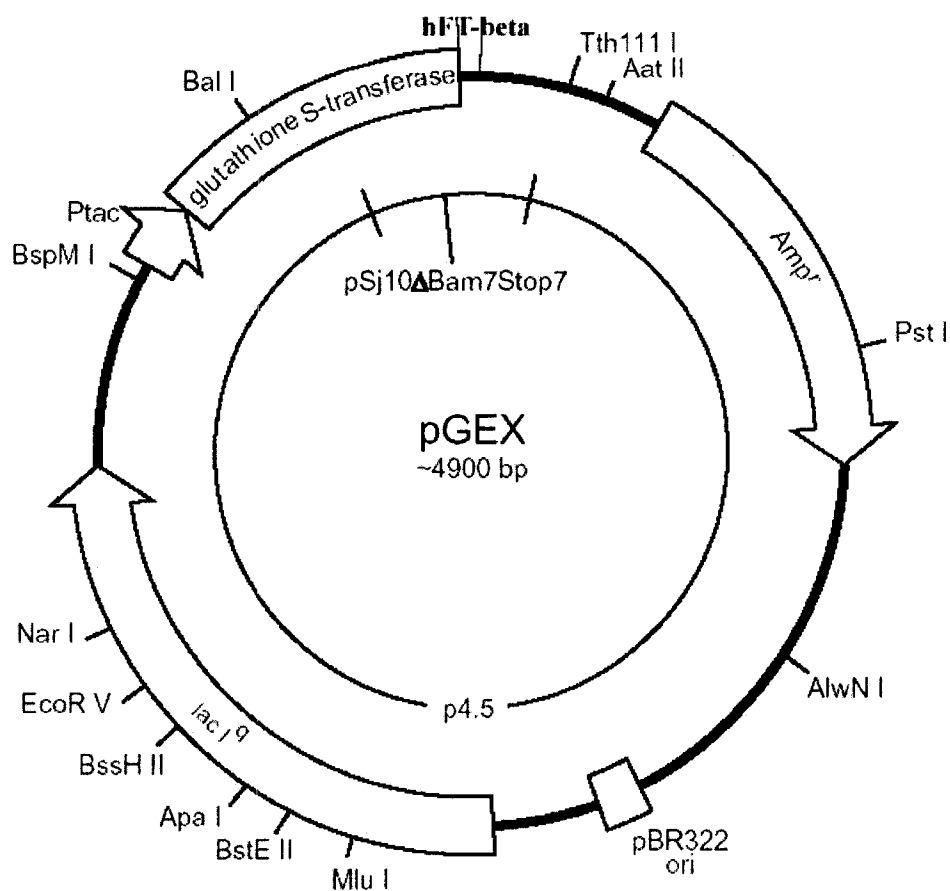


FIG. 8. Plasmid map of pGEX. The plasmid pGEXhFT β construct contained ampicillin resistance sequence and the glutathione S-transferase (GST) gene sequence.

IN VITRO FTASE ASSAY USING FTASE EXPRESSED IN AN *E. COLI* EXPRESSION SYSTEM

FTase can transfer the farnesyl group of farnesylpyrophosphate (FPP) to protein substrates (such as lamin B or Ras protein) to generate farnesylated protein and pyrophosphate. The *in vitro* FTase assay quantitates the amount of radio-labeled farnesylated protein using radio-labeled FPP as a substrate (34, 74). The FTase activity was determined by measuring the incorporation of the ^3H -farnesyl group of ^3H -FPP to the substrate peptide. The usage of radioactive materials and the experimental procedures were approved by the Radiation Safety Committee (RSC) of Old Dominion University (Norfolk, VA).

The Farnesyltransferase Scintillation Proximity Assay (SPA) Kit was purchased from Amersham Life Science (TRKO 7010). Scintillation proximity assay uses fluoromicrospheres (yttrium silicate beads) coated with streptavidin (12, 34, 46). Protein substrates were labeled with biotin. Farnesylpyrophosphate was labeled with tritium (^3H) that emits low energy radiation. During the FTase assay reaction, radioactively labeled farnesylated-biotinylated-protein was generated relative to total farnesyltransferase activity. When this product bound to the beads and, by its proximity, the emitted short-range electrons of the isotope excited the fluorophor in the bead. The light emitted was measured using a standard liquid scintillation counter. The enzymatic reaction was started by adding 20 μl of purified FTase (0.1 $\mu\text{g}/\mu\text{l}$) into 80 μl of assay buffer consisting of [^3H]-FPP (120 nM), zinc chloride (100 μM), and biotin lamin-B peptide (0.5 μM). The tubes containing the combined reaction solutions were incubated at 37°C water bath for

60 minutes. The assay was stopped by the addition of STOP/bead reagent into the reaction. The resulting solution was counted using a liquid scintillation counter.

A standard curve of FTase activity was generated using increasing amounts of cell protein (0.4-4 μg) produced from the FTase expression and purification procedures (Fig 9). Reactions without cell protein and reactions without the addition of arglabin-DMA were used as negative controls. Reactions using a known FTI, FPT inhibitor II (Calbiochem 344152) or FTase Inhibitor II (Calbiochem 344512) were used as positive controls. Various concentrations of arglabin-DMA were tested in FTase assays. The FTase enzymatic activity was expressed as the amount of radiolabeled farnesylated protein per minute of reaction ($\mu\text{Ci}/\text{min}$). The 50% inhibition concentration (IC_{50}) of known FTIs and arglabin-DMA were determined. Various concentrations of radio-labeled FPP were used to determine the velocity of enzyme reaction (pmol/min). Lineweaver-Burk plots of known FTIs and arglabin-DMA were generated to show the type of inhibition of farnesyltransferase.

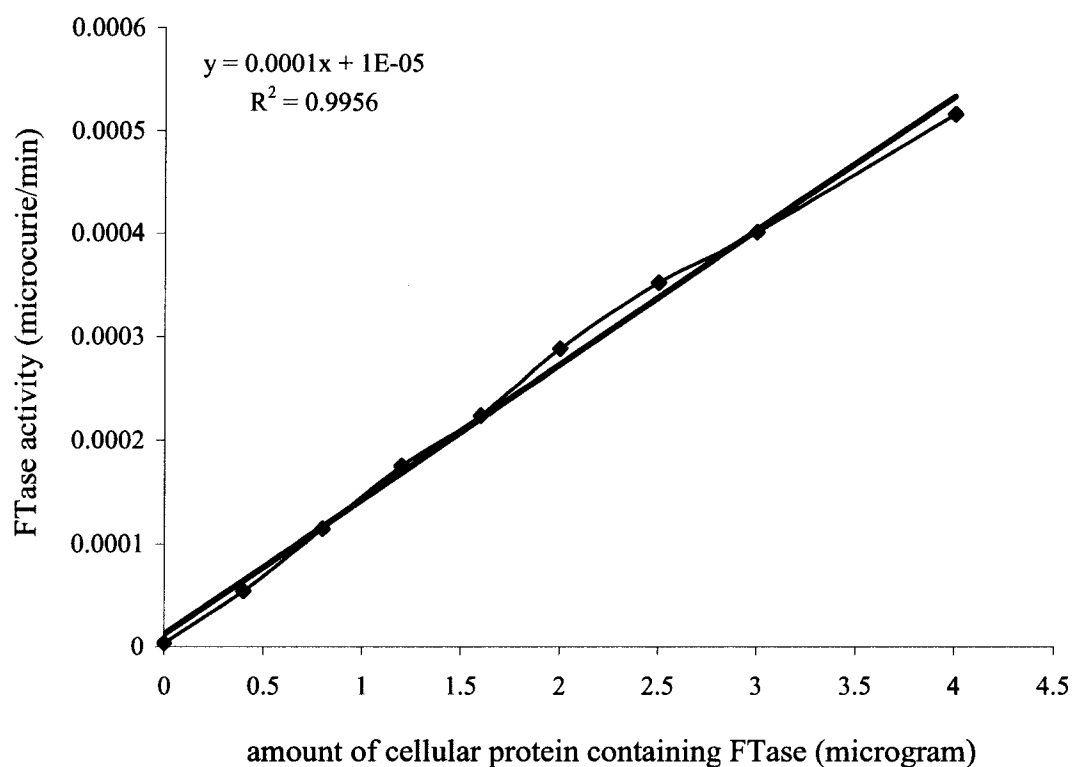


FIG. 9. Standard curve of FTase assay. Various amount of expressed and purified FTase (0.4 μg – 4 μg) was used for FTase standard curve generation. Generation of ^3H -farnesylated-biotin-lamin B peptide was measured by liquid scintillation counter.

CELL LYSATE PREPARATION

An equal number of Ras/3T3 cells was seeded in T25 flasks. After cells had grown to the mid-log phase, various concentrations of arglabin-DMA (0.1, 1, 10, 50, and 100 μ M) were introduced into cell culture media. Once the cells had been treated for 2 hours, 24 hours, or 72 hours, the culture media were removed. Cells were washed with 1x phosphate buffered saline (PBS) and removed from tissue culture flasks using lysis buffer containing sodium chloride (150 mM), magnesium chloride (5 mM), DTT (1mM), sodium phosphate (1 mM), triton X-100 (1%), sodium dodecylsulfate (0.05%), HEPES (50 mM), phenylmethylsulfonyl fluoride (1 mM), sodium vanadate (1 mM), aprotinin (10 μ g/mL), and leupeptin (10 μ g/mL) (37, 38, 39, 45). Cell suspensions in lysis buffer were sonicated at 10 watts for a total of 60 seconds. After sonication, cell lysates were centrifuged at 10,000 relative centrifugal force (rcf) for 10 minutes. The supernatants were transferred to new centrifuge tubes and used for experiments. Protein concentrations of cell lysates were quantificated using BCA assays. Samples with the equal amounts of cellular protein were utilized.

The negative control was the cell lysate generated from cells without arglabin-DMA treatment. The positive control was the cell lysate obtained from cells treated with known farnesyltransferase inhibitor.

PROTEIN QUANTIFICATION

The BCA protein assay[™] detects and quantitates total protein in samples by using reagents containing bicinchoninic acid (BCA). The purple-colored reaction product of this assay was formed by the chelation of two molecules of BCA with one cuprous ion,

which generated from reduction of Cu^{+2} to Cu^{+1} by protein. Bovine serum albumin (BSA) ranging from 25 $\mu\text{g/mL}$ to 750 $\mu\text{g/mL}$ was used for standard curve generation. Linearity exists over the protein concentration range of 25 $\mu\text{g/mL}$ to 750 $\mu\text{g/mL}$ ($R^2=0.9971$, Fig. 10). The BCA protein assay was started by addition of 200 μl of working reagent which contained BCA and cuprous cation (Cu^{+2}) to 25 μl of testing solution (such as cell lysate) in a 96-well assay plate. The plate was incubated at 37°C for 30 minutes, and the optical densities of the standard and test samples were measured at absorbency of 570 nm in a plate reader. The protein concentrations of the testing samples were calculated by comparing the optical density at 570 nm with the standard curve generated for each assay. A minimum of three replicates of each testing sample was used for every protein assay.

FTASE ASSAY USING FTASE PRODUCED IN H-RAS TRANSFORMED NIH/3T3 CELLS

The endogenous farnesyltransferase activity was tested by an *in vitro* FTase assay. This *in vitro* FTase Assay uses cell lysate as a source of FTase (47, 57, 68, 69). The cell lysates were generated from Ras/3T3 cells incubated with various concentrations of arglabin-DMA for 2 hours, 1 day, or 2 days. Tritiated farnesylpyrophosphate and Ras protein were used as the substrates. Tritiated farnesylated Ras protein was generated in proportion to the FTase activity of the cell lysate.

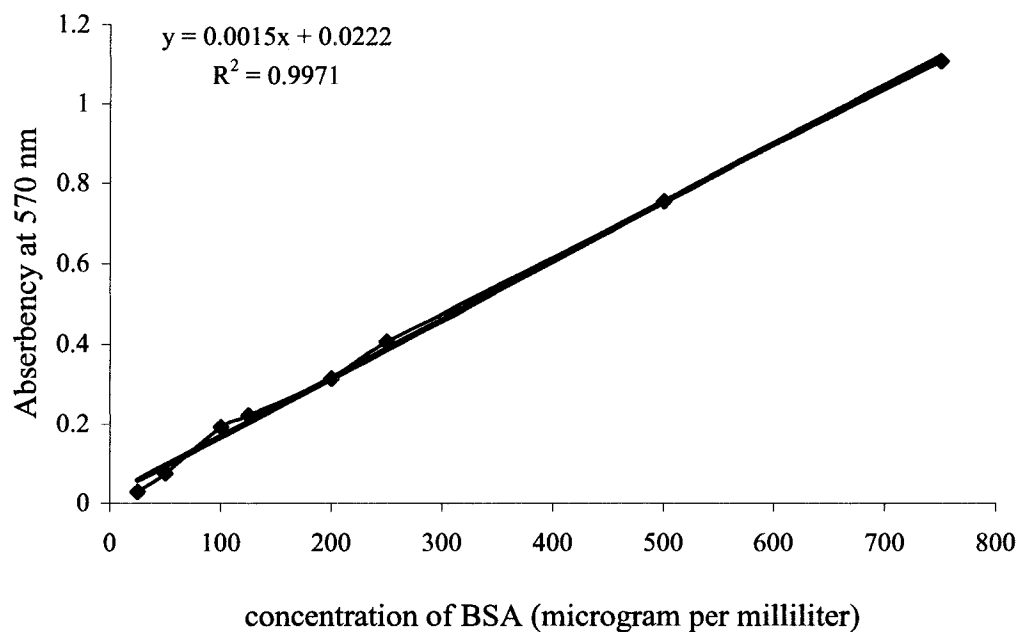


FIG. 10. Standard curve for BCA Assay. Bovine serum albumin (BSA) ranging from 25 $\mu\text{g/mL}$ to 750 $\mu\text{g/mL}$ was used for standard curve generation. The absorbency of BSA was measured at 570 nm in a plate reader.

The *in vitro* FTase assay was initiated by adding 5 μ l of cell lysate (15-20 μ g protein) into 45 μ l of assay buffer. The assay buffer contained H-Ras protein (100 nM), [3 H]FPP (100 nM, 0.1 μ Ci), $MgCl_2$ (5 mM), dTT (5 mM), and HEPES (50 mM), and the pH was adjusted to 7.5 with 1N HCl (47). The reaction was maintained at 37°C for 1 hour and stopped by adding 1M of ice-cold hydrochloride (HCl) prepared with ethanol. The resulting solution was filtered through GF/C filter paper and rinsed by 1 ml of ice-cold ethanol. The filter paper was dried in air and transferred into scintillation fluid. The radioactivity was measured by liquid scintillation counter.

Reactions without cell lysate were used as blank negative controls. Reactions using cell lysate generated from cells without arglabin-DMA treatment, and reactions using farnesyltransferases expressed and purified through prokaryotic system were used as the other negative controls. Reactions using a known FTI were the positive controls. The nonspecific activity of the blank negative control was subtracted from the total radioactivity of each sample. The specific activity of each sample was calculated by dividing the radioactivity (counts per minute) by the amount of protein. The percentage of farnesyltransferase inhibition of arglabin-DMA in cells was calculated by comparing the specific activity of each sample to the cell lysate negative control (without arglabin-DMA treatment). Three replicates were used for each test and control group. Dose-response curves for arglabin-DMA were generated.

GEL ELECTROPHORESIS

SDS-polyacrylamide gels (12% or 4-15%) were purchased from Bio-Rad. Precision pre-stained protein standards ranging from 10 to 250 kD (BioRad, 161- 0373) were used

to assess the relative protein size and transfer efficiency. Equal amounts of sample buffer (BioRad, 161-0737) containing beta-mercaptoethinal and protein samples were mixed, then denatured in boiling water for 5 minutes and stored in wet ice until they were used. Thirty microliter samples were loaded into each well, and 200 volts of electricity was used to separate various sizes of proteins in samples. After 1 hour of electrophoresis in 1x Tris-Glycine-SDS (TGS) running buffer (BioRad, 161-0772), the gel was ready for Coomassie blue staining or protein transfer.

COOMASSIE BLUE STAINING

The SDS-polyacrylamide gel was fixed in solution containing 50% methanol and 10% acetic acid for 30 minutes. After removing fixing solution, the gel was stained with Coomassie blue stain (BioRad, R-250) and agitated at room temperature for 3 hours. Approximately 1 μ g of protein per band was needed for detection using Coomassie blue R-250 staining. The gel was destained with solution containing 5% methanol and 7% acetic acid overnight on an orbital shaker with slow agitation. A photo of the gel was taken after destaining process and used for documentation and analysis.

PROTEIN TRANSFER

SDS-polyacrylamide gels from electrophoresis were submerged in 1x transfer buffer containing 20% methanol and 1x Tris-Glycine buffer (BioRad, 161-0771) for 15 minutes. The proteins separated through electrophoresis were transferred to polyvinylidene difluoride (PVDF) membrane in 1x transfer buffer at 350 mA for 1 hour using Mini

Trans-Blot Cell (Bio-Rad, 170-3930). The transfer efficiency was assessed by examining the prestained protein standard.

IMMUNOPRECIPITATION

Immunoprecipitation before electrophoresis was used to increase the sensitivity of Western blot (65, 67). Specific primary antibody (1 μ g) was added to 1 mL of cell lysates according to various manufacturer instructions. After incubating the cell lysate at 4°C for 2-4 hours, the antigen-antibody complexes were generated. ProteinG agarose beads (20 μ L) were introduced into cell lysate containing antigen-antibody (Ag-Ab) complexes. The immunoprecipitation were performed on a rocker at 4°C overnight. Antigen-antibody complexes attached to agarose beads were separated from cell lysates by centrifugation at 1,000 g for 5 minutes. The precipitates were washed with 1 mL of phosphate buffered saline (1x PBS) 3-4 times. The final precipitates were resuspended in sample buffer (BioRad, 161-0737), denatured in boiling water for 5 minutes, and loaded into SDS-polyacrylamide gel for electrophoresis. Antibodies used for immunoprecipitation were listed in Table 1.

WESTERN BLOT

Following the protein transfer, non-specific protein binding sites were blocked by agitation PVDF membrane in blocking reagents containing 3% casein and 0.15% Tween-20 for 2 hours. The membrane was then incubated with a primary antibody specific to the antigen of interest for 2 hours with slow agitation at room temperature. After washing away unbounded antibody, the blot was incubated with a secondary antibody linked to

horseradish peroxidase (HRP). Following washing unbounded secondary antibody, the blot was incubated in the Opti-4CN substrate for up to 30 minutes, or until the desired sensitivity was attained. The Opti-4CN detection system (Bio-Rad, 170-8235) uses colorimetric horseradish peroxidase substrate, 4-chloro-1-naphthol (4CN), which can generate the detection sensitivity of 100 pg. The primary and secondary antibodies used in this study are listed in Table 1.

SMALL GTPASE-PULL DOWN ASSAY

The EZ-Detect™ Ras Activation Kit (Pierce, 89855) and EZ-Detect™ Rho Activation Kit (Pierce, 89854) were purchased from PIERCE. This assay quantitates the active Ras protein (or RhoA protein) by isolating them via their specific downstream effector Raf protein (or Rhotekin for RhoA protein). The Ras-binding domain (RBD) of Raf protein was expressed as a Glutathione-fusion protein (GST), which was used to pull down the active or GTP-bound Ras protein. The Rho-binding domain (RBD) of Rhotekin was expressed as GST protein as well, which was used to precipitate cellular GTP-bound RhoA protein. After immobilized bait protein (GST-RBD) was incubated with cell lysates at 4°C for 1 hour in the presence of a SwellGel Immobilized Glutathione Disc, GST-RBD of Raf1 or GST-RBD of Rhotekin pulled down active Ras protein or active RhoA protein. The SwellGel Immobilized Glutathione Disc was washed 3 times with 400 µL of 1xLysis/Binding/Wash buffer. The “interactors” were selectively eluted with sample buffer by boiling the samples at 95-100°C for 5 minutes. Samples were collected by centrifugation at 7,200 g for 2 minutes and introduced into SDS-polyacrylamide gel to

TABLE 1. List of antibodies used for immunoprecipitation (IP) and Western blot (WB)

Antigen	Antibody for IP	Primary Antibody for WB	Secondary Antibody for WB
FTase	N/A	Rabbit anti-FTase (341285 ^a)	Goat anti-Rabbit-IgG-HRP
H-Ras	Mouse anti-Ras IgG (89855 ^b)	Rat anti-v-H-Ras (OP ^c 1)	Rabbit anti-Rat-IgG-HRP
K-Ras	Mouse anti-Ras IgG (89855)	Mouse anti-K-Ras (sc-30)	Goat anti-Mouse-IgG-HRP
RhoA	Rabbit anti-RhoA IgG (sc ^d -179)	Mouse anti-RhoA (sc-418)	Goat anti-Mouse-IgG-HRP
Rho B	Rabbit anti-RhoB Ig G(sc-180)	Mouse anti-RhoB (sc-8048)	Goat anti-Mouse-IgG-HRP
P21WAF1	Rabbit anti-p21 IgG (ab ^e -7960)	Mouse anti-p21WAF1 (OP76)	Goat anti-Mouse-IgG-HRP

^a 341285: Antibody from Calbiochem-Novabiochem Corporation (San Diego, CA). ^b 89855: Antibody from PIERCE Biotechnology, Inc. (Rockford, IL). ^c OP: Antibodies from Oncogene Research Products (San Diego, CA). ^d sc: Antibodies from Santa Cruz Biotechnology, Inc. (Santa Cruz, CA). ^e ab: Antibodies from Abcam Limited (Cambridgeshire, UK).

separate different sizes of proteins. The pulled-down active Ras and Rho protein were detected by a Western blot.

DENSITOMETRY ANALYSES

The intensity of the bands from Western blot was determined by densitometry using the Quantity One system (4.6) from Bio-Rad according to the manufacturer instruction. Briefly, the images of blots were scanned and stored in a computer. The bands of interest were selected using Quantity One program. Values of maximum intensity (INT), minimum intensity (INT), mean (INT), standard deviation, volume area (mm^2), density (INT/mm^2), and background intensity (INT) were assessed and calculated using Quantity One program.

STATISTICAL ANALYSES

Each data point consists of at least 3 replicates in all statistical analyses. Linear regression analyses were used to derive standard curves. An analysis of variance (ANOVA) was used to determine the significant differences among all experimental groups. Two-sample t-tests were performed to compare the differences between any 2 specific groups. A confidence level of 95% was considered to be statistically significant.

RESULTS

IN VITRO CYTOTOXICITY OF ARGLABIN-DMA

Characterization of H-Ras Transformed NIH-3T3 Cells and NIH/3T3 Cells

Both Ras/3T3 cells and NIH/3T3 cells were propagated in Dulbecco's Modified Eagle's Medium (DMEM) containing 10% fetal bovine serum and 4 mM of L-glutamine at 37 °C in a CO₂ incubator containing 5% CO₂/95% air. Photos of representative cell morphologies of NIH/3T3 cells and Ras/3T3 cells were taken using a digital camera attached to the microscope (Fig. 11). NIH/3T3 cells showed monolayer morphology when cells reached confluence (Fig. 11A). Ras/3T3 cells showed cluster formation and loss of "contact inhibition" (piled up) in culture (Fig. 11B). Normal diploid mammalian cells, such as NIH/3T3 cells, have a phenomenon called density-dependent inhibition of growth or "contact inhibition", which means the cell-cell contact stops cell replication (61). The transformed cells, such as Ras/3T3, not only have decreased density-dependent inhibition of growth, but also loss of anchorage dependence (Fig. 12A). Ras/3T3 cells had grown in suspension culture where the plates were coated with poly-HEME (Fig. 12B).

Viable cell numbers were counted using the Trypan Blue exclusion method for a continuous seven days after seeding 5,000 cells/cm² on day 0. The seven-day growth curves showed that the number of NIH/3T3 cells plateau at 60,080 cells/cm² (Fig. 13), while the number of Ras/3T3 cells plateau at 308,200 cells/cm². Population doubling time (PDT) from day 1 to day 4 was 23.51 hours for NIH/3T3 cells and 17.45 hours for Ras/3T3 cells. The number of Ras/3T3 cells increased significantly for 5 days until the

nutrients in culture media were exhausted. The number of NIH/3T3 cells increased for 4 days until cells reached confluence.

In Vitro Cytotoxicity Assessment of Arglablin-DMA

Arglablin-DMA at concentrations of 0.1 μM , 1 μM , 10 μM , 50 μM , and 100 μM were prepared with DMEM containing 10% FBS and 4 mM of L-glutamine. Equal numbers of Ras/3T3 cells and NIH/3T3 cells were seeded in 96-well plates. After 48 hours of incubation at 37 °C in a CO₂ incubator containing 5% of CO₂/95% air, the culture media was replaced by culture media containing various concentrations of arglablin-DMA. Cells incubated in medium alone were used as negative controls. Cells incubated with 5% sodium azide were used as a positive control. After 72 hours of incubation with arglablin-DMA, *in vitro* cytotoxicity assays were performed using the MTT (3-[4,5-dimethylthiazol-2-yl]-2,5-diphenyl tetrazolium bromide) based *in vitro* toxicology assay kit from Sigma (TOX-1). An increase or decrease in cell number results in a concomitant change in the amount of formazan formed, indicating the degree of cytotoxicity caused by the test material. Absorbencies of viable cells were measured using a plate reader (Labsystems, MultiSkan Ascent).

The absorbency of the Ras/3T3 cell control (OD = 1.014) was more than twice that of the NIH/3T3 cell control (OD = 0.4457) after 72 hours of incubation. Dose-response curves for arglablin-DMA were generated for both cell lines (Fig. 14). Concentrations of arglablin-DMA (μM) were plotted in logarithmic scale. A trend line was generated from the plot using percentage of growth inhibition (compared to the positive control cells without arglablin-DMA treatment) versus logarithmic scale of arglablin-DMA concentrations (μM) (Fig. 15). Regression analysis showed 96% correlation between

concentration of arglabin-DMA and percentage of growth inhibition. The 50% inhibition concentration (IC₅₀) of arglabin-DMA for Ras/3T3 cells estimated from the plot was 10.34 μ M, and the IC₉₀ was 79.28 μ M. The concentration of arglabin-DMA used to inhibit half of Ras/3T3 cell growth was 10.34 μ M, while the concentration of arglabin-DMA used to inhibit the same number of NIH/3T3 cells was more than 100 μ M, approximately 10-fold greater than the concentration for Ras/3T3 cells.

THE EFFECT OF ARGLABIN-DMA ON FTASE ACTIVITY

Binding Affinity of Arglabin-DMA and FTase

The X-ray diffraction structure of the FTase and FPP complex was taken from the Brookhaven National Library Protein Data Bank. The 3-D molecular structures of all ligands were drawn based on the 2-D structure diagram using the Insight II software. The intermolecular energy of FTase and various ligands were measured using the Insight II docking program (Appendix A).

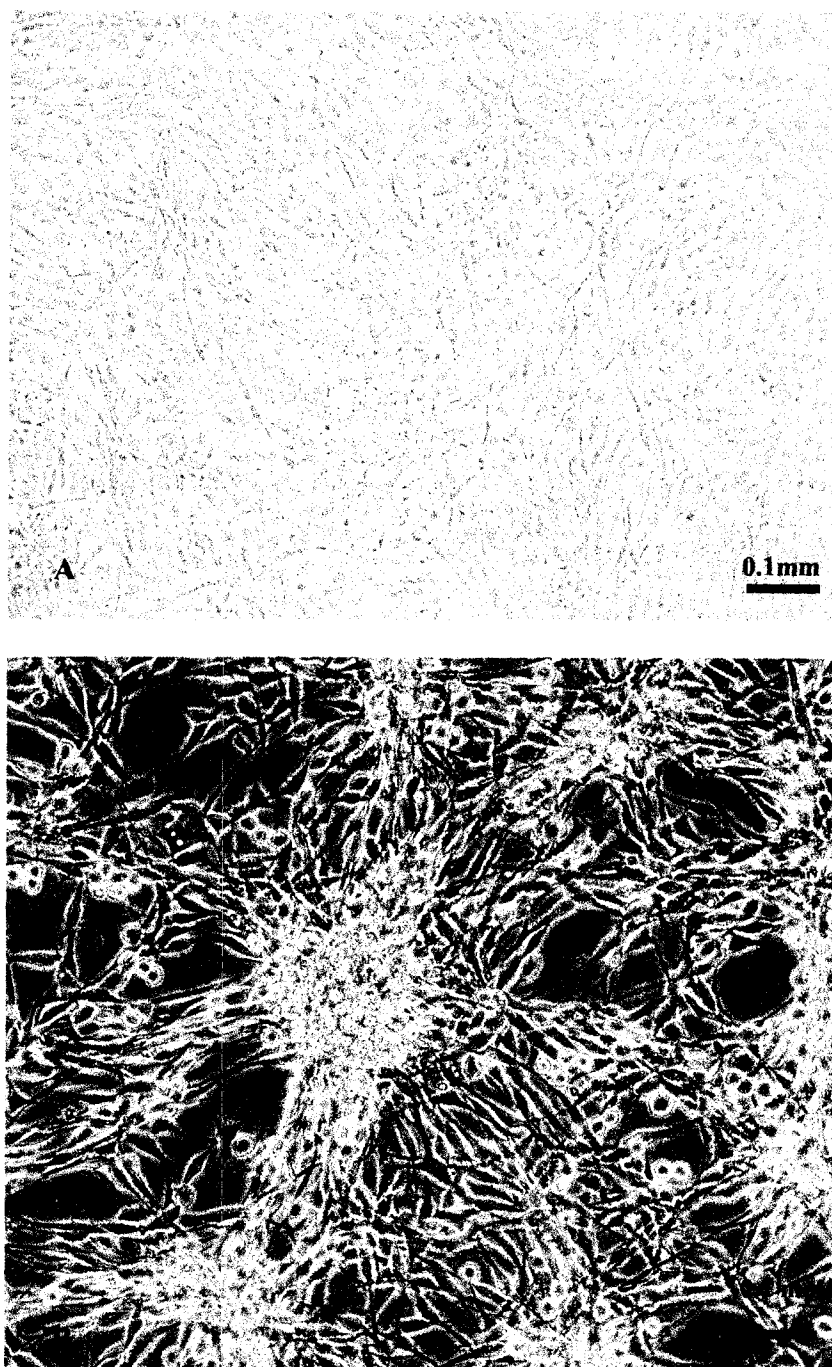


FIG. 11. Confluent Ras/3T3 cells and NIH/3T3 cells in culture. Figure 11A - monolayer of NIH/3T3 cells after reaching confluence. Figure 11B - Ras/3T3 cells formed clusters and loss of "contact inhibition" (piled up) in culture. All of the photos shown here were taken at 100x magnification.

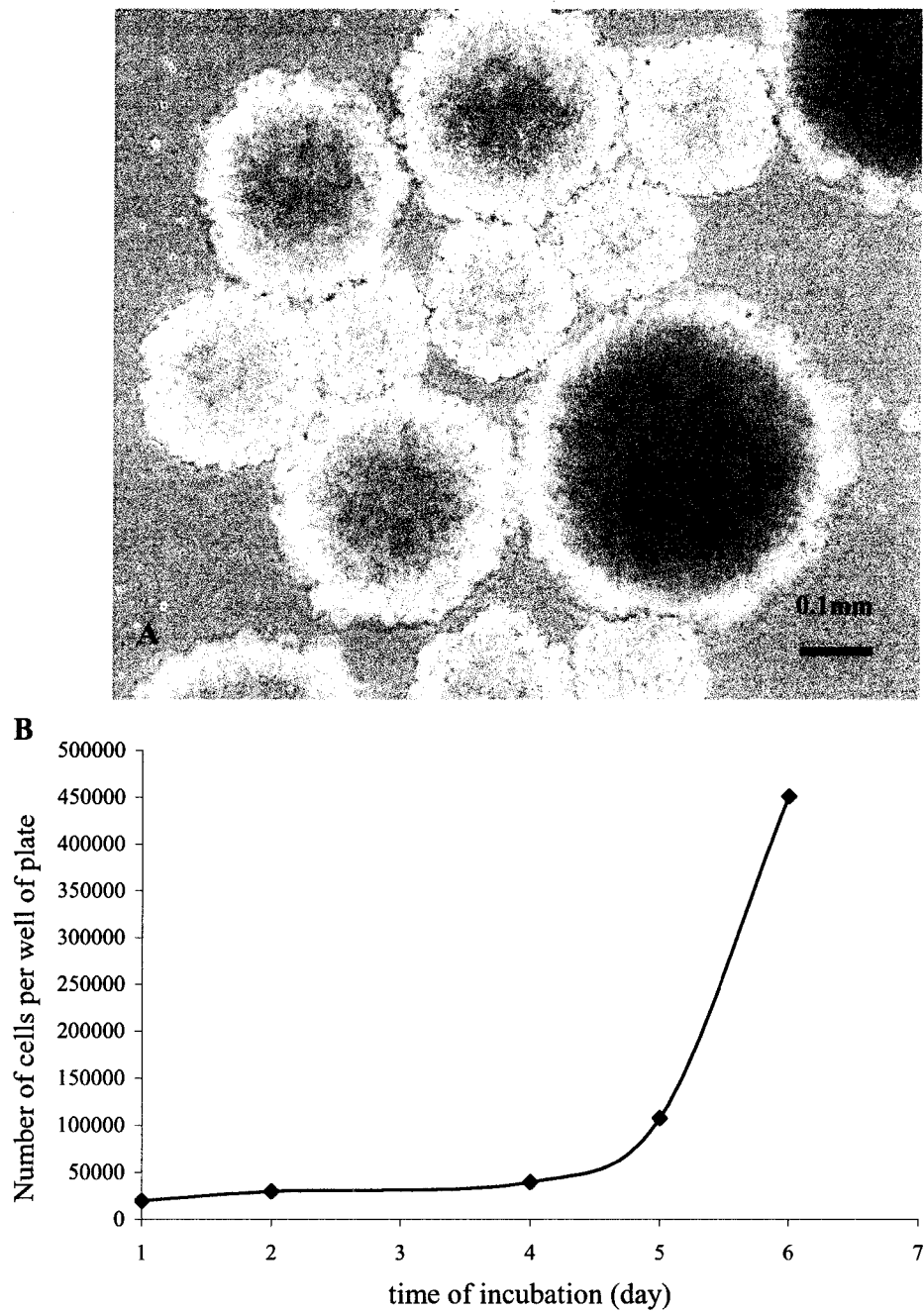


FIG. 12. Growth of Ras/3T3 cells in suspension. Figure 12A - Ras/3T3 cells grown in poly-HEME coated tissue culture plates. Figure 12B - growth curve for Ras/3T3 cells grown in suspension in poly-HEME coated tissue culture plates. The photo shown here was taken at 100x magnification.

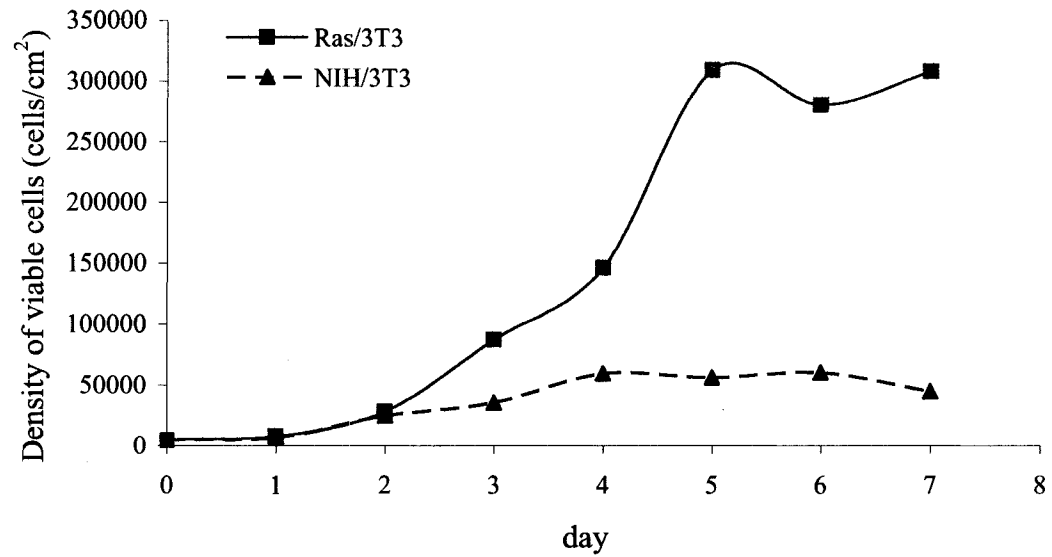


FIG. 13. Growth curves of Ras/3T3 cells and NIH/3T3 cells. Viable cell numbers were counted each day for 7 days. The number of Ras/3T3 cells increased significantly for 5 days until the nutrients in culture media were exhausted. The number of NIH/3T3 cells increased for 4 days until cells reached confluence.

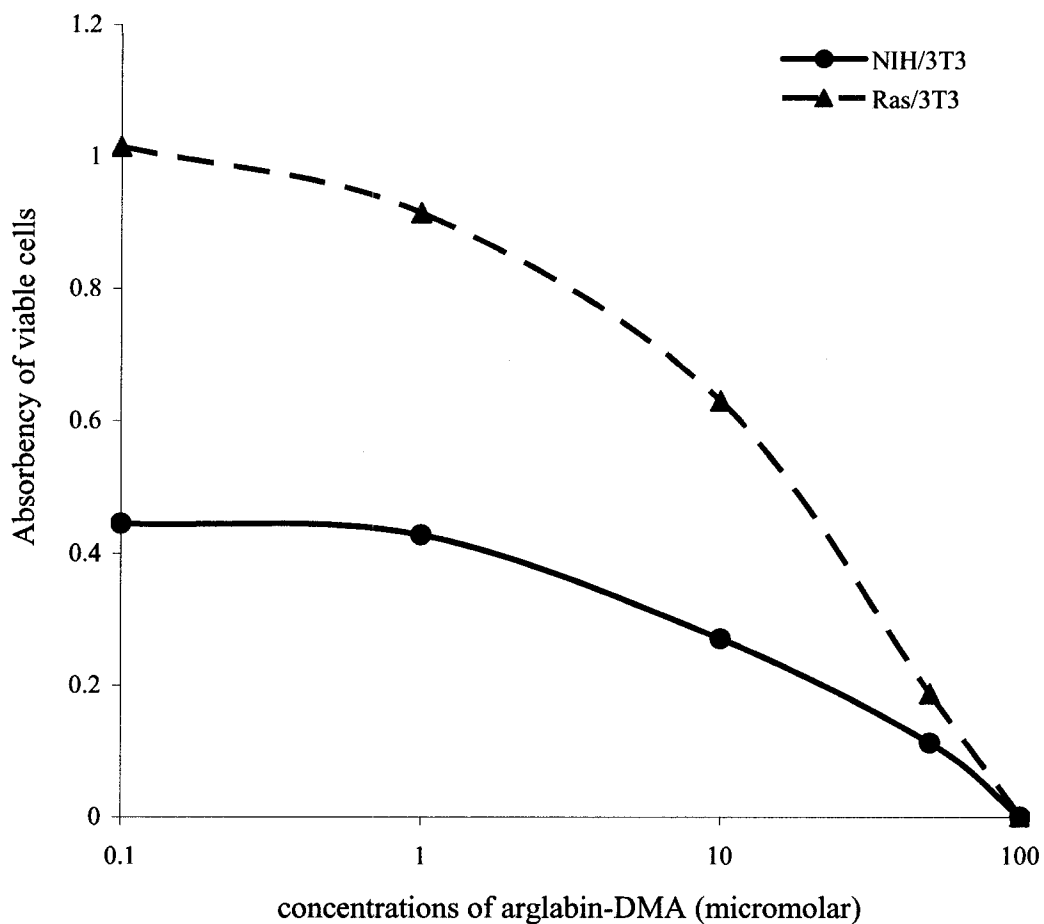


FIG.14. Dose-response curves of NIH/3T3 cells and Ras/3T3 cells to arglabin-DMA. Culture media containing various concentrations of arglabin-DMA (0.1, 1, 10, 50, or 100 μ M) were used to incubate with cells for 72 hours. The absorbencies obtained from MTT assays reflect the viable cell number for both cell lines, indicating the degree of cytotoxicity caused by the test material. For the Ras/3T3 cell control and NIH/3T3 cell control (not shown in this figure), the absorbency of viable Ras/3T3 cells (OD = 1.014) was more than twice as much as the absorbency of viable NIH/3T3 cells (OD = 0.4457).

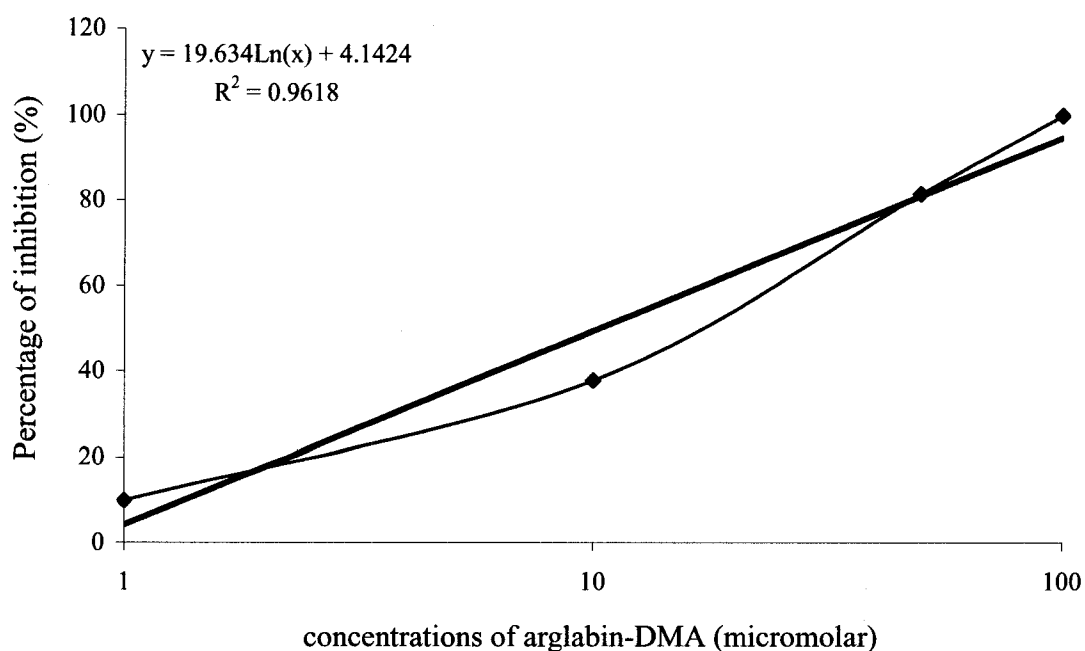


FIG.15. Percentage Ras/3T3 cell growth inhibition by arglabin-DMA. A trend line was generated from the plot using percentage of growth inhibition (compared to the positive control cells without arglabin-DMA treatment) versus logarithmic scale of arglabin-DMA concentrations (μM). The 50% inhibition concentration (IC_{50}) of arglabin-DMA for Ras/3T3 cells estimated from the plot was $10.34 \mu\text{M}$, and the IC_{90} was $79.28 \mu\text{M}$.

The mean of the intermolecular energy of all ten possible frames and standard deviation for each pair of ligand and FTase were calculated and shown in Table 2. The difference in intermolecular energy was statistically significant between pairs of all seven ligands (Appendix B) ($p < 0.05$). The lower the intermolecular energy, the higher the binding affinity of ligand and FTase will be (18, 30). The intermolecular energy between arglabin-DMA and FTase (-46.97 kCal/mol) was significantly higher than the intermolecular energy between FPP and FTase (-60.8 kCal/mol) ($p < 0.05$) (Table 2), which means that arglabin-DMA was not able to compete for the FTase binding site with FPP. The intermolecular energy between FTase inhibitor II and FTase (-57.57 kCal/mol), the energy between phosphorylated arglabin-DMA and FTase, and the energy between FTI-277 and FTase were not significantly different from the intermolecular energy between FPP and FTase ($p > 0.05$). Intermolecular energy between FPT inhibitor II and FTase and intermolecular energy between FPI inhibitor III and FTase were significantly lower than the intermolecular energy between FPP and FTase ($p < 0.05$). These results suggested that arglabin-DMA itself may not bind to FTase directly and arglabin-DMA itself is not a potent FTase inhibitor.

TABLE 2. Intermolecular energy between FTase and various ligands

<i>Ligands</i>	<i>Intermolecular Energy (kCal/mol)</i>	<i>Stdev</i>
FPT Inhibitor II	-82.19	12.16
FPT Inhibitor III	-78.90	5.37
FTI-277	-65.93	10.26
Phosphorylated Arglabin-DMA	-63.70	4.76
FPP	-60.80	5.56
FTase Inhibitor II	-57.57	7.31
Arglabin-DMA	-46.97	4.62

The Effect of Argabin-DMA on Expressed and Purified FTase Activity

Verification of the Expressed and Purified FTase

Human FTase α and β subunits were expressed in competent *E.coli* cells, purified through glutathione affinity chromatography and concentrated by centrifugation using centrifugal filters with 100 kilodalton molecular weight cutoff (MWCO). The protein concentration of the purified FTase was determined by BCA protein assay. The relative protein size was confirmed by electrophoresis of the purified protein on SDS-polyacrylamide gel stained with Coomassie blue. Coomassie blue staining showed two separate bands: one band had a relative size of 90 kD the second band with a relative size of 70 kD when compared to the ladder (Fig. 16). The relative protein size of MBP-FT α should be 74.1 kD, which included MBP (29.7 kD) and the FT α -subunit (44.4 kD). The relative size of GST-FT β should be 90.2 kD, including GST (42 kD) and the FT β -subunit (48.8 kD).

The enzymatic activity of the expressed and purified FTase was determined by *in vitro* FTase assay. The standard curve of FTase activity was generated using increasing amounts of cellular protein (0.4-4 μ g) (Fig. 9). Generation of ^3H -farnesylated-biotin-lamin B peptide was measured by liquid scintillation counter (microcurie/min). Linearity existed over the range of 0.4 μ g to 4 μ g of purified protein ($R^2 = 0.9956$, Fig. 9). Two micrograms of cellular protein was chosen to use for the following *in vitro* FTase assays.

FTase Assay using expressed and purified FTase

The FTase activity was determined by measuring the incorporation of the ^3H -farnesyl group of ^3H -FPP to the substrate peptide, lamin-B. Various concentrations of argabin-

DMA (50, 100, 1000, 2000, 4000, and 8000 μ M), FPT inhibitor II (1, 10, 50, 100, 1,000, 5,000, and 10,000 nM), or FTase inhibitor II (0.01, 0.05, 0.1, 0.5, 1, 5, and 10 μ M) were tested in FTase assays. The FTase enzymatic activity was expressed as the amount of radiolabeled farnesylated protein per minute of reaction (μ Ci/min). Dose-response curves for arglabin-DMA, FPT inhibitor II, and FTase inhibitor II are shown in Figure 17, Figure 19, and Figure 21. Percentages of FTase inhibition by various compounds were calculated by comparing the FTase activity to the no-treatment control. Trend lines were generated from percentage inhibition plots (Fig. 18, Fig. 20, Fig. 22). The 50% inhibition concentration (IC₅₀) of known FTIs and arglabin-DMA were estimated from the equation of the linear regression.

FPT inhibitor II is a phosphonic acid, an FPP analogue, which competes for the FPP binding site of FTase. FTase assay showed significant inhibition at nanomolar concentrations of FPT inhibitor II (Fig. 17). Linearity exists over FPT inhibitor II concentrations ranging from 10 nM to 1000 nM ($R^2 = 0.975$, Fig. 18). The IC₅₀ of FPT inhibitor II calculated from the equation of the linear regression was 119 nM. FTase inhibitor II is a peptidomimetic inhibitor of FTase, which competes for the protein binding site of FTase. FTase assays indicated significant inhibition of FTase activity at

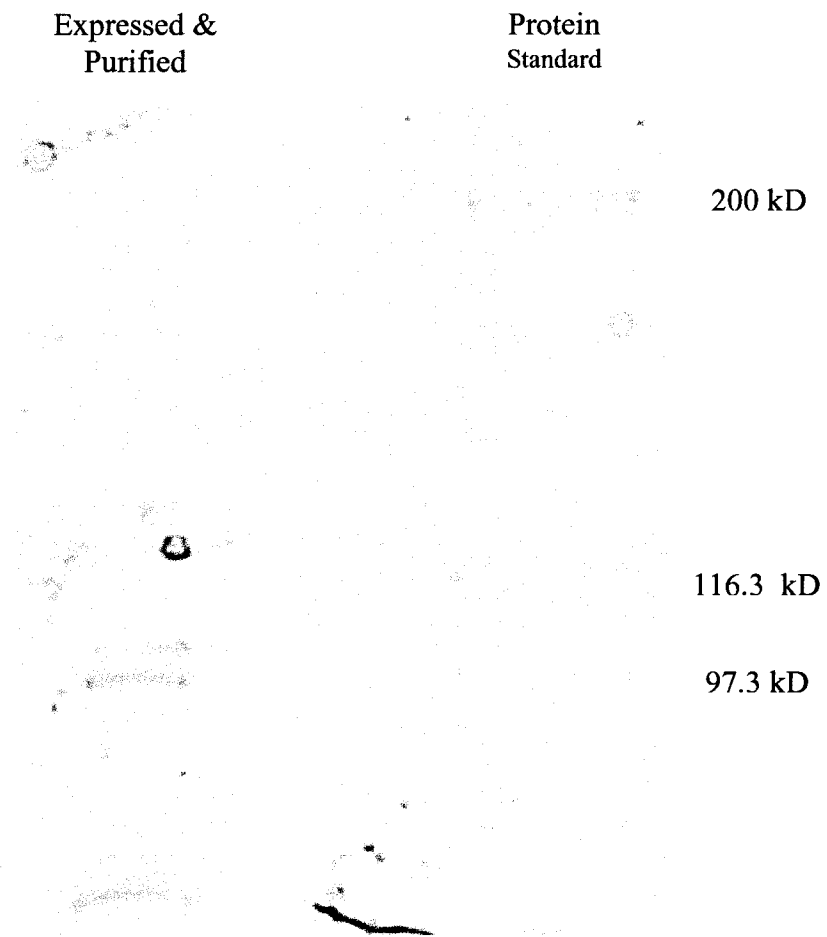


FIG. 16. Coomassie blue staining of expressed and purified FTase. The relative protein size of MBP-FT α was 74.1 kD, which included MBP (29.7 kD) and FT α -subunit (44.4 kD). The relative size of GST-FT β was 90.2 kD that included GST (42 kD) and FT β -subunit (48.8 kD).

micromolar concentrations of FTase inhibitor II (Fig. 19). The IC_{50} of FTase inhibitor II calculated from the equation of the linear regression of the percentage inhibition plot was $5.09 \mu\text{M}$ ($R^2 = 0.972$, Fig. 20). FTase assay using various concentrations of arglabin-DMA showed that FTase activity was inhibited by arglabin-DMA at millimolar concentrations (Fig. 21). Linearity exists over the arglabin-DMA concentration ranging from $500 \mu\text{M}$ to $8000 \mu\text{M}$ ($R^2 = 0.9776$, Fig. 22). The IC_{50} for Argabin-DMA calculated from the equation of the linear regression was 2.9 mM .

Lineweaver-Burk Double Reciprocal Plot of Argabin-DMA and Known FTIs

The Lineweaver-Burk plot shows $1/v$ (velocity) versus $1/[S]$ (substrate concentration), which gives a straight line with a slope of K_m/V_m and a y-intercept of $-1/K_m$. Thus, V_m (maximum velocity) and K_m (Michaelis constant) can be obtained from the plot. The Michaelis constant is an indication of the relative affinity of the enzyme for the substrate (51, 58). The lower the Michaelis constant, the higher affinity between substrate and enzyme. Various concentrations of tritium-labeled FPP (2, 4, 8, and $16 \mu\text{M}$) were used to determine the velocity of enzyme reaction (pmol/min). The Lineweaver-Burk plot of FPT inhibitor II was generated from FTase assays using various concentrations of tritium-labeled FPP and three concentrations of FPT inhibitor II (0 nM, 10 nM, 100 nM) (Fig. 23). The Lineweaver-Burk plot of FTase inhibitor II was generated from FTase assays using various concentrations of tritium-labeled FPP and three concentrations of FTase inhibitor II (0 nM, 500 nM, 5,000 nM) (Fig. 24). The Lineweaver-Burk plot of arglabin-DMA was generated from FTase assay using various

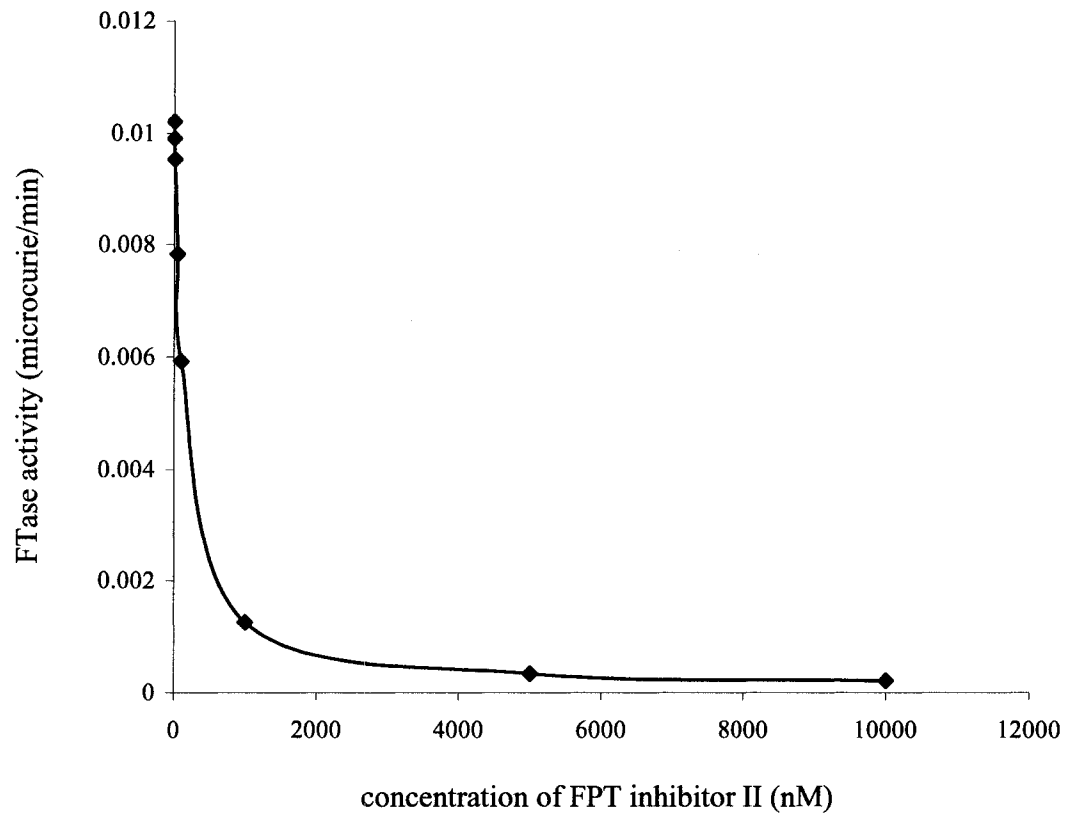


FIG. 17. Dose response curve of FPT inhibitor II. Various concentrations of FPT inhibitor II (1, 10, 50, 100, 1,000, 5,000, and 10,000 nM) were used for FTase assay. FTase activity was reduced significantly when the concentration of FPT inhibitor II was between 10 nM to 1,000 nM.

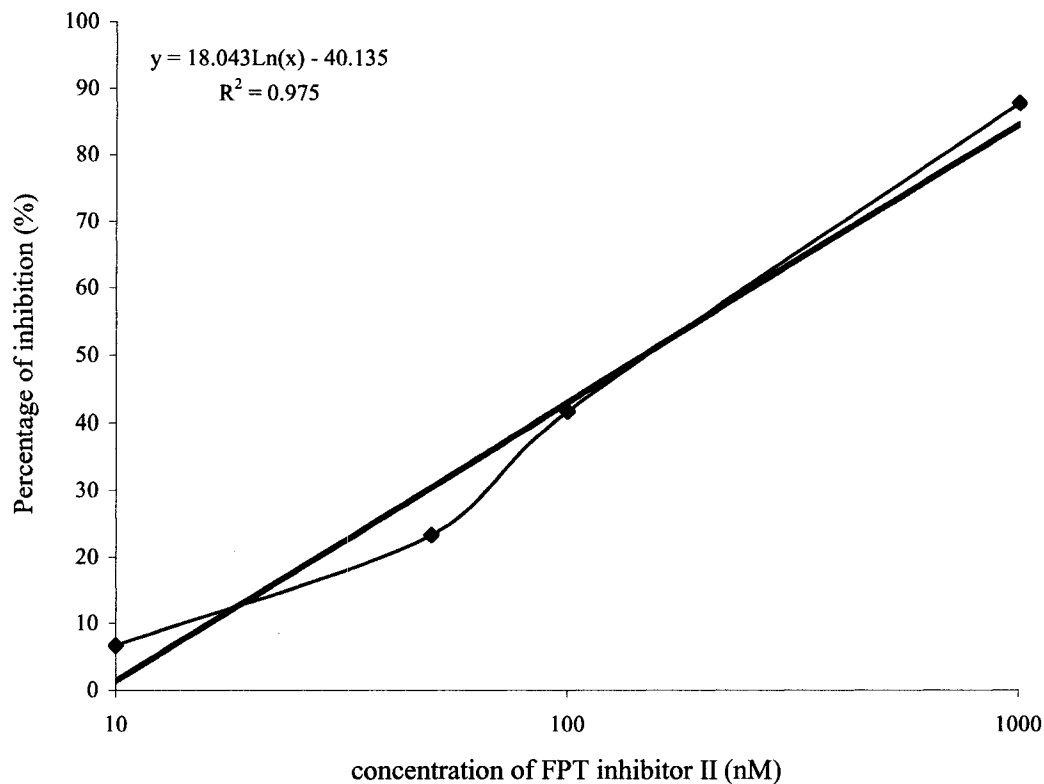


FIG. 18. Percentage of inhibition of FTase activity by FPT inhibitor II. A trend line was generated from the plot using percentage of inhibition versus logarithmic scale of FPT inhibitor II concentrations (nM). Linearity exists over FPT inhibitor II concentration ranging from 10 nM to 1000 nM ($R^2 = 0.975$). IC₅₀ of FPT inhibitor II calculated from the equation of linear regression was 119 nM.

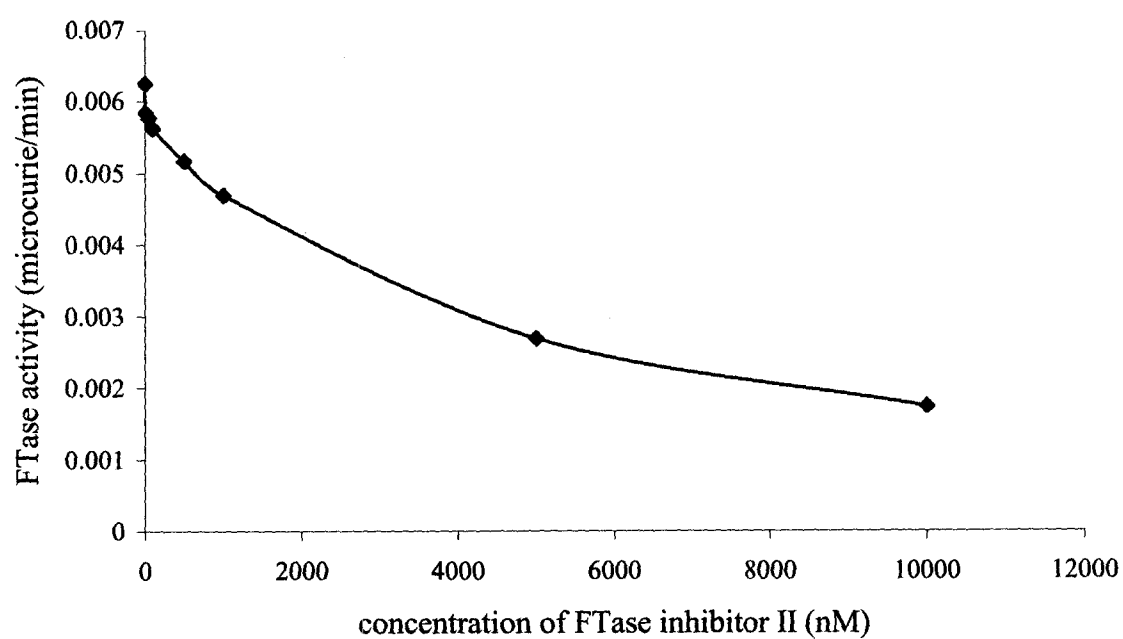


FIG. 19. Dose response curve of FTase inhibitor II. Various concentrations of FTase inhibitor II (0.01, 0.05, 0.1, 0.5, 1, 5, and 10 μ M) were used for FTase assay. FTase activity was reduced significantly when the concentration of FTase inhibitor II was between 1 μ M to 10 μ M.

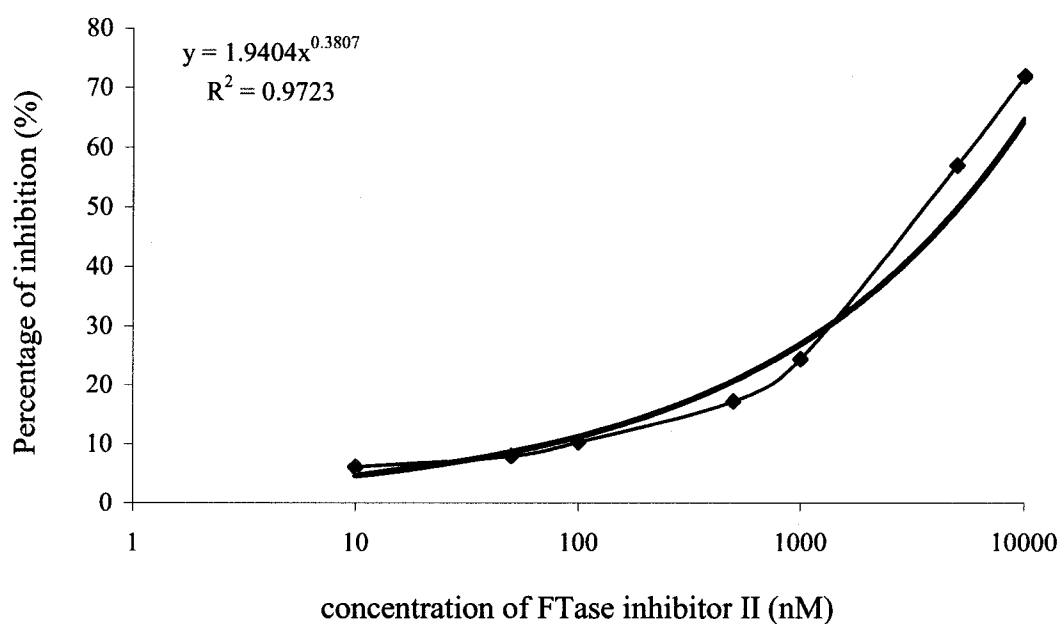


FIG. 20. Percentage of inhibition of FTase activity by FTase Inhibitor II. A trend line was generated from the plot using percentage of inhibition versus logarithmic scale of FTase inhibitor II concentrations (nM) ($R^2 = 0.972$). IC₅₀ of FTase inhibitor II calculated from the equation of the trend line was 5.09 μ M.

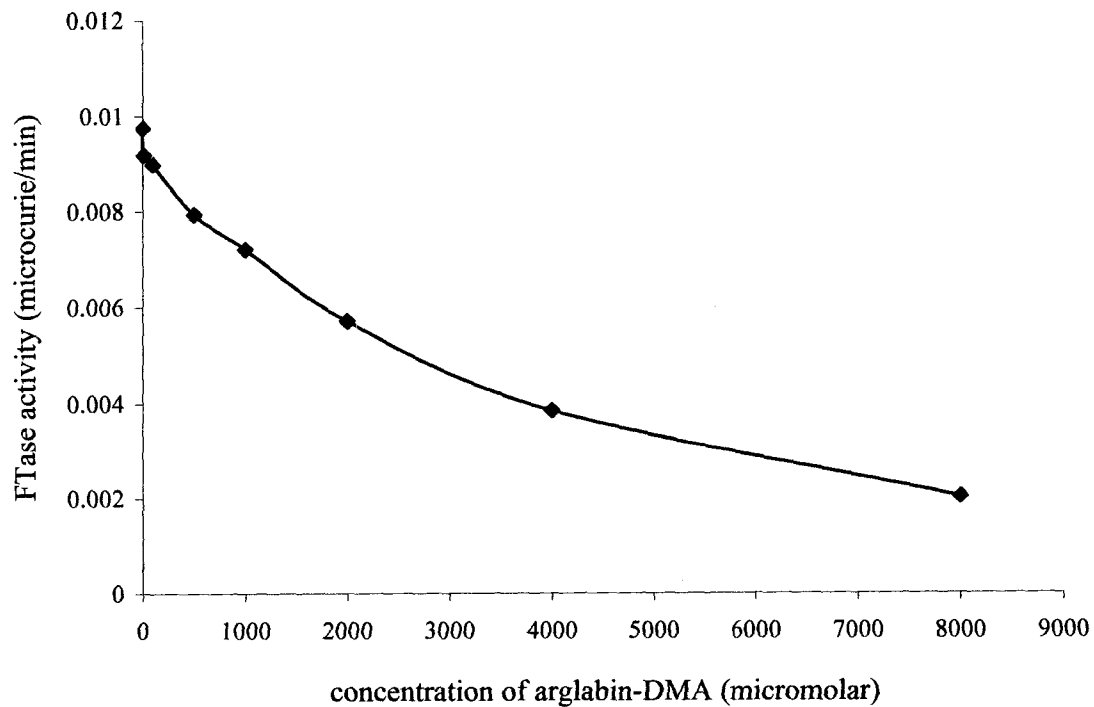


FIG. 21. Dose response curve of arglabin-DMA. Various concentrations of FTase inhibitor II (50, 100, 1000, 2000, 4000, and 8000 μM) were used for FTase assay. FTase activity was reduced significantly when the concentration of arglabin-DMA was between 1 mM and 8 mM.

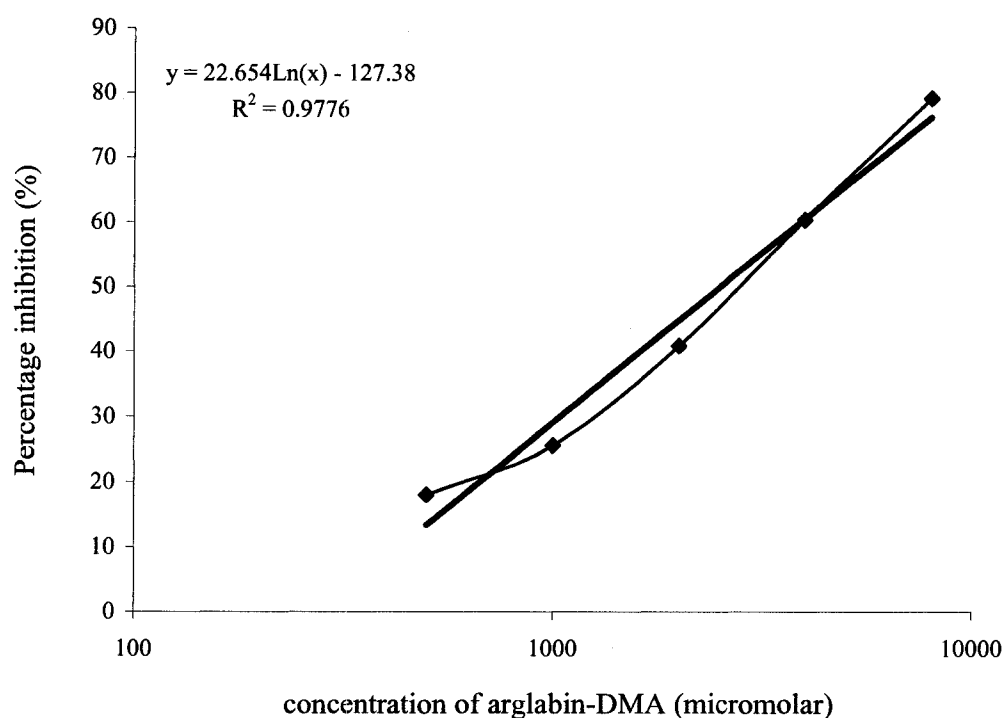


FIG. 22. Percentage of inhibition of FTase activity by arglabin-DMA. A trend line was generated from the plot using percentage of inhibition versus logarithmic scale of arglabin-DMA concentrations (μM). Linearity exists over arglabin-DMA concentration ranging from 100 μM to 8,000 μM ($R^2 = 0.976$). The IC_{50} of arglabin-DMA calculated from the equation of linear regression was 2.9 mM.

concentrations of tritium-labeled FPP and three concentrations of arglabin-DMA (0 μ M, 1 μ M, 4 μ M) (Fig. 25).

Lineweaver-Burk double reciprocal plots of $1/v$ versus $1/[S]$ showed that V_m (0.75 pmol/min) were nearly identical for three different concentrations of FPT inhibitor II (Fig. 23). K_m changed at different FPT inhibitor concentrations. The plot indicates competitive inhibition of FTase by FPT inhibitor II, which means that FTI inhibitor II competes with the FPP for binding to the active site of FTase. The Lineweaver-Burk double reciprocal plot of FTase inhibitor II showed a constant slope (K_m/V_m), but both K_m and V_m changed with various concentrations of FTase inhibitor II. These results indicated that FTase inhibitor II was an uncompetitive inhibitor of FTase (Fig 24), which means FTase inhibitor II binds to the FPP-FTase complex, not FTase. The Lineweaver-Burk double reciprocal plot of arglabin-DMA was more like the double reciprocal plot of FTase inhibitor II with a constant slope (K_m/V_m) (Fig. 25). This suggests that arglabin-DMA may bind to FPP-FTase complex and inhibits FTase activity at higher concentrations than FPT inhibitor II and FTase inhibitor II.

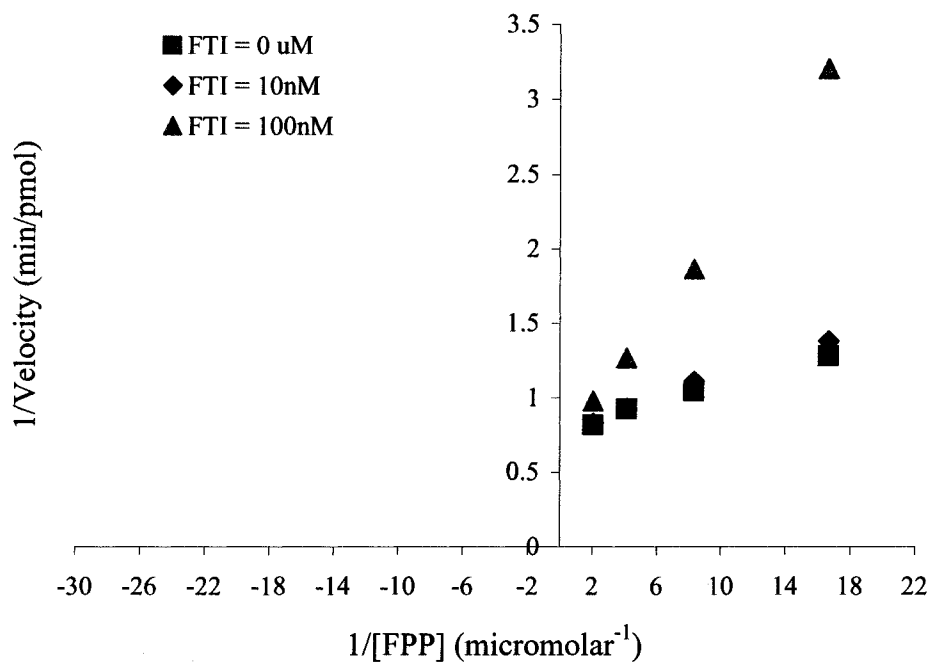


FIG. 23. Lineweaver-Burk double reciprocal plots of FPT inhibitor II. FTase-catalyzed reaction velocity ($1/v$) versus substrate concentration ($1/[S]$) using various concentrations of FPT inhibitor II (0 nM, 10 nM, 100 nM). V_m was constant for three different concentrations of FPT inhibitor II (0.75 pmol/min). K_m was changed at different FPT inhibitor II concentrations.

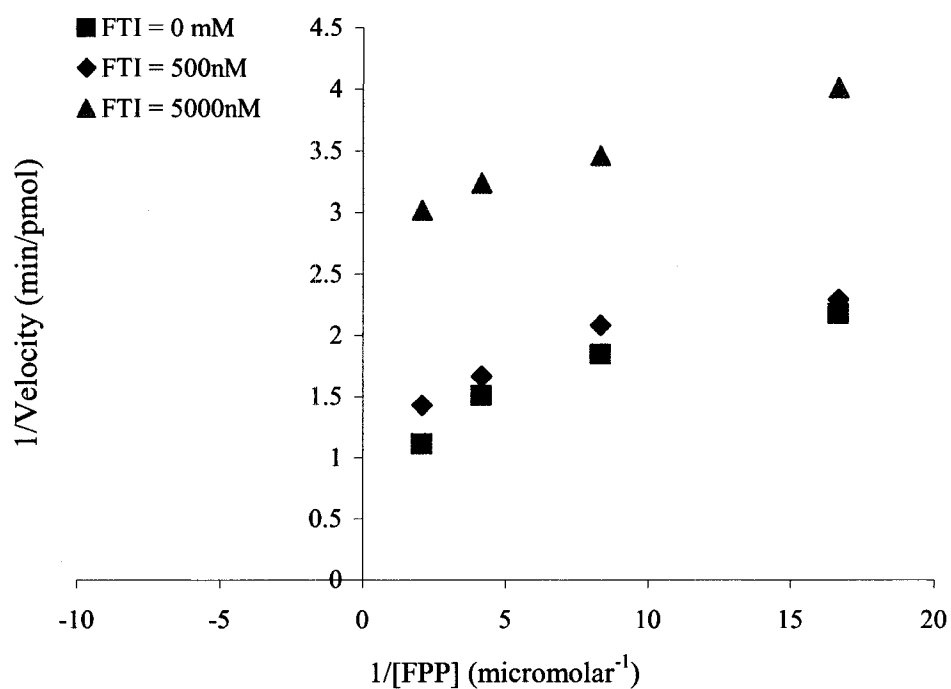


FIG. 24. Lineweaver-Burk double reciprocal plots of FTase inhibitor II. FTase-catalyzed reaction velocity ($1/v$) versus substrate concentrations ($1/[S]$) using 0 nM, 500 nM, or 5,000 nM of FTase inhibitor II. A constant slope (K_m/V_m) and various K_m and V_m were found in three different concentrations of FTase inhibitor II.

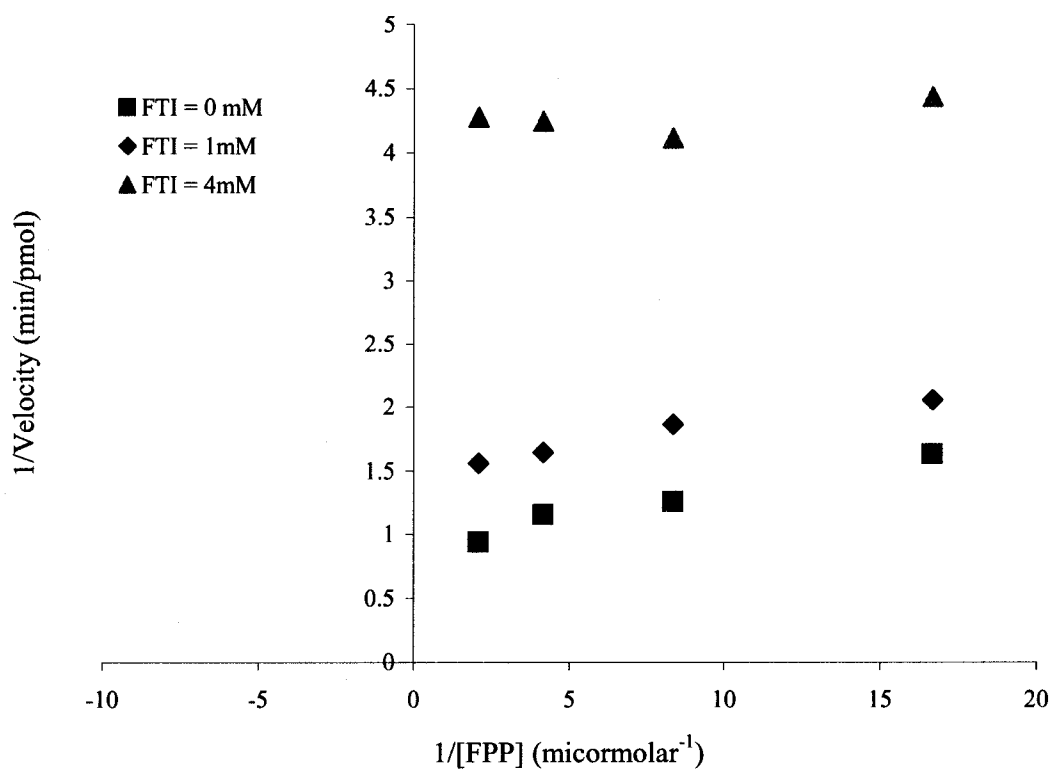


FIG. 25. Lineweaver-Burk double reciprocal plots of arglabin-DMA. FTase-catalyzed reaction velocity ($1/v$) versus substrate concentration ($1/[S]$) using various concentrations of arglabin-DMA (0 μ M, 1 μ M, 4 μ M). The slopes (K_m/V_m) of all three concentrations of arglabin-DMA were constant, but both K_m and V_m changed with various concentrations of arglabin-DMA.

The Effect of Arglabin-DMA on FTase Produced in Transformed Cells

Farnesyltransferase Production in Arglabin-DMA Treated Ras/3T3 Cells

Equal numbers of Ras/3T3 cells were incubated with various concentrations of arglabin-DMA (0, 0.1, 1, 10, 50, and 100 μM), or 0.25 μM of FTI-277 for 24 hours or 72 hours, since the half-life of FTase in cells is around 24 hours. Cell lysates were generated, and the concentrations of cellular protein were determined by BCA protein assays. Equal amounts of cellular protein were separated in SDS-polyacrylamide gel, and the amounts of FTase in gels were determined by Western blot using rabbit anti-farnesyltransferase monoclonal antibody. The densities of each band were quantitated using Quantity One densitometry software from Bio-Rad.

Two band sizes appear on Western blots: the top band (48.8 kDa) represents the FT β -subunit, and the bottom band (44.4 kDa) represents the FT α -subunit. Western blots for FTase after 24 hours and 72 hours of incubation with arglabin-DMA or FTI-277 are shown in figure 26A and figure 27A. There was no significant difference between densities of bands detected by densitometry (Fig. 26 B and Fig.27B). These results suggested that neither arglabin-DMA nor FTI-277 affected FTase production in Ras/3T3 cells.

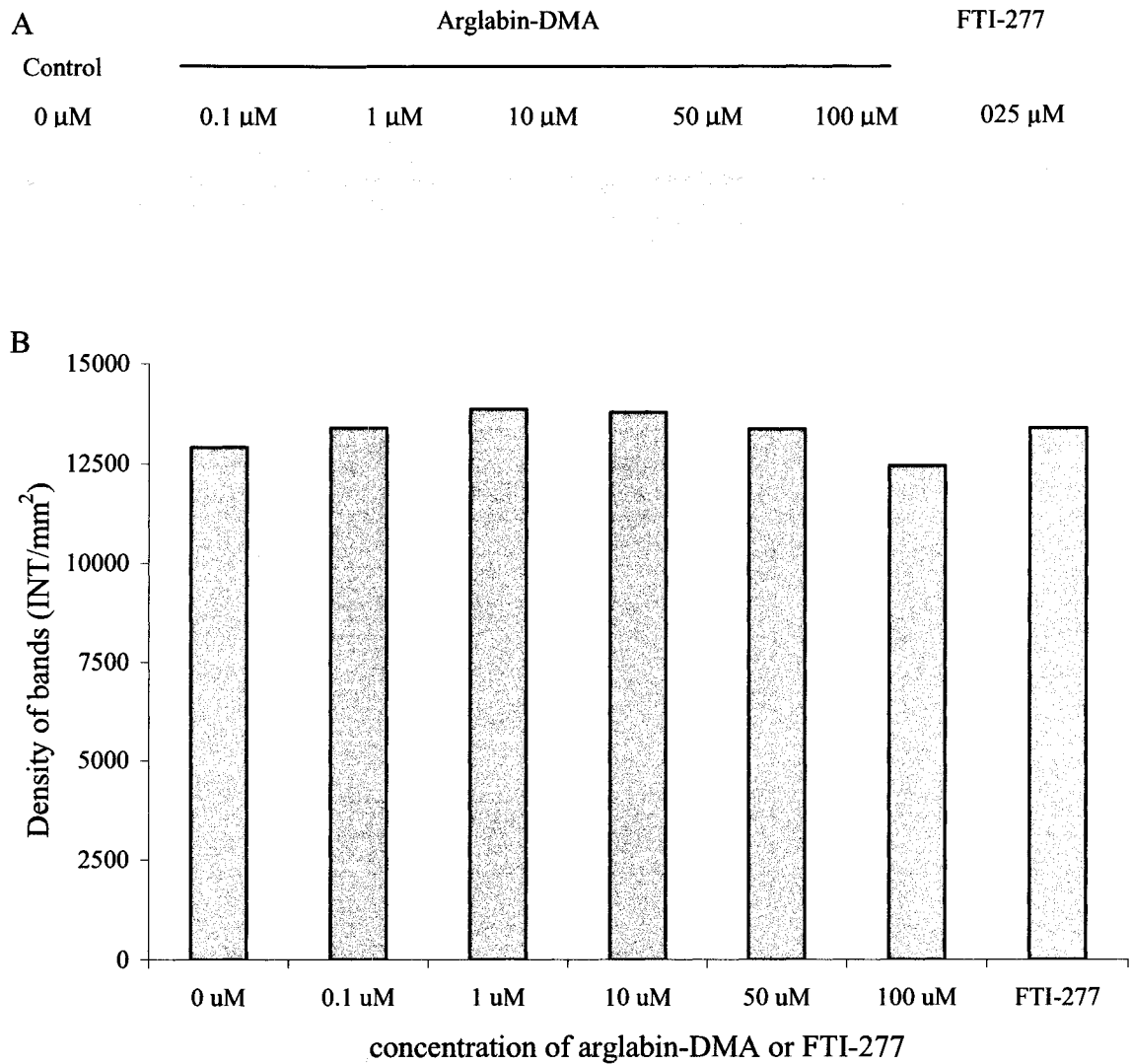


FIG. 26. Western blot of FTase after 24-hour incubation with arglabin-DMA or FTI-277. Ras/3T3 cells were incubated with complete cell culture media containing 0, 0.1, 1, 10, 50, or 100 μ M of arglabin-DMA or 0.25 μ M of FTI-277 for 24 hours. FTase in cellular protein was detected and shown in figure 26A. The total densities of bands for each concentration group were shown in figure 26B. No significant difference was found between groups.

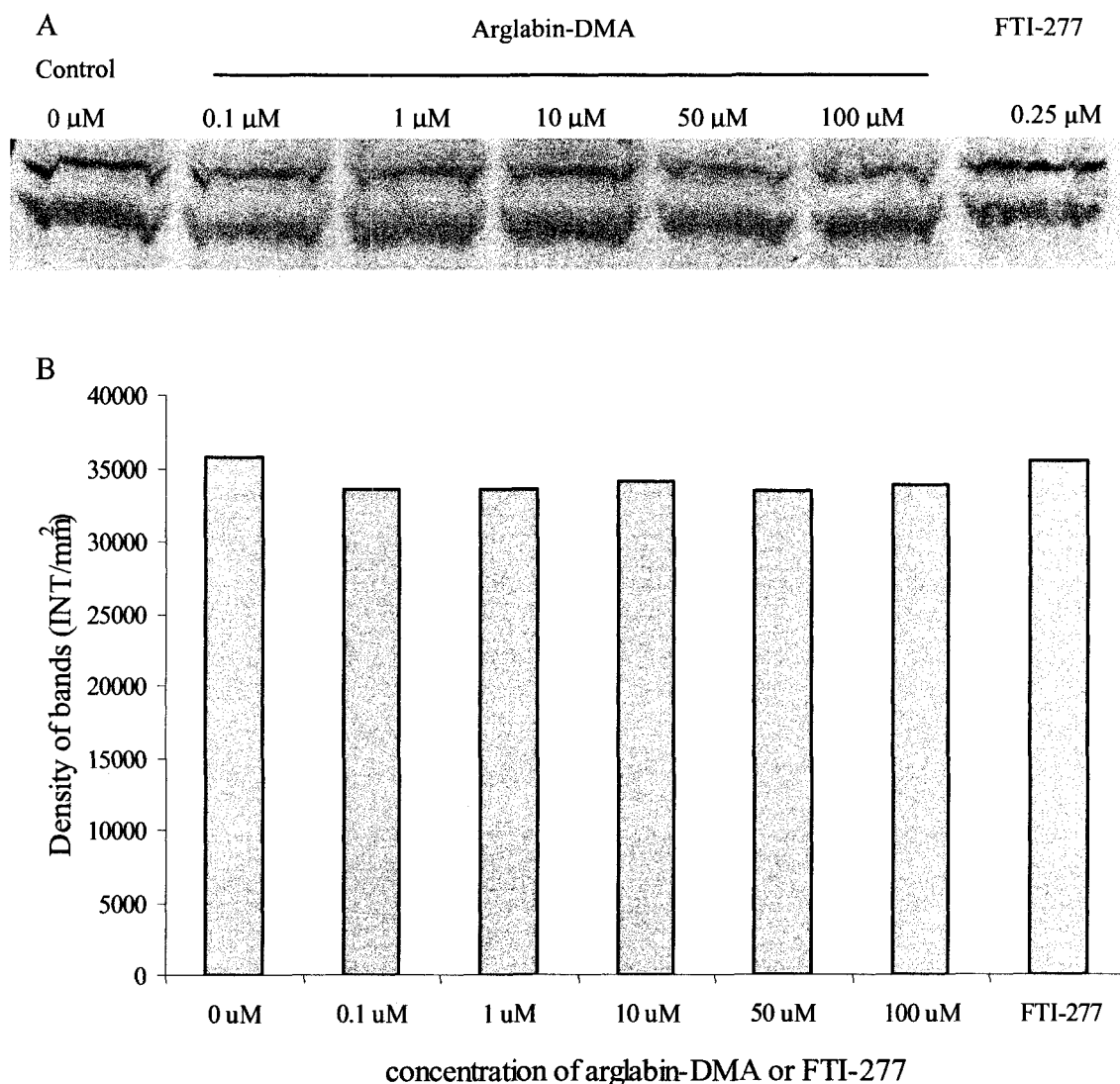


FIG. 27. Western blot of FTase after 72-hour incubation with arglabin-DMA and FTI-277. Ras/3T3 cells were incubated with complete cell culture media containing 0, 0.1, 1, 10, 50, or 100 μ M of arglabin-DMA, or 0.25 μ M of FTI-277 for 72 hours. FTase in cellular protein was detected and shown in figure 27A. The total densities of bands for each concentration group were shown in figure 27B. No significant difference was found between groups.

FTase Assay using FTase Produced in Ras/3T3 Cells

Equal numbers of Ras/3T3 cells were incubated with various concentrations of arglabin-DMA or FTI-277 for 2 hours, 1 day or 2 days. Cell lysates were generated, and the concentrations of cellular protein were determined by BCA protein assays. Equal amounts of cellular protein were used in the FTase assays. Tritiated farnesylpyrophosphate and Ras protein were used as the substrates. Tritiated farnesylated Ras protein was generated in proportion to the FTase activity of the cell lysate. Reactions using cell lysates generated from cells without arglabin-DMA treatment were used as the negative control. Reactions using cell lysates incubated with FTI-277 were the positive controls.

When low concentrations of arglabin-DMA (10, 50, 100, and 1,000 nM) were used on Ras/3T3 cells for a short period (2 hours), a significant reduction in the specific activity of FTase was found at the 10 nM concentration of arglabin ($p < 0.05$) (Fig. 28). The reduction plateaued when the concentration of arglabin-DMA reached 100 nM. The specific activity difference between 100 nM and 1,000 nM arglabin-DMA groups was not significant ($p > 0.05$). Percentage of FTase inhibition was calculated by comparing the specific activity with the no arglabin-DMA control. The highest inhibition of FTase activity was 59% when 100 nM arglabin-DMA was used on Ras/3T3 cells for 2 hours (Fig. 29). These results were derived from 3 separate experiments. The percentage of inhibition of FTase activity by 1,000 nM of FTI-277 was 90%. These results suggested that low concentrations (10-1,000 nM) of arglabin-DMA inhibited FTase activity after 2 hours of incubation with Ras/3T3 cells. However, this inhibition was limited by the substrate availability in cells that may transform arglabin-DMA to a farnesyltransferase

inhibitor, such as phosphorylated arglabin-DMA.

When higher concentrations of arglabin-DMA (25, 50, 75, and 100 μM) were used on Ras/3T3 cells for longer times (1 day or 2 days), percentage inhibitions plateaued at 75 μM for both incubation times (Fig. 30 and Fig. 31). After incubation with arglabin-DMA for these longer times, the enzyme activity of the newly synthesized FTase was inhibited by much higher concentrations of arglabin-DMA (50 μM to 100 μM). This may imply that arglabin-DMA was transformed to an FTase inhibitor inside of cells and this transformation was not reversible. Another possibility was that some arglabin-DMA or its derivatives were degenerated inside of cells after longer period of incubation. Therefore, after large amount of newly synthesized FTase appeared in cells, more arglabin-DMA was needed to inhibit FTase activity.

THE EFFECT OF ARGLABIN-DMA ON RAS PROTEIN IN TRANSFORMED CELLS

The Effect of Argabin-DMA on H-Ras Protein in Transformed Cells

Equal numbers of Ras/3T3 cells were incubated with various concentrations of arglabin-DMA (0.1, 1, 10, 50, and 100 μM) or 0.25 μM of FTI-277 (control) for 24 hours or 72 hours. Cell lysates were generated, and the concentrations of cellular protein were determined by BCA protein assays. Equal amounts of cellular protein were separated in SDS-polyacrylamide gel, transferred to PVDF membrane, and the amounts of H-Ras protein determined by western blot using rat anti-v-H-Ras monoclonal antibody. The recombinant H-Ras protein (Sigma, R-9894) was used as a positive control for the

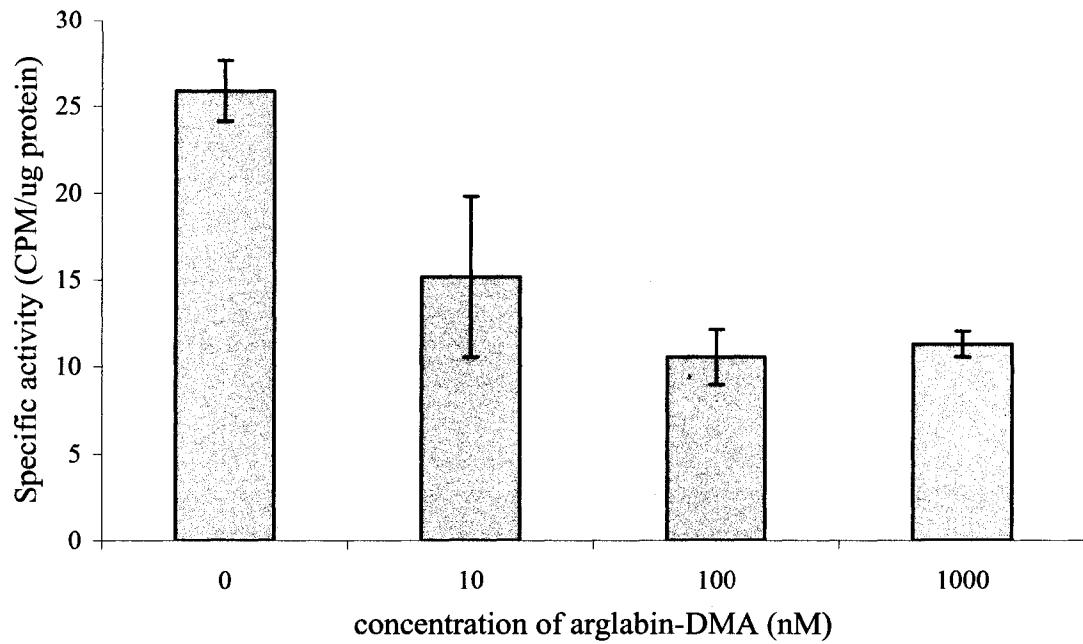


FIG. 28. Specific activity of FTase after 2-hour incubation with arglabin-DMA. A significant reduction in specific activity of FTase was found at 10 nM concentration of arglabin ($p < 0.05$). The reduction plateaued when the concentration of arglabin reached 100 nM. The specific activity difference between 100 nM and 1,000 nM arglabin-DMA groups was not significant ($p > 0.05$).

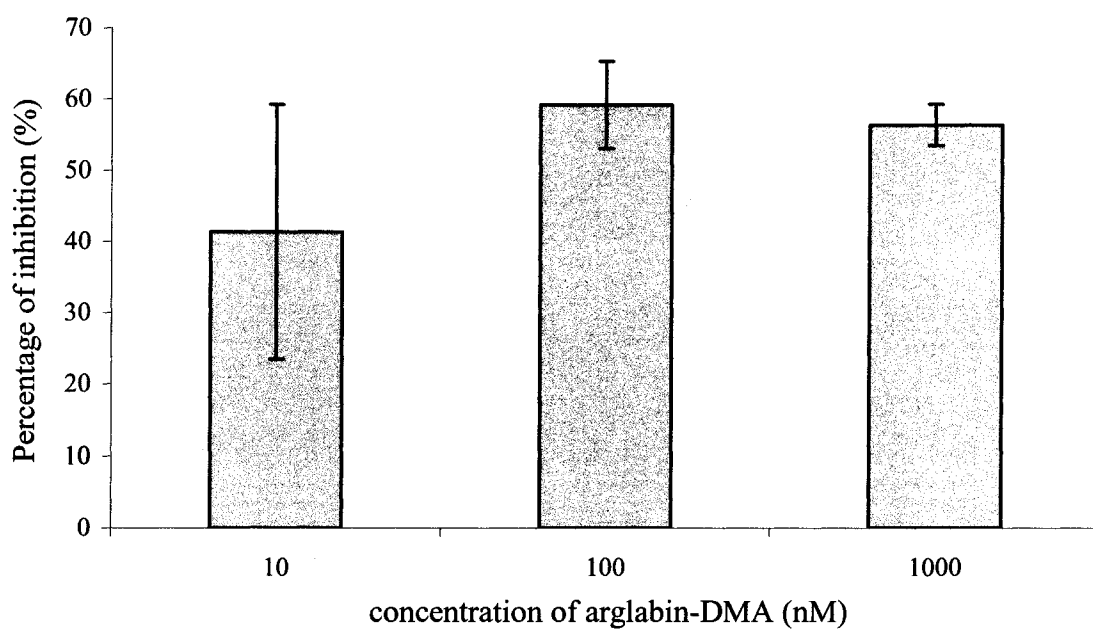


FIG. 29. Percentage of FTase inhibition after 2-hour incubation with arglabin-DMA. Percentage of FTase inhibition was calculated by comparing the specific activity with the no arglabin-DMA control. The highest inhibition of FTase activity was 59% when 100 nM arglabin-DMA was used to incubate Ras/3T3 cells for 2 hours.

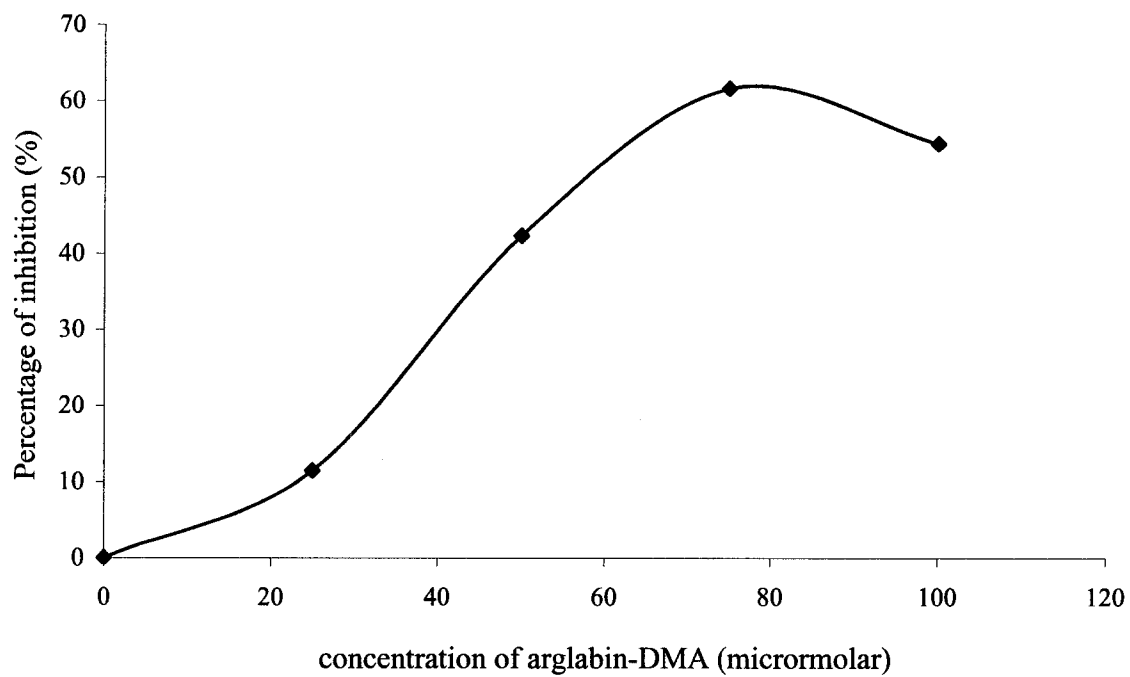


FIG. 30. Percentage of FTase inhibition after 1-day incubation with arglabin-DMA. Percentage of inhibitions plateaued after 1-day incubation with 75 μM of arglabin-DMA.

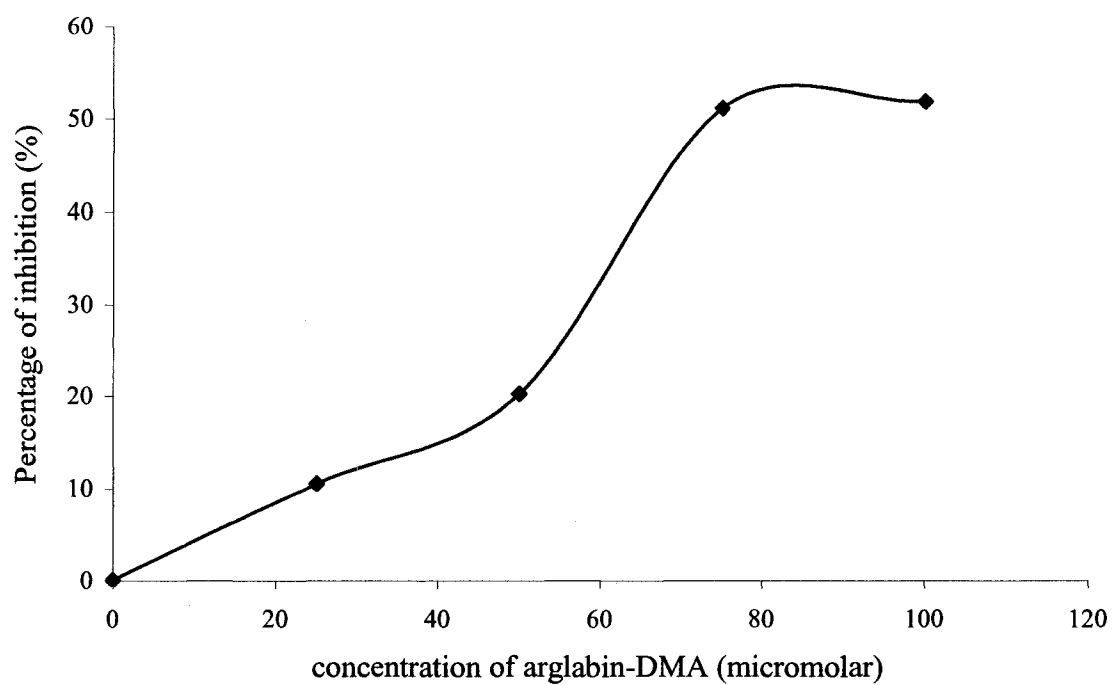


FIG. 31. Percentage of FTase inhibition after 2-day incubation with arglabin-DMA. Percentage of inhibitions plateaued after 2-day incubation with 75 μ M of arglabin-DMA.

western blot. The densities of each band were quantitated using Quantity One densitometry software from Bio-Rad.

The prenylated (processed) and non-prenylated (non-processed) Ras proteins were separated by electrophoresis and detected by Western blot (53, 58). The faster-migrating immunoreactive bands represented mature, fully processed protein, whereas the slower-migrating form was unprocessed protein (62) (Fig. 32, 33).). The relative molecular weight of the processed protein estimated from the Precision protein standard (BioRad, 161-0373) was 21 ± 1 kD. The Western blots for cells incubated with arglabin-DMA (0, 0.1, 1, 10, 50, 100 μ M) or FTI-277 (0.25 μ M) for 24 hours or 72 hours are shown in Figures 32A and 33A, respectively. A trend of increasing densities of the slower-migrating bands was found as the concentration of arglabin-DMA increased from 0 μ M to 100 μ M, and the density of the slower-migrating band for the FTI-277 group reached the highest level (Fig. 32A and Fig. 33A). The ratio of densities of faster-migrating bands (processed H-Ras protein) to densities of slower-migrating bands (unprocessed H-Ras protein) was calculated and shown in Figures 32B and 33B. The percentage reduction of the ratio was calculated by comparing the ratio of densities to the no arglabin-DMA treatment control. After cells were incubated with 100 μ M of arglabin-DMA for 24 hours or 72 hours, percentages of reduction of ratio of processed to unprocessed H-Ras protein were 18.6% and 9.5%, respectively (Fig. 32B and Fig. 33B). When cells were incubated with FTI-277 for 24 hours or 72 hours, the percentages of ratio reduction were 46% and 26.5%, respectively. These results were derived from 4 separate experiments.

Equal amounts of cellular protein from various treatment groups were utilized in small GTPase-pull down assays. The complexes of GST-Raf1-RBD and active Ras

protein were selectively eluted from glutathione discs, separated in SDS-polyacrylamide gel, transferred to PVDF membrane, and the amounts of H-Ras protein were determined by western blot using rat anti-v-H-Ras monoclonal antibody. There were multiple bands detected in the western blots (Fig. 34A-B). When cell lysates incubated with arglabin-DMA or FTI-277 for 24 hours were used for the pull-down assay, the bands with the highest density were found at relative molecular weight of 40 ± 2 kD compared to the protein standard (Fig. 34A). No band with molecular weight of 21 ± 1 kD was detected. This may be due to the Ras protein dimer formation during the pull-down process. The densities of bands were reduced significantly on lanes of 50 μ M and 100 μ M arglabin-DMA (Fig. 34A). When cell lysates incubated with arglabin-DMA or FTI-277 for 72 hours were used for the pull-down assay, bands with relative molecular weight of 39 ± 1 kD were detected in all tested samples (Fig. 34B). Significant density reductions were found in lanes of 1 μ M, 10 μ M, 50 μ M, and 100 μ M arglabin-DMA and FTI-277. These data suggested that arglabin-DMA or FTI-277 inhibited active H-Ras formation in Ras/3T3 cells.

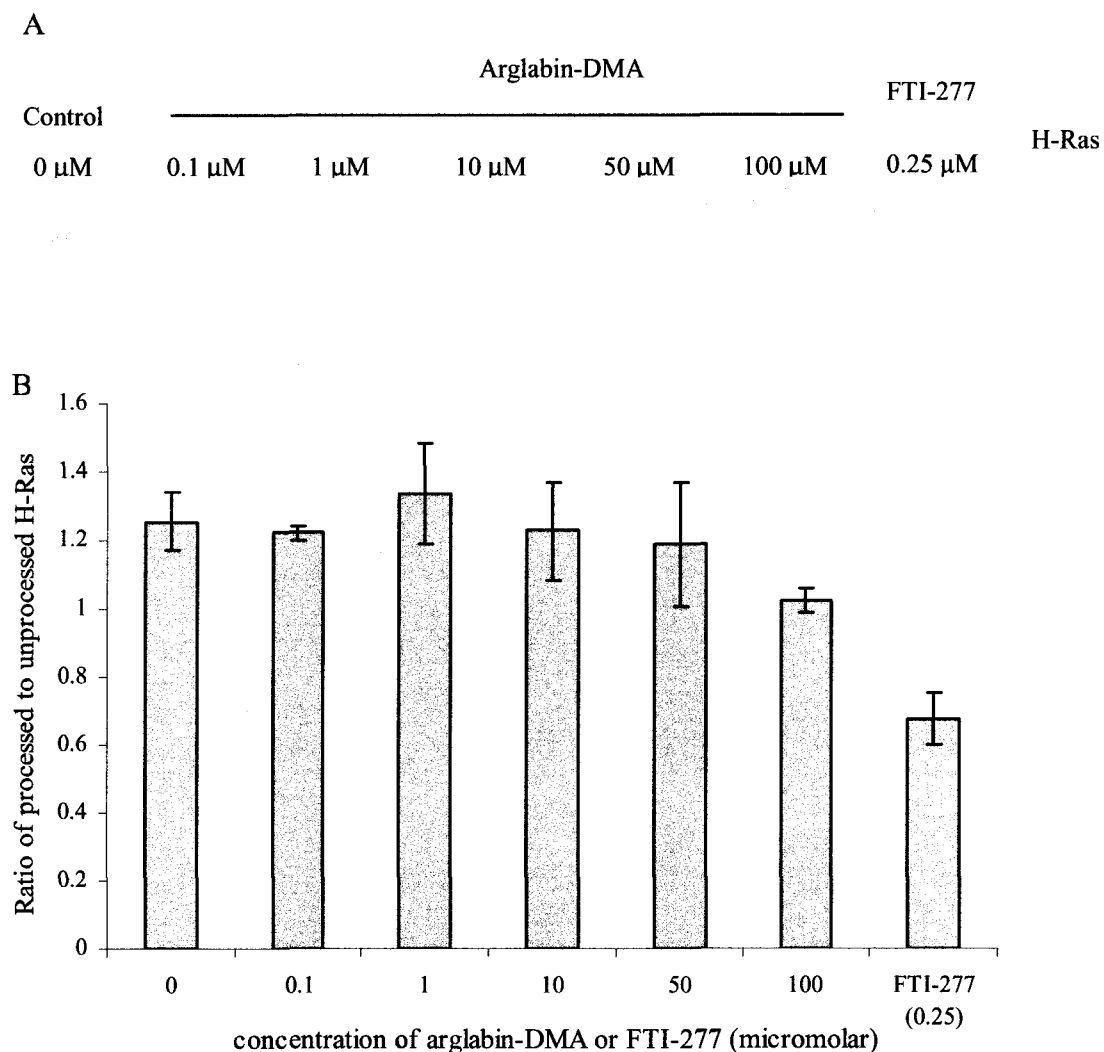


FIG. 32. Western Blot of H-Ras after 24-hour incubation with Arglabin-DMA or FTI-277. A trend of increasing densities of slower-migrating bands was found as the concentrations of arglabin-DMA increased from 0 μ M to 100 μ M, and the density of the slower-migrating band for FTI-277 group reached its highest level (Fig. 32A). The ratios of densities of faster-migrating bands (processed H-Ras protein) to densities of slower-migrating bands (unprocessed H-Ras protein) were calculated and shown in figure 32B.

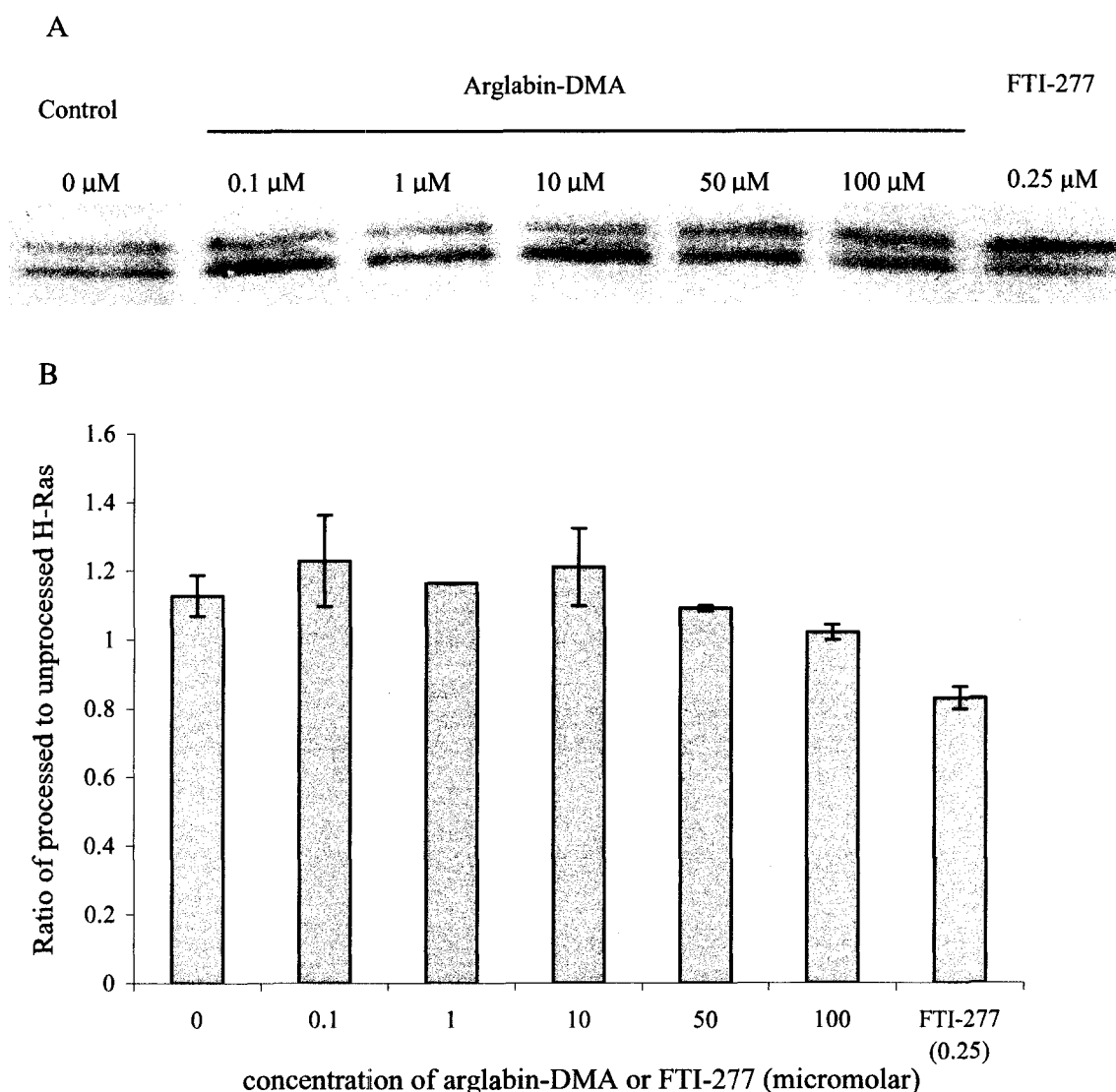


FIG. 33. Western Blot of H-Ras after 72-hour incubation with Arglablin-DMA or FTI-277. A trend of increasing on densities of slower-migrating bands was found as the concentrations of arglablin-DMA increased from 0 μ M to 100 μ M, and the density of the slower-migrating band for FTI-277 group reached the highest (Fig. 33A). The ratios of densities of faster-migrating bands (processed H-Ras protein) to densities of slower-migrating bands (unprocessed H-Ras protein) were calculated and shown in figure 33B.

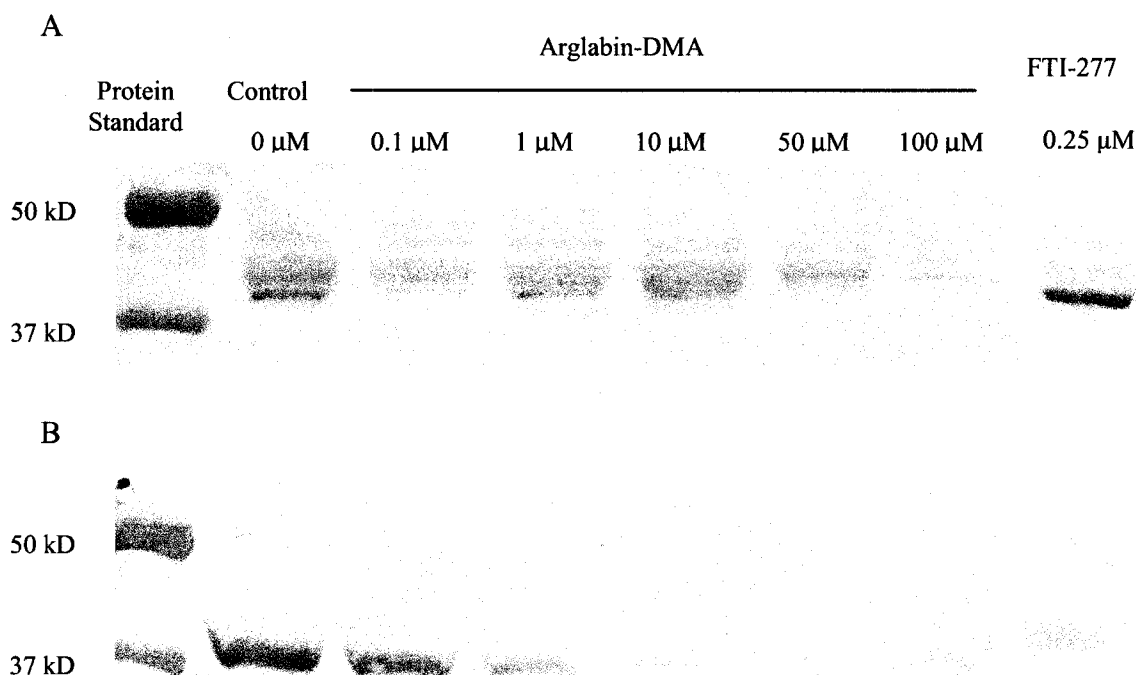


FIG. 34. Western blot of H-Ras protein after small GTPase pull-down assays. When cell lysates incubated with arglabin-DMA or FTI-277 for 24 hours were used for the pull-down assay, the bands with the highest density were found at relative molecular weight of 40 ± 2 kD compared to the protein standard (Fig. 34A). The densities of bands reduced significantly after 50 μ M and 100 μ M arglabin-DMA incubation. When cell lysates incubated with arglabin-DMA or FTI-277 for 72 hours were used for the pull-down assay, bands with relative molecular weight of 39 ± 1 kD were detected in all tested samples (Fig. 34B). Significant density reductions were found in lanes of 1 μ M, 10 μ M, 50 μ M, and 100 μ M arglabin-DMA and FTI-277.

The Effect of Arglabin-DMA on K-Ras Protein in Transformed Cells

Equal numbers of Ras/3T3 cells were incubated with various concentrations of arglabin-DMA (0.1, 1, 10, 50, and 100 μ M) or 0.25 μ M of FTI-277 (positive control) for 24 hours. Cell lysates were generated, and the concentrations of cellular protein were determined by BCA protein assays. Equal amounts of cellular protein were separated in SDS-polyacrylamide gel, transferred to PVDF membrane, and the amounts of K-Ras protein were determined by Western blot using mouse anti-K-Ras monoclonal antibody. Cell lysates from rat K-Ras transformed kidney (KNRK) cells (Santa Cruz, Inc. SC-2214), was used as a positive control for Western blot. The densities of each band in tested samples were quantitated using Quantity One densitometry software from Bio-Rad.

The KNRK cell lysate control showed two bands, one faster-migrating band (processed K-Ras protein) and one slower-migrating band (unprocessed K-Ras protein) (Fig. 35A). The relative molecular weight of the processed protein estimated from the Precision protein standard (BioRad, 161-0373) was 21 ± 1 kD. Only one band in each sample was detected in Western blot for Ras/3T3 cell lysates that was incubated with arglabin-DMA, FTI-277, or no treatment control (Fig. 35A). All tested samples have only the faster-migrating bands (processed K-Ras protein) when compared to the KNRK cell lysate control. The densities of each test samples are shown in figure 35B. No significant difference was found between band densities of all test samples. The data was collected from two separate experiments. These results suggested that FTase inhibitors have no effect on K-Ras prenylation, since all K-Ras were post-translational modified by geranylgeranylation of GGTaseI.

A

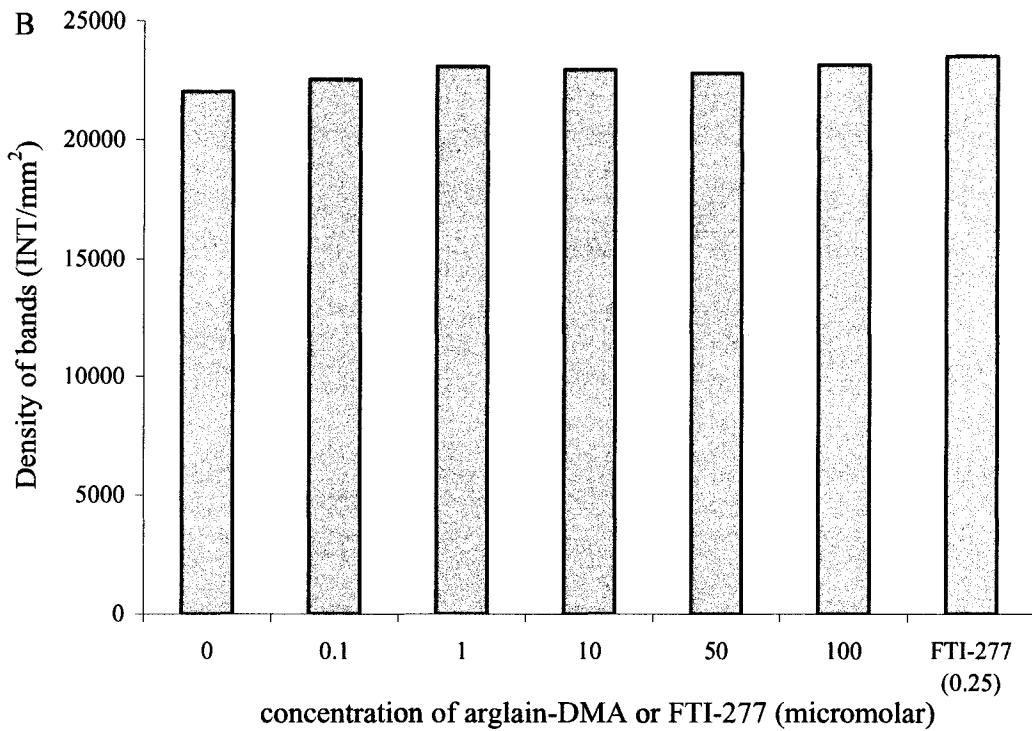
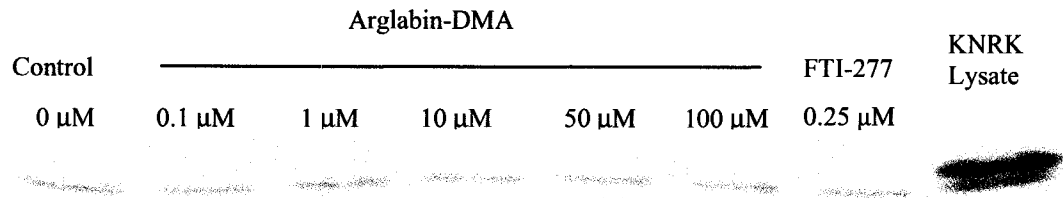


FIG. 35. Western blot of K-Ras after 24-hour incubation with arglabin-DMA or FTI-277. All tested samples only have the faster-migrating bands (processed K-Ras protein) when compared to the KNRK cell lysate control (Fig. 35A). No significant differences were found between band densities of all test samples (Fig. 35B).

THE EFFECT OF ARGLABIN-DMA ON RHO PROTEIN IN TRANSFORMED CELLS

The Effect of Arglabin-DMA on RhoA Protein in Transformed Cells

Equal numbers of Ras/3T3 cells were incubated with various concentrations of arglabin-DMA (0.1, 1, 10, 50, and 100 μ M) or 0.25 μ M of FTI-277 (positive control) for 24 hours and 72 hours. Cell lysates were generated, and the concentrations of cellular proteins were determined by BCA protein assays. Equal amounts of cellular protein were separated in SDS-polyacrylamide gel, transferred to PVDF membrane, and the amount of RhoA protein were determined by western blot using mouse anti-RhoA monoclonal antibody. The Hela cell lysate (Santa Cruz, Inc. SC-2200) from human epithelioid carcinoma cells was used as a positive control for western blot. The densities of each band of all tested samples were quantitated using Quantity One densitometry software from Bio-Rad.

Two bands were detected from Hela cell lysate control: the faster migrating band (processed RhoA protein) and the slower migrating band (unprocessed RhoA protein) (Fig. 36A-B and Fig. 37A). The relative molecular weight of the processed protein estimated from the Precision protein standard (BioRad, 161-0373) was 21 ± 1 kD. After 24 hours of incubation with various concentrations of arglabin-DMA or FTI-277, one band from each sample was detected in Western blots (FIG. 36A-B). The bands from 10 μ M, 50 μ M, 100 μ M arglabin-DMA, and FTI-277 were the slower migrating bands when compared to the Hela cell lysate control. The densities of bands from lanes of control (0 μ M) and 0.1 μ M arglabin-DMA were higher than the rest of the bands and moved faster than the rest of the samples. These faster migrating bands may be caused by an uneven

distribution of electrical voltage of the gel, or caused by processed RhoA protein (faster-migrating RhoA protein) in control and 0.1 μ M arglabin-DMA treated sample. The densitometry data is shown in figure 36C. The bands from control samples showed the highest densities. The error bars showed the range from two separate experiments.

After 72 hours incubation with various concentrations of arglabin-DMA or FTI-277, still only one band was detected in all tested samples (Fig. 37A-B). The migration pattern of bands was similar to the 24-hour incubation samples. The bands from 10 μ M, 50 μ M, 100 μ M arglabin-DMA and FTI-277 controls were slower-migrating bands when compared to the Hela cell lysate control (Fig. 37A-B). The bands from control (0 μ M) and 0.1 μ M arglabin-DMA were faster-migrating compared to the Hela cell lysate control. The densities of bands from two separate experiments were summarized in figure 37C. After 72 hours of incubation, there was no significant density difference between bands of all samples.

Equal amounts of cellular protein from various treatment groups were utilized in small GTPase-pull down assays. The complexes of GST-Rhotekin-RBD and active RhoA protein were selectively eluted from glutathione discs, separated in SDS-polyacrylamide gel, transferred to a PVDF membrane, and the amounts of RhoA protein determined by western blot using mouse anti-RhoA monoclonal antibody. When cell lysates incubated with arglabin-DMA or FTI-277 for 72 hours were used for the pull-down assay, two bands with the highest densities were found at relative molecular weight of 40 ± 2 kD and 36 ± 1 kD, respectively (Fig. 38). The 36 ± 1 kD bands were detected in all tested samples, while the 40 ± 2 kD bands were detected in lanes for the control and 0.1 μ M, 1 μ M, 10 μ M and 50 μ M arglabin-DMA. The fusion protein of GST-Rhotekin has the

molecular weight of 36 kD, according to the manufacturer's guide. The protein with molecular weight of 40 ± 2 kD could be the dimer of active RhoA protein. This protein was not found in 100 μ M arglabin-DMA and 0.25 μ M of FTI-277. These results indicated that arglabin-DMA and FTI-277 may have inhibited active RhoA formation in Ras/3T3 cells.

The Effect of Arglabin-DMA on RhoB Protein in Transformed Cells

Equal numbers of Ras/3T3 cells were incubated with various concentrations of arglabin-DMA (0.1, 1, 10, 50, and 100 μ M) or 0.25 μ M of FTI-277 (control) for 24 hours. Cell lysates were generated and the concentrations of cellular protein were determined by BCA protein assays. Equal amounts of cellular protein were used for immunoprecipitation with Rabbit anti-RhoB IgG. The eluted material from protein G-agarose beads containing antigen-antibody complex were separated in SDS-polyacrylamide gel, transferred to PVDF membrane, and the amounts of RhoB protein were determined by Western blot using mouse anti-RhoB monoclonal antibody. The densities of each band of all tested samples were quantitated using Quantity One densitometry software from Bio-Rad.

After 24-hour incubation with various concentrations of arglabin-DMA or FTI-277, two bands from each sample were detected in western blot (Fig. 39A). The band with significantly higher density was the faster-migrating band (processed RhoB) and the band with lower density was the slower-migrating band (unprocessed RhoB) (Fig. 39A). The relative molecular weight of the processed protein estimated from the Precision protein standard was 21 ± 1 kD. The densities of the fast migrating bands quantitated by densitometry showed no significant difference between all samples (Fig. 39B).

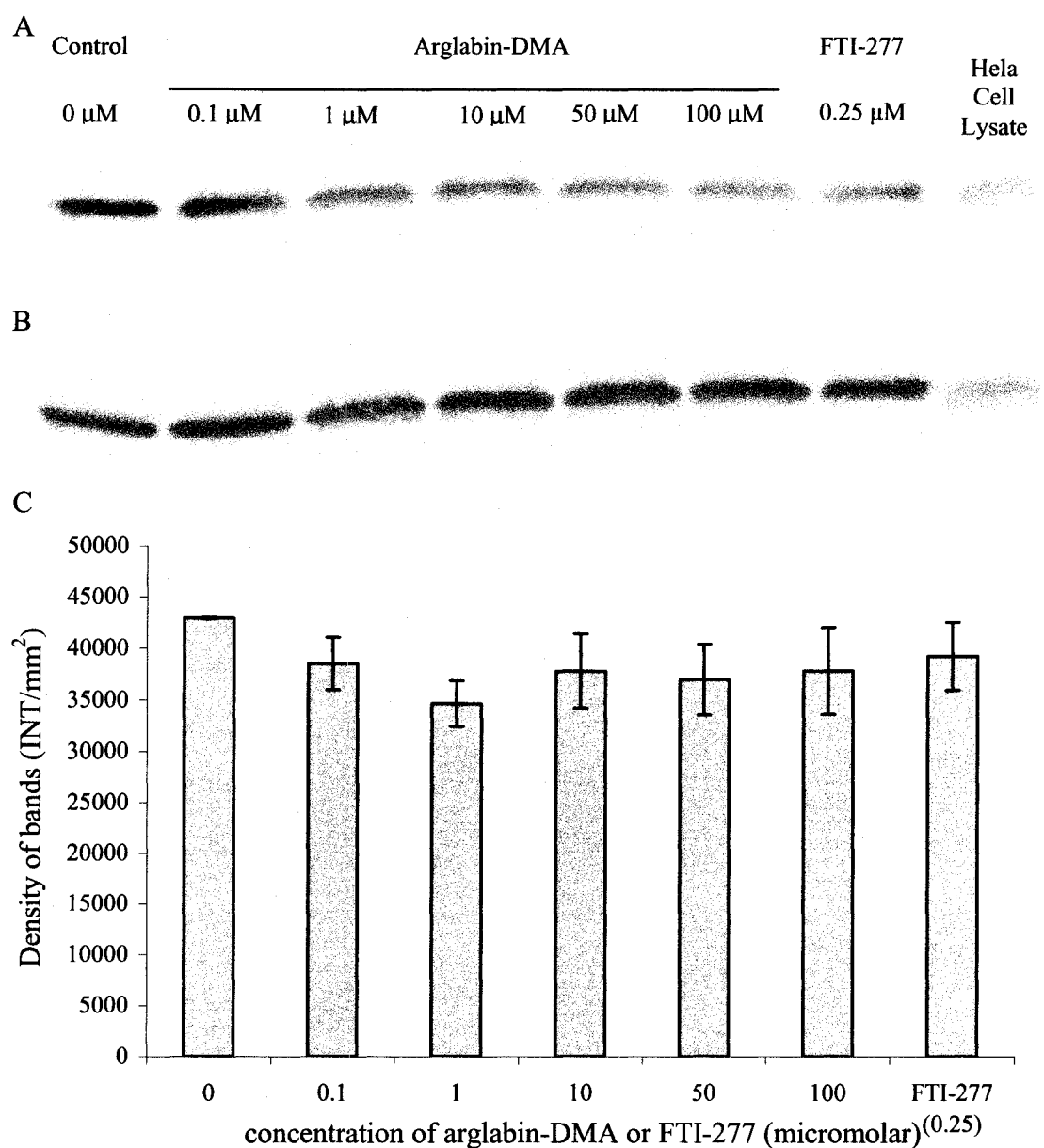


FIG. 36. Western blot of RhoA after 24-hour incubation with arglablin-DMA or FTI-277. The bands from 10 μ M, 50 μ M, 100 μ M arglablin-DMA, and FTI-277 were the slower migrating bands when compared to the HeLa cell lysate control (Fig. 36A-B). The densities of bands from control (0 μ M) and 0.1 μ M arglablin-DMA were higher than the rest of bands and moving faster than the rest of samples. The bands from control samples showed the highest densities (Fig. 36C).

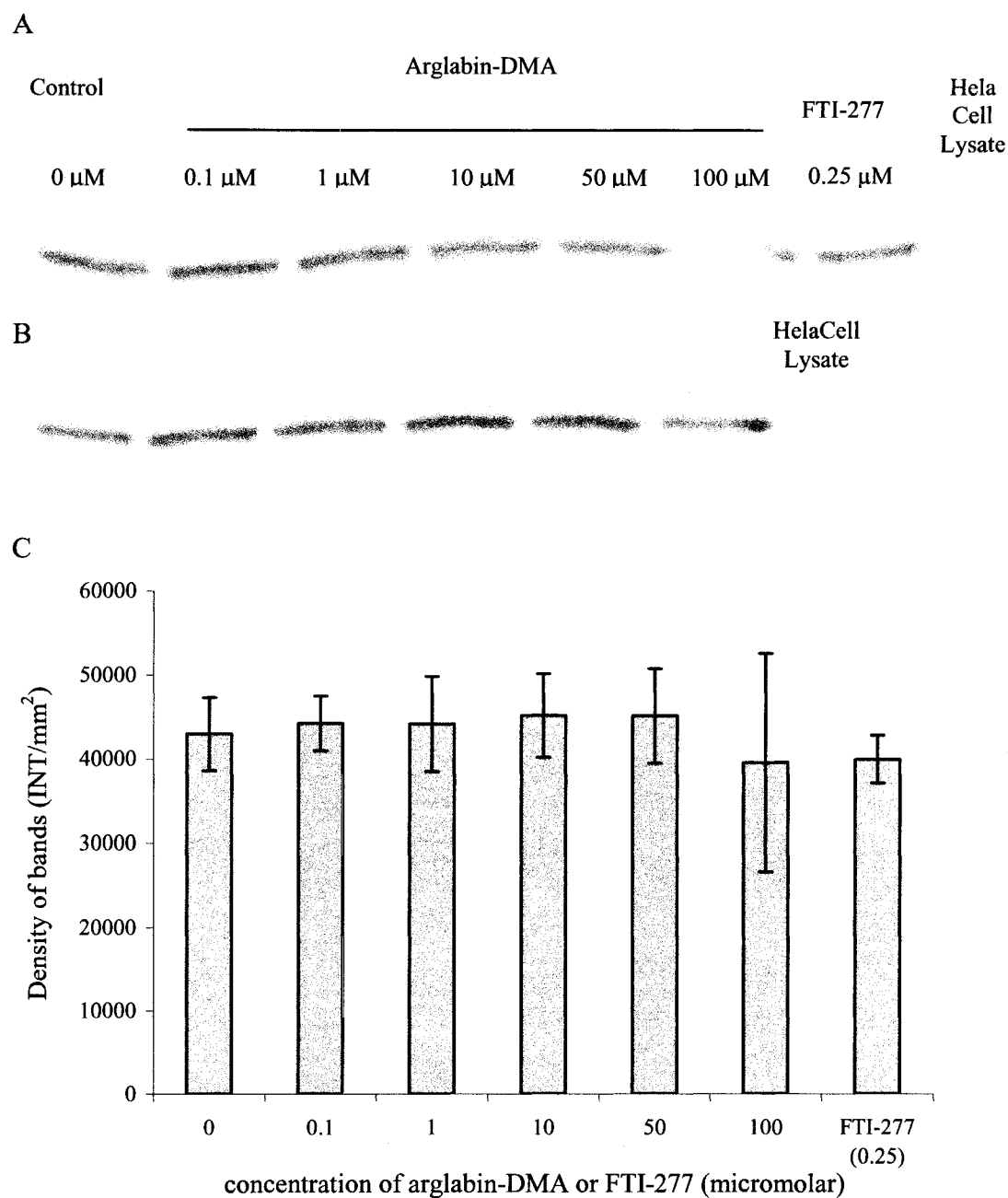


FIG. 37. Western blot of RhoA after 72-hour incubation with Arglabin-DMA or FTI-277. The bands from 10 μ M, 50 μ M, 100 μ M arglabin-DMA and FTI-277 controls were slower-migrating bands when compared to the Hela cell lysate control (Fig. 37A-B). After 72 hours of incubation, there was no significant density difference between bands of all samples (Fig. 37C).

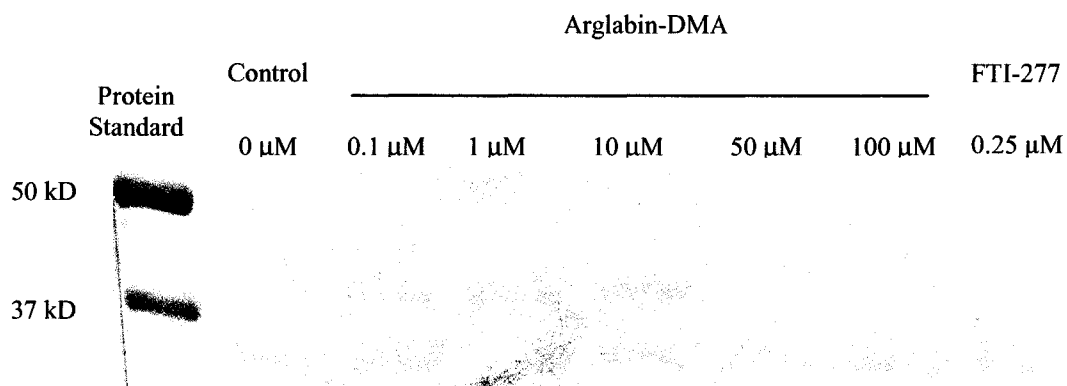


FIG. 38. Western blot of RhoA protein after GTPase pull-down assay. When cell lysates incubated with arglabin-DMA or FTI-277 for 72 hours were used for the pull-down assay, two bands with the highest densities were found at relative molecular weights of 40 ± 2 kD and 36 ± 1 kD, respectively. The 36 ± 1 kD bands were detected in all tested samples, while the 40 ± 2 kD bands were detected in lanes for control and 0.1 μ M, 1 μ M, 10 μ M and 50 μ M arglabin-DMA.

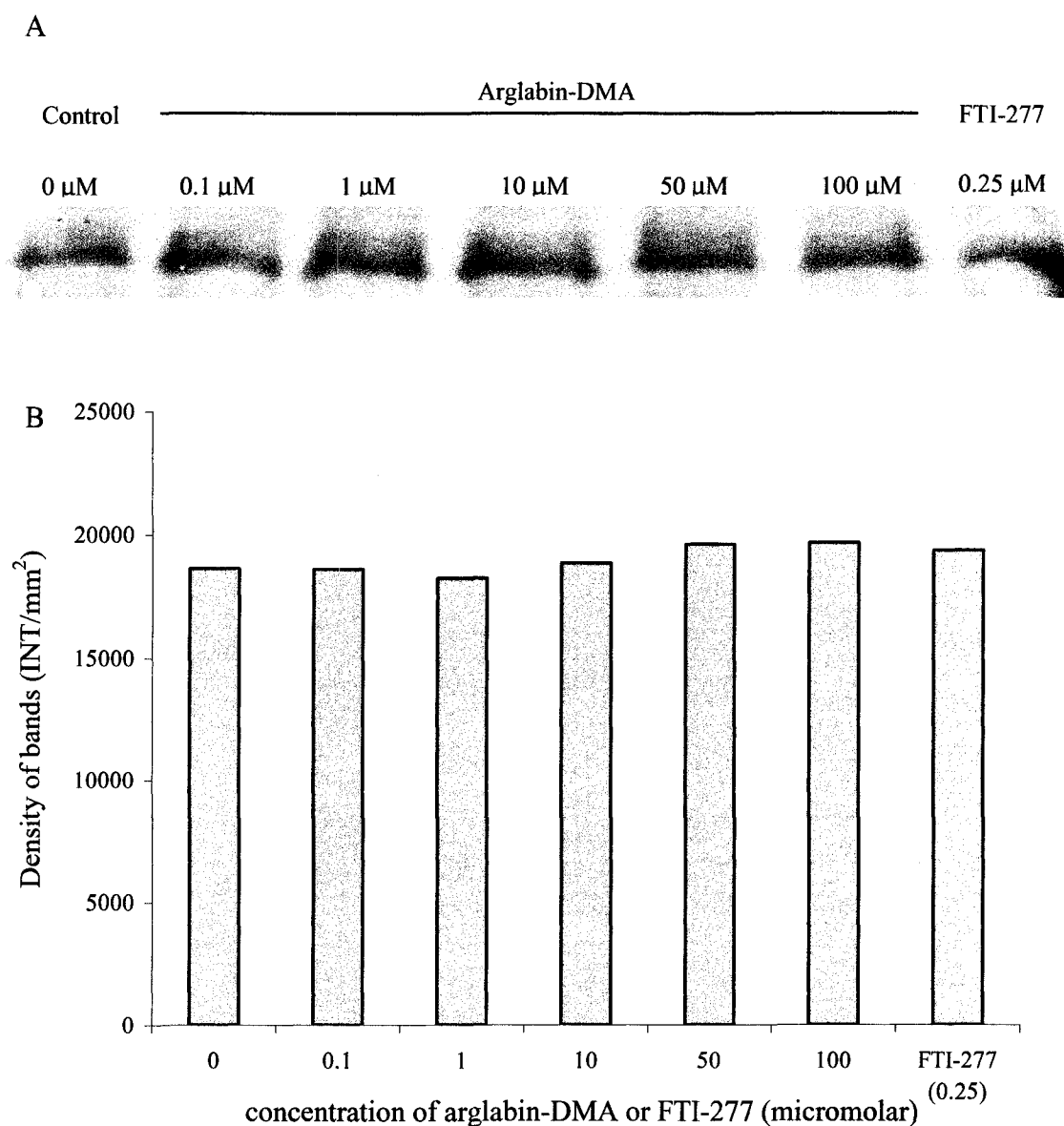


FIG. 39. Western blot of RhoB after 24-hour incubation with arglabin-DMA or FTI-277. The bands with significantly higher density were the faster-migrating bands (processed RhoB protein) and the bands with lower density were the slower-migrating bands (unprocessed RhoB protein) (Fig. 39A). The densities of bands quantitated by densitometry showed no significant difference between all samples (Fig. 39B).

THE EFFECTS OF ARGLABIN-DMA ON P21/WAF1/CIP1 PROTEIN IN TRANSFORMED CELLS

Equal numbers of Ras/3T3 cells were incubated with various concentrations of arglabin-DMA (0.1, 1, 10, 50, and 100 μ M) or 0.25 μ M of FTI-277 (control) for 24 hours and 72 hours. Cell lysates were generated, and the concentrations of cellular protein were determined by BCA protein assays. Equal amounts of cellular protein were used for immunoprecipitation using rabbit anti-p21 IgG. The protein G-agarose beads containing antigen-antibody complex were separated in SDS-polyacrylamide gel, transferred to PVDF membrane, and the amount of p21/WAF1/CIP1 protein were determined by Western blot using mouse anti-p21/WAF1 monoclonal antibody. Direct Western blots without immunoprecipitation were also performed using equal amounts of cellular protein. The full-length p21/WAF1/CIP1 (SC-4078) from mouse origin produced in *E. coli* was used as a positive control for Western blot. The densities of each band of all tested samples were quantitated using Quantity One densitometry software from Bio-Rad.

After 24 hours incubation with various concentrations of arglabin-DMA or FTI-277, one major band around 20 kD was detected in all samples (Fig. 40A-C). No significant density difference was found between samples incubated with various concentrations of arglabin-DMA ($p > 0.05$) (Fig. 40D). These data were derived from three separate experiments. Decreased overall density in the FTI-277 control was found in two of three experiments.

After 72 hours of incubation, a trend of increasing density was found from the no treatment control group to the 100 μ M of arglabin-DMA treatment group (Fig. 41A-C).

Density increased compared to the no treatment control ($23 \pm 5\%$ and $36 \pm 9\%$ for 50 μM and 100 μM of arglabin-DMA treatment groups, respectively) (Fig. 41D). These were the results from three separate experiments. Decreased densities in the FTI-277 control were found in all three experiments. This data suggested that arglabin-DMA and FTI-277 affected Ras/3T3 cell cycle by different mechanisms.

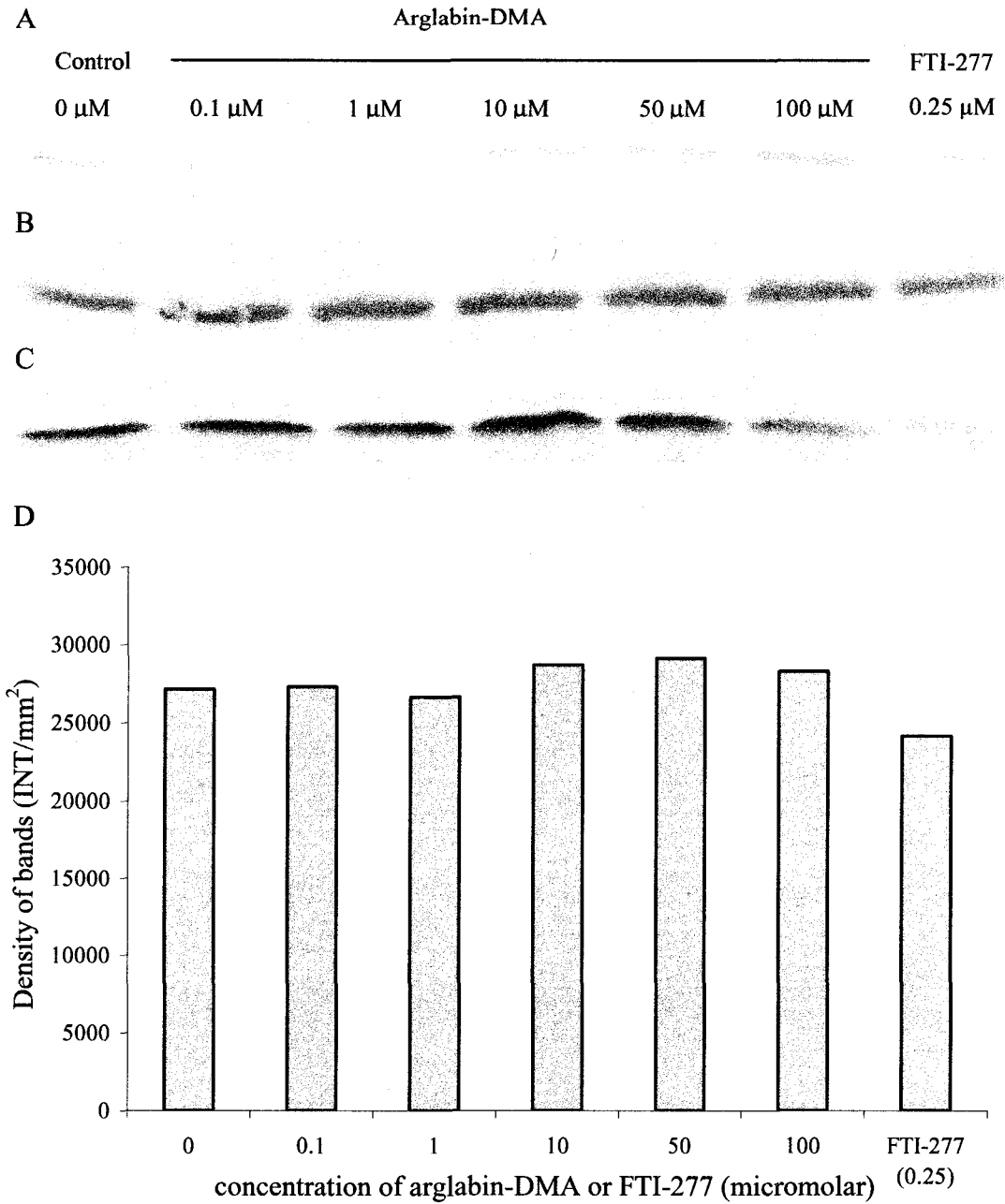


FIG. 40: Western blot of p21/WAF1/CIP1 after 24-hour incubation with arglabin-DMA or FTI-277. No significant density difference was found between samples incubated with various concentration of arglabin-DMA ($p > 0.05$) (Fig. 40A-D). These data were derived from three separate experiments. Decreased density in lane of FTI-277 control was found in two of the three experiments.

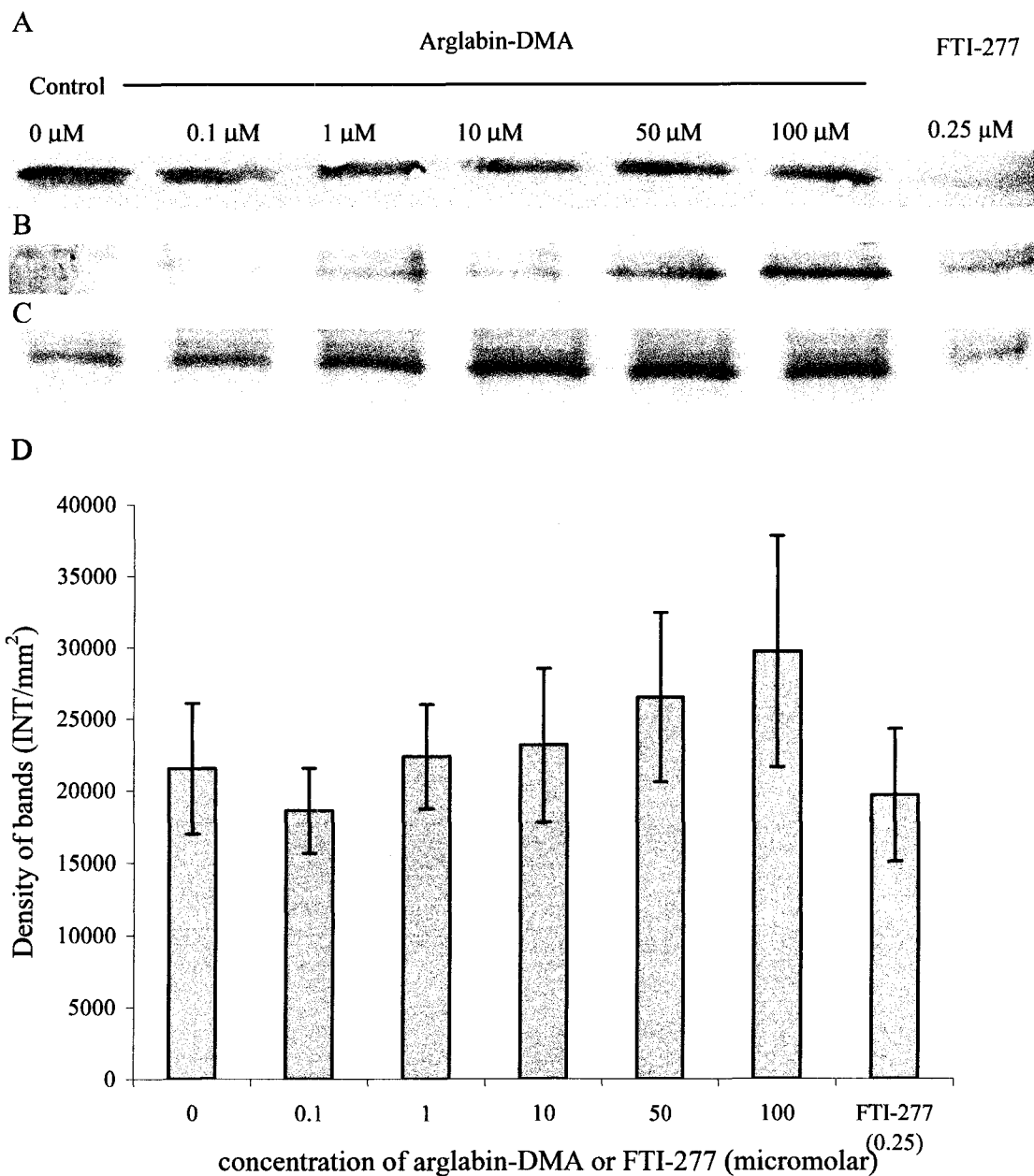


FIG. 41. Western blot of p21/WAF1/CIP1 after 72-hour incubation with arglabin-DMA or FTI-277. A trend of increasing density was found from no treatment control group to 100 μ M of arglabin-DMA treatment group (Fig. 41A-D). Decreased densities in lanes of FTI-277 control were found in all three experiments.

DISCUSSION

The most frequently detected alterations in oncogenes in human cancers are mutations in the *ras* family of oncogenes (49). The first and most critical post-translational modification of the Ras protein is farnesylation catalyzed by farnesyltransferase (20). Consequently, inhibitors of farnesyltransferase have been proposed as potential agents for treating cancers. Three major groups of farnesyltransferase inhibitors have been developed (20): CAAX pepidomimetics (such as FTI-277), heterocyclic FTIs (such as SCH66336), and FPP competitive compounds (such as FPT inhibitor II). Arglabin-dimethylaminohydrochloride (arglabin-DMA) is used in current anti-tumor treatments in the Republic of Kazakhstan (1, 2, 51). Shaikenov's studies showed that arglabin-DMA inhibited the incorporation of farnesylpyrophosphate into H-Ras protein by FTase with an IC₅₀ of 25 μ M (51, 52). Their studies have shown promise in suppressing the growth of various tumor cells by arglabin-DMA (51, 52). However, the mechanism of arglabin-DMA cytotoxicity and cytostatic effects on tumor cells at the molecular and cellular level is still unclear. The current study was undertaken to determine the farnesyltransferase inhibitory activity of arglabin-DMA and to investigate the effects of arglabin-DMA on Ras protein, Rho protein and cyclin kinase inhibitor p21/WAF1/CIP1.

Based on Shaikenov's studies, arglabin-DMA inhibits the anchorage-dependent proliferation and anchorage-independent growth of neuroblastoma cells at the similar concentrations (IC₅₀ = 10 μ g/mL or 30.5 μ M), and inhibits H-Ras transformed cells (Ras/3T3 cells) at concentration of 2 μ g/mL (6.1 μ M) (IC₅₀) in the soft-agar colony

formation assay (52). The present study used a MTT based *in vitro* toxicology assay kit to measure metabolic activity of Ras/3T3 cells that were incubated with various concentrations of arglabin-DMA. The data revealed that the 50% inhibition concentration of arglabin-DMA for Ras/3T3 cells was 10.34 μ M, which is close to the IC₅₀ in the soft-agar colony formation assay.

Studies of the effect of arglabin-DMA on farnesyltransferase showed different results when using expressed FTase and Ras/3T3 cell lysates. When the FTase assay was performed using expressed and purified FTase, the IC₅₀ for Arglablin-DMA was 2.9 mM, which was 24,000 times higher than FPT inhibitor II (119 nM). Lineweaver-Burk double reciprocal plots indicated competitive inhibition of FTase by FPT inhibitor II, and uncompetitive inhibition of FTase by FTase Inhibitor II and arglabin-DMA. When the FTase assay was performed using Ras/3T3 cell lysates as a source of FTase, the highest percentage of arglabin-DMA inhibition was 50-60% compared to the no arglabin-DMA treatment control, and this inhibition plateaued when the arglabin-DMA concentration reached 100 nM or higher. These results suggest that arglabin-DMA was transformed in cells and this transformation was limited by the substrate availability in cells. Data generated in Shaikenov's laboratory suggested that arglabin-DMA is transformed by phosphorylation within cells and that the phosphorylated derivative of arglabin-DMA can prevent farnesylation of Ras proteins (51). The molecular modeling results from the present study also indicated that the phosphorylated arglabin-DMA has significantly higher binding affinity than arglabin-DMA alone. Unprocessed arglabin-DMA alone was not a potent FTase inhibitor. However, a derivative of arglabin-DMA in Ras/3T3 cells showed inhibitory activity to FTase at nanomolar or higher concentrations, and this

inhibitory capability was limited by the availability of other substrates that can be used to transform arglabin-DMA within cells. ATP is a possible substrate based on Dr. Saikenov's study.

The Rho GTPases are essential for Ras-induced oncogenic transformation (35) and activated Rho acts synergistically with activated Raf in cell transformation. Raf, with activated serine/threonine kinase activity, sends positive signals down a kinase cascade (the mitogen-activated protein kinase pathway) and prompts cells to move through the G1 phase of the cell cycle towards S phase (42, 44, 50). Excessive signaling from Ras/Raf induces p21/WAF1/CIP1, which blocks entry into S phase. RhoA overcomes the cell-cycle block by suppressing expression of p21/WAF1/CIP1 (42, 44, 50) (Fig. 3). Although some evidence showed the involvement of RhoB in the anti-tumor activity of FTIs (11,17), direct evidence implicating RhoB in the mechanism of action of FTIs in human tumors is lacking.

FTIs were originally developed as a Ras-targeted therapy, because Ras protein plays a crucial role in cellular signal transduction pathways, and the first and most critical post-translational modification of Ras is farnesylation catalyzed by the FTase (20, 40). Four isoforms of Ras proteins have been discovered (63). Ki-Ras4A, Ki-Ras4B, and N-Ras proteins can be either farnesylated or geranylgeranylated, whereas H-Ras proteins are singly farnesylated (48, 63). Expressions of H-Ras and K-Ras (including both Ki-Ras4A and Ki-Ras4B) in Ras/3T3 cells that were incubated with various concentrations of arglabin-DMA (0.1, 1, 10, 50, and 100 μ M) or 0.25 μ M of FTI-277 (control) were examined in this study. Western blots and densitometry showed significant decreases in the ratio of processed to unprocessed H-Ras protein in cell lysates incubated with 100 μ M

of arglabin-DMA and cell lysates incubated with FTI-277 for 24 hours and 72 hours. Western blots of active H-Ras protein from small GTPase pull-down assays showed significant reduction of active H-Ras production after incubation with 50 μ M of arglabin-DMA for 24 hours, or 1 μ M of arglabin-DMA for 72 hours. The K-Ras can undergo geranylgeranylation catalyzed by GGT-I when cells are treated with FTIs (63). Thus, tumors bearing the mutant Ki-ras4B isoform should be resistant to FTIs; however, some tumors bearing Ki-ras4B mutations are clearly responsive to FTI treatments. In the present study, only processed K-Ras protein was detected and no significant density differences between bands of all samples were found after 24 hours of incubation with arglabin-DMA. This result indicated that processing of K-Ras protein was not affected by arglabin-DMA or FTI-277. Farnesylation of H-Ras was affected by arglabin-DMA; however, this inhibition cannot account for the cytotoxicity of arglabin-DMA alone, since H-Ras is one of the four Ras proteins in Ras/3T3 cells and H-Ras is only involved in part of Ras signaling pathway. K-Ras was not affected by arglabin-DMA or FTI-277.

Dr. Prendergast and his research team at the Wistar Institute suggested that cell growth inhibition by farnesyltransferase inhibitors is mediated by gain of geranylgeranylated RhoB (17, 32). Dr. Chen's results (11) supported the conclusion that alteration of RhoB prenylation is both necessary and sufficient to the FTI mechanism in malignant cells. Both RhoB-F and RhoB-GG induce apoptosis, inhibit oncogenic signaling, and suppress transformation *in vitro* and *in vivo* (11). RhoB proteins can be either farnesylated or geranylgeranylated, whereas RhoA proteins are singly geranylgeranylated (48, 63). The half-life of RhoB protein is about 2 hours and that of RhoA protein is around 30 hours. The results of the present study showed that only

unprocessed RhoA was detected by Western blot after 24 hours or 72 hours of incubation with 10 μ M, 50 μ M, 100 μ M arglabin-DMA, and FTI-277. There were no significant density differences between bands of all samples. Western blots of active RhoA protein from small GTPase pull-down assays showed significant reduction of active RhoA production after 72 hours of incubation with 50 μ M of arglabin-DMA. These results suggested that production of processed or activated RhoA protein was affected by arglabin-DMA and FTI-277. In the present study, only processed RhoB protein was detected and no significant density difference between bands of all samples was found after 24 hours of incubation with arglabin-DMA. This result indicated that processing of RhoB protein was not affected by arglabin-DMA or FTI-277.

The 21 kD protein of the WAF1 gene is found in a complex involving cyclins, CDKs, and proliferating cell nuclear antigen (PCNA) in normal cells but not in transformed cells and appears to be a universal inhibitor of CDK activity (24). One consequence of p21/WAF1/CIP1 binding to and inhibiting CDKs is the prevention of CDK-dependent phosphorylation and subsequent inactivation of the retinoblastoma (Rb) protein that is essential for cell cycle progression (24). P21/WAF1/CIP1 is, therefore, a potent and reversible inhibitor of cell cycle progression at both the G1 and G2 check points, presumably to allow sufficient time for DNA repair to be completed (19). Study of the effects of arglabin-DMA on cyclin kinase inhibitor p21/WAF1/CIP1 protein was performed using the Ras/3T3 cell line. Equal amounts of protein lysates from Ras/3T3 cells that were incubated with various concentrations of arglabin-DMA (0.1, 1, 10, 50, and 100 μ M) or 0.25 μ M of FTI-277 (control) for 24 hours or 72 hours were used to detect p21/WAF1/CIP1 proteins. This study showed a trend of increasing

p21/WAF1/CIP1 production after 72 hours of incubation with arglabin-DMA and this trend was not found in the FTI-277 control, which suggested a different cellular mechanism of cytotoxic effect for arglabin-DMA and FTI-277. However, this study only detected p21/WAF1/CIP1 protein in the whole cell lysates, which include the p21/WAF1/CIP1 protein in a complex involving cyclins, CDKs, and proliferating cell nuclear antigen (PCNA) and p21/WAF1/CIP1 protein free in cytoplasm.

In summary, cellular mechanism of arglabin-DMA cytotoxic effect was investigated in the present study. First, arglabin-DMA itself is not a potent FTase inhibitor, however, arglabin-DMA was transformed to a derivative in Ras/3T3 cells that can inhibit FTase activity at nanomolar or higher concentrations, and this inhibitory capability was limited by the availability of other substrates that can be used to transform arglabin-DMA within cells. Secondly, H-Ras farnesylation, RhoA geranylgeranylation, and p21/WAF1/CIP1 production were affected by arglabin-DMA, while K-Ras prenylation and RhoB prenylation were not influenced by arglabin-DMA treatments (Fig. 42).

Since geranylgeranylations of RhoB and K-Ras were not affected by arglabin-DMA and farnesylation of RhoB and K-Ras were inhibited by arglabin-DMA, the balances between RhoB-F and RhoB-GG or K-Ras-F and K-Ras-GG were disturbed. The half-life of RhoB is 2 hours and the half-life of K-Ras protein is around 24 hours. This means that large amounts of geranylgeranyltransferase (GGT) and geranylgeranylpyrophosphate (GGPP) were used for RhoB and K-Ras prenylation. The half-life of RhoA is around 30 hours, RhoA can only be geranylgeranylated and the availabilities of GGT and GGPP for geranylgeranylation of RhoA were affected by arglabin-DMA treatments. When H-Ras protein prenylation was inhibited by arglabin-DMA, K-Ras protein prenylation was not

affected by arglabin-DMA, the overall signals from Ras to Raf may be reduced, but most of signals still existed, which can induce p21/WAF1/CIP1 expression. RhoA should overcome the cell-cycle block by suppressing expression of p21/WAF1/CIP1 in normal circumstances (42, 44, 50), but RhoA geranylgeranylation was inhibited due to lack of GGT and GGPP after arglabin-DMA treatments. Thus, the increased expressions of p21/WAF1/CIP1 were found after 72 hours treatment of arglabin-DMA. However, this increasing p21/WAF1/CIP1 was not found in FTI-277 treated group, which suggests that the cellular mechanism of arglabin-DMA cytotoxic effect is different from the cellular mechanism of FTI-277.

Taken together, arglabin-DMA can be transformed to a derivative in Ras/3T3 cells that will inhibit FTase activity at nanomolar or higher concentrations. The inhibition of Ras and RhoB protein farnesylation will shift more active K-Ras and RhoB proteins to geranylgeranylated forms after 24 to 72 hours incubation. The availability of GGT and GGPP for RhoA geranylgeranylation will be reduced, which can decrease the inhibitory effect of RhoA on p21/WAF1/CIP1 production. Increasing p21/WAF1/CIP1 production can block Ras/3T3 cells at G1 phase of cell cycle, thus inhibits DNA synthesis and cell proliferation. Understanding of the cellular mechanism of arglabin-DMA cytotoxic effects should help clinicians to determine the dose of arglabin-DMA for treatment and to use arglabin-DMA in combination with metabolical substrate (such as ATP) in cancer treatments. Detection of p21/WAF1/CIP1 in tumor cells may be used as a marker of effectiveness of arglabin-DMA treatments.

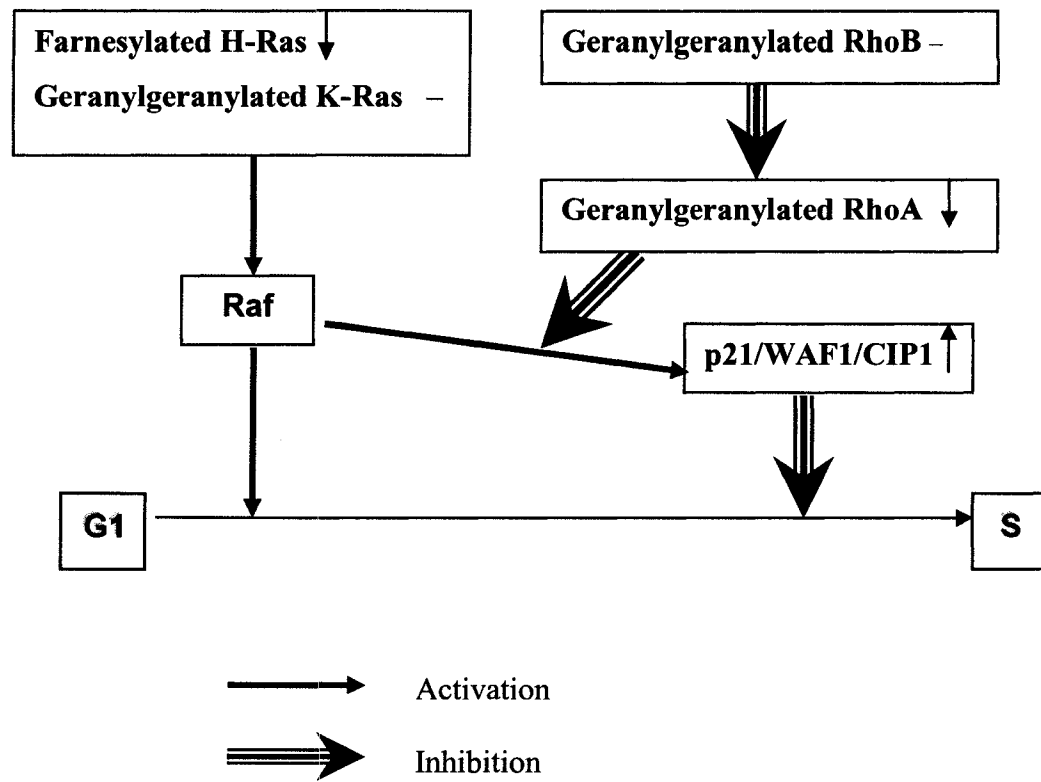


FIG. 42. Diagram of active Ras, Rho, and p21/WAF1/CIP1 protein production affected by arglabin-DMA in Ras/3T3 cells.

SUMMARY

Arglabin-DMA itself is not a potent FTase inhibitor, however, arglabin-DMA was transformed to a derivative in Ras/3T3 cells that can inhibit FTase activity at nanomolar or higher concentrations, and this inhibitory capability was limited by the availability of other substrates that can be used to transform arglabin-DMA within cells. H-Ras farnesylation, RhoA geranylgeranylation, and cyclin kinase inhibitor p21/WAF1/CIP1 production were affected by arglabin-DMA, while K-Ras prenylation and RhoB prenylation were not influenced by arglabin-DMA treatments.

REFERENCES

1. **Adekenov, S. M., M. N. Mukhametzhanov, A. D. Kagarlitskii, and A. N. Kupriyanov.** 1983. Argabin-a new sesquiterpene lactone from *artemisia glabella*. *Chem. Nat. Comp.* **18**:623-624.
2. **Apolloni, A., I. A. Prior, M. Lindsay, R. G. Parton, J. F. Hancock.** 2000. H-ras but not K-ras traffics to the plasma membrane through the exocytic pathway. *Mol. Cell. Biol.* **20**:2475-2487.
3. **Appendino, G., P. Gariboldi, and F. Menichini.** 1991. The stereochemistry of argabin, a cytotoxic guaianolide from *artimisia myriantha*. *Fitoterapia.* **62**:275-276.
4. **Armstrong, S. A., V. C. Hannah, J. L. Goldstein, and M. S. Brown.** 1995. CAAX geranylgeranyl transferase transfers farnesyl as efficiently as geranylgeranyl to RhoB. *J. Biol. Chem.* **270**:7864-7868.
5. **Backlund, P. S. Jr.** 1997. Post-translational processing of RhoA. *J. Biol. Chem.* **272**:33175-33180.
6. **Banyard, J., B. Anand-Apte, M. Symons, and B. R. Zetter.** 2000. Motility and invasion are differentially modulated by Rho family GTPases. *Oncogene.* **19**:580-591.
7. **Bar-Sagi, D. and A. Hall.** 2000. Ras and Rho GTPases: a family reunion. *Cell.* **103**:227-238.
8. **Barton, R. M., H. J. Worman.** 1999. Prenylated prelamins A interacts with Narf, a novel nuclear protein. *J. Biol. Chem.* **274**:30008-30018.
9. **Beekman, A. C., P. K. Wierenga, H. J. Woerdenbag, W. V. Uden, N. Pras, A. W. T. Konings, and H. V. Wikstrom.** 1998. Artemisinin-derived sesquiterpene lactones as potential antitumor compounds: cytotoxic action against bone marrow and tumour cells. *Planta Medica.* **64**:615-619.
10. **Bishop, W. R., R. Bond, J. Petrin, L. Wang, R. Patton, R. Doll, G. Njoroge, J. Catino, J. Schwartz, W. Windsor, R. Syto, J. Schwartz, D. Carr, L. James, and P. Kirschmeier.** 1995. Novel tricyclic inhibitors of farnesyl protein transferase. Biochemical characterization and inhibition of Ras modification in transfected Cos cells. *J. Biol. Chem.* **270**:30611-30618.

11. **Bork, P. M., M. L. Schmitz, M. Kuhnt, C. Escher, and M. Heinrich.** 1997. Sesquiterpene lactone containing Mexican Indian medicinal plants and pure sesquiterpene lactones as potent inhibitors of transcription factor NF- κ B. *FEBS Letters*. **402**:85-90.
12. **Bosworth, N., and P. Towers.** 1989. Scintillation proximity assay. *Nature* **341**:167-168.
13. **Bottex-Gauthier, C., D. Vidal, F. Picot, P. Potier, F. Menichini, and G. Appendino.** 1993. In vitro biological activities of arglabin, a sesquiterpene lactone from the Chinese herb *Artemisia myriantha* Wall. (Asteraceae). *Biotechnol. Ther.* **4**:77-98.
14. **Boyd, D. B., and K. B. Lipkowitz.** 1982. Molecular Mechanics. *J. Chem. Education*. **59**:269-277.
15. **Chen, Z., J. Sun, A. Pradines, G. Favre, J. Adnane, and S. M. Sebti.** 2000. Both farnesylated and geranylgeranylated RhoB inhibit malignant transformation and suppress human tumor growth in nude mice. *J. Biol. Chem.* **275**:17974-17978.
16. **Chiu, V. K., T. Bivona, A. Hach, J. B. Sajous, J. Silletti, H. Wiener, R. L. Johnson, A. D. Cox, M. R. Phillips.** 2002. Ras signaling on the endoplasmic reticulum and the Golgi. *Nature Cell Biol.* **4**:343-350.
17. **Choy, E., V. K. Chiu, J. Silletti, M. Feoktistov, T. Morimoto, D. Michaelson, I. E. Ivanov, M. R. Phillips.** 1999. Endomembrane trafficking of Ras: the CAAX motif targets proteins to the ER and Golgi. *Cell* **98**:69-80.
18. **Cohen, N. C., A. Itai., M. Y. Mizutani, Y. Nishibata, and N. Tomioka.** 1996. Computer-assisted new lead design. *Guidebook on molecular modeling in drug design* **4**:93-137.
19. **Del Villar, K., H. Mitsuzawa, W. Yang, I. Sattler, and F. Tamanoi.** 1997. Amino acid substitutions that convert the protein substrate specificity of farnesyltransferase to that of geranylgeranyltransferase type I. *J. Biol. Chem.* **272**:680-687.
20. **Del Villar, K., J. Urano, L. Guo, and F. Tamanoi.** 1999. A mutant form of human protein farnesyltransferase exhibits increased resistance to farnesyltransferase inhibitors. *J. Biol. Chem.* **274**:27010-27017.
21. **Desrosiers, R. R., F. Gauthier, J. Lanthier, and R. Beliveau.** 2000. Modulation of Rho and cytoskeletal protein attachment to membranes by a prenylcysteine analog. *J. Biol. Chem.* **275**:14949-14957.

22. **Dolence, J. M., and C. D. Poulter.** 1995. A mechanism for posttranslational modifications of proteins by yeast protein farnesyltransferase. *Proc. Natl. Acad. Sci. U. S. A.* **92**:5008-5011.
23. **Dolence, J. M., P. B. Cassidy, J. R. Mathis, and C. D. Poulter.** 1995. Yeast protein farnesyltransferase: steady-state kinetic studies of substrate binding. *Biochemistry* **34**:16687-16694.
24. **Du, W., P. F. Lebowitz, and G. C. Prendergast.** 1999. Cell growth inhibition by farnesyltransferase inhibitors is mediated by gain of geranylgeranylated RhoB. *Mol. Cell. Biol.* **19**:1831-1840.
25. **Dunten, P., U. Kammlott, R. Crowther, D. Weber, R. Palermo, and J. Birktoft.** 1998. Protein farnesyltransferase: structure and implications for substrate binding. *Biochemistry* **37**:7907-7912.
26. **El-Deiry, W. S., J. W. Harper, P. M. O'Connor, V. E. Velculescu, C. E. Canman, J. Jackman, J. A. Pietenpol, M. Burrell, D. E. Hill, and Y. Wang.** 1994. WAF1/CIP1 is induced in p53-mediated G1 arrest and apoptosis. *Cancer Res.* **54**:1169-1174.
27. **End, D. W.** 1999. Farnesyl protein transferase inhibitors and other therapies targeting the Ras signal transduction pathway. *Invest. New Drugs* **17**:241-258.
28. **Furfine, E. S., J. J. Leban, A. Landavazo, J. F. Moomaw, and P. J. Casey.** 1995. Protein farnesyltransferase: kinetics of farnesyl pyrophosphate binding and product release. *Biochemistry* **34**:6857-6862.
29. **Goalstone, M. L., B. Draznin,** 1996. Effect of insulin on farnesyltransferase activity in 3T3-L1 adipocytes. *J. Biol. Chem.* **271**:27585-27589.
30. **Goodsell, D. S., G. M. Morris, and A. J. Olson.** 1996. Automated docking of flexible ligands: applications of AutoDock. *J. Mol. Recognit.* **9**:1-5.
31. **Harper, J. W., G. R. Adami, N. Wei, K. Keyomarsi, and S. J. Elledge.** 1993. The p21 Cdk-interacting protein Cip1 is a potent inhibitor of G1 cyclin-dependent kinases. *Cell* **75**:805-816.
32. **Hehner, S. P., M. Heinrich, P. M. Bork, M. Vogt, F. Ratter, V. Lehmann, K. Schulze-Osthoff, W. Droge, and M. L. Schmitz.** 1998. Sesquiterpene lactones specifically inhibit activation of NF- κ B by preventing the degradation of I κ B- α and I κ B- β . *J. Biol. Chem.* **273**:1288-1297.
33. **Holstein, S. A., L. C. Wohlford-Lenane, and R. J. Hohl.** 2002. Consequences of Mevalonate Depletion. *J. Biol. Chem.* **277**:10678-10682.

34. **Hood, C. M., V. A. Kelly, M. I. Bird, and C. J. Britten.** 1998. Measurement of alpha(1-3) fucosyltransferase activity using scintillation proximity. *Anal. Biochem.* **255**:8-12.
35. **Kesley, R. G., and F. Shafizadeh.** 1979. Sesquiterpene lactones and systematics of the genus *Artemisia*. *Phytochemistry* **18**:1591-1611.
36. **Koch, G., C. Benz, G. Schmidt, C. Olenik, and K. Aktories.** 1997. Role of Rho protein in lovastatin-induced breakdown of actin cytoskeleton. *J. Pharmacol. Exp. Ther.* **283**:901-909.
37. **Kohl, N. E., F. R. Wilson, S. D. Mosser, E. Giuliani, S. J. Desolms, M. W. Conner, N. J. Anthony, W. J. Holtz, R. P. Gomez, T. J. Lee, R. L. Smith, S. L. Graham, G. D. Hartman, J. B. Gibbs, and A. Oliff.** 1994. Protein farnesyltransferase inhibitors block the growth of ras- dependent tumors in nude mice. *Proc. Natl. Acad. Sci. U. S. A.* **91**:9141-9145.
38. **Kumar, A., M. H. Beresini, P. Dhawan, and K. D. Mehta.** 1996. Alpha-subunit of farnesyltransferase is phosphorylated in vivo: effect of protein phosphatase-1 on enzymatic activity. *Biochem. Biophys. Res. Commun.* **222**:445-452.
39. **Law, B. K., P. Norgaard, L. Gnudi, B. B. Kahn, H. S. Poulson, and H. L. Moses.** 1999. Inhibition of DNA synthesis by a farnesyltransferase inhibitor involves inhibition of the p70(s6k) pathway. *J. Biol. Chem.* **274**:4743-4748.
40. **Lebowitz, P. F., D. Sakamuro, and G. C. Prendergast.** 1997. Farnesyl transferase inhibitors induce apoptosis of Ras-transformed cells denied substratum attachment. *Cancer Res.* **57**:708-713.
41. **Lebowitz, P. F., P. J. Casey, G. C. Prendergast, and J. A. Thissen.** 1997. Farnesyltransferase inhibitors alter the prenylation and growth- stimulating function of RhoB. *J. Biol. Chem.* **272**:15591-15594.
42. **Lebowitz, P. F., J. P. Davide, and G. C. Prendergast.** 1995. Evidence that farnesyltransferase inhibitors suppress Ras transformation by interfering with Rho activity. *Mol. Cell. Biol.* **15**:6613-6622.
43. **Lebowitz, P. F., W. Du, and G. C. Prendergast.** 1997. Prenylation of RhoB is required for its cell transforming function but not its ability to activate serum response element-dependent transcription. *J. Biol. Chem.* **272**:16093-16095.
44. **Lee, S. H., M. J. Kim, S. H. Bok, H. Lee, and B. M. Kwon.** 1998. Artiminolide, and inhibitor of farnesyltransferase from *artemisia sylvatica*. *J. Org. Chem.* **63**:7111-7113.

45. **Leftheris, K., T. Kline, G. D. Vite, Y. H. Cho, R. S. Bhide, D. V. Patel, M. M. Patel, R. J. Schmidt, H. N. Weller, M. L. Andahazy, J. M. Carboni, J. L. Gullo-Brown, F. Y. F. Lee, C. Ricca, W. C. Rose, N. Yan, M. Barbacid, J. T. Hunt, C. A. Meyers, B. R. Seizinger, R. Zahler, and V. Manne.** 1996. Development of highly potent inhibitors of Ras farnesyltransferase possessing cellular and in vivo activity. *J. Med. Chem.* **39**:224-236.
46. **Lerner, C. G. and A. Y. C. Saiki.** 1996. Scintillation proximity assay for human DNA topoisomerase I using recombinant biotinyl-fusion protein produced in baculovirus-infected insect cells. *Anal. Biochem.* **240**:185-196.
47. **Lerner, E. C., T. T. Zhang, D. B. Knowles, Y. Qian, A. D. Hamilton, and S. M. Sebti.** 1997. Inhibition of the prenylation of K-Ras, but not H- or N-Ras, is highly resistant to CAAX peptidomimetics and requires both a farnesyltransferase and a geranylgeranyltransferase I inhibitor in human tumor cell lines. *Oncogene* **15**:1283-1288.
48. **Long, S. B., P. J. Hancock, A. M. Kral, H. W. Hellinga, and L. S. Beese.** 2001. The crystal structure of human protein farnesyltransferase reveals the basis for inhibition by CaaX tetrapeptide and their mimetics. *Proc. Natl. Acad. Sci. U. S. A.* **98**:12948-12953.
49. **Long, S. B., P. J. Casey, and L. S. Beese.** 1998. Cocystal structure of protein farnesyltransferase complexed with a farnesyl diphosphate substrate. *Biochemistry* **37**:9612-9618.
50. **Lyb, G., A. Knorre, T. J. Schmidt, H. L. Pahl, and I. Merfort.** 1998. The anti-inflammatory sesquiterpene lactone helenalin inhibits the transcription factor NF- κ B by directly targeting p65. *J. Biol. Chem.* **273**:33508-33516.
51. **Matallanas, D., V. Sanz-Moreno, I. Arozarena, F. Calvo, L. Agudo-Ibanez, E. Santox, M. T. Berciano, and P. Crespo.** 2006. Distinct utilization of effectors and biological outcomes resulting from site-specific Ras activation: Ras functions in lipid rafts and golgi complex are dispensable for proliferation and transformation. *Mol. Cell. Biol.* **26**:100-106.
52. **McCormick, F.** 1998. Why Ras needs Rho. *Nature* **394**:220-221.
53. **Morris, G. M., D. S.Goodsell, R. Huey, and A. J. Olson.** 1996. Distributed automated docking of flexible ligands to proteins: parallel applications of AutoDock 2.4. *J. Comput. Aided Mol. Des.* **10**:293-304.
54. **Olson, M. F., H. F. Paterson, and C. J. Marshall.** 1998. Signals from Ras and Rho GTPases interact to regulate expression of p21^{Waf1/Cip1}. *Nature* **394**:295-299.

55. **Olson, M. F., and R. Marais.** 2000. Ras Protein Signalling. *Seminars in Immunology* **12**:63-73.
56. **Prendergast, G. C., R. Khosravi-Far, P. A. Solski, H. Kurzawa, P. F. Lebowitz, and C. J. Der.** 1995. Critical role of Rho in cell transformation by oncogenic Ras. *Oncogene* **10**:2289-2296.
57. **Prendergast, G. C., J. P. Davide, S. J. Desolms, E. A. Giuliani, S. L. Graham, J. B. Gibbs, A. Oliff, and N. E. Kohl.** 1994. Farnesyltransferase inhibition causes morphological reversion of ras-transformed cells by a complex mechanism that involves regulation of the actin cytoskeleton. *Mol. Cell. Biol.* **14**:4193-4202.
58. **Robyt, J. F., and B. J. White.** 1987. *Enzymology. Biochemical techniques theory and practice* **9**:291-320.
59. **Rocks, O., A. Peyker, M. Kahms, P. J. Verveer, C. Koerner, M. Lumbierres, J. Kuhlmann, H. Waldmann, A. Wittinghofer, P. H. Bastiaens.** 2005. An acylation cycle regulates localization and activity of palmitoylated Ras isoforms. *Science* **307**:1746-1751.
60. **Rowell, C. A., J. J. Kowalczyk, M. D. Lewis, and A. M. Garcia.** 1997. Direct Demonstration of Geranylgeranylation and Farnesylation of Ki-Ras in Vivo. *J. Biol. Chem.* **272**:14093-14097.
61. **Ruddon, R. W.** 1995. Phenotypic Characteristics of Human Cancer. *Cancer Biology.* **4**:96-140.
62. **Sahai, E., F. M. Olson, and C. J. Marshall.** 2001. Cross-talk between Ras and Rho signaling pathways in transformation favours proliferation and increased motility. *EMBOJ* **20**:755-766.
63. **Shaikenov, T. E., S. M. Adekenov, S. Basset, M. Trivedi, and L. Wolfinbarger.** 1998. Arglabin As a Novel Inhibitor of the Farnesylation of Ras Proteins. *Reports of Ministry of Science-Academy of Sciences, Republic of Kazakstan.* 64-74.
64. **Shaikenov, T. E., S. M. Adekenov, R. M. Williams, N. Prashad, F. L. Baker, T. L. Madden, and R. Newman.** 2001. Arglabin-DMA, a plant derived sesquiterpene, inhibits farnesyltransferase. *Oncol. Rep.* **8**:173-179.
65. **Stamellos, K. D., J. E. Shackelford, I. Shechter, G. Jiang, D. Conrad, G. A. Keller, and S. K. Krisans.** 1993. Subcellular localization of squalene synthase in rat hepatic cells. Biochemical and immunochemical evidence. *J. Biol. Chem.* **268**:12825-12836.

66. **Strickland, C. L., W. T. Windsor, R. Syto, L. Wang, R. Bond, Z. Wu, J. Schwartz, H. V. Le, L. S. Beese, and P. C. Weber.** 1998. Crystal structure of farnesyl protein transferase complexed with a CaaX peptide and farnesyl diphosphate analogue. *Biochemistry* **37**:16601-16611.
67. **Sun, J., Y. Qian, A. D. Hamilton, and S. M. Sebti.** 1998. Both farnesyltransferase and geranylgeranyltransferase I inhibitors are required for inhibition of oncogenic K-Ras Prenylation but each alone is sufficient to suppress human tumor growth in nude mouse xenografts. *Oncogene* **16**:1467-1473.
68. **Suzuki, N., J. Urano, and F. Tamanoi.** 1998. Farnesyltransferase inhibitors induce cytochrome c release and caspase 3 activation preferentially in transformed cells. *Proc. Natl. Acad. Sci. U. S. A.* **95**:15356-15361.
69. **Suzuki, N., K. Del Villar, and F. Tamanoi.** 1998. Farnesyltransferase inhibitors induce dramatic morphological changes of KNRK cells that are blocked by microtubule interfering agents. *Proc. Natl. Acad. Sci. U. S. A.* **95**:10499-10504.
70. **Weisz, B., K. Giehl, M. Gana-Weisz, Y. Egozi, G. Ben-Baruch, D. Marciano, P. Gierschik, and Y. Kloog.** 1999. A new functional Ras antagonist inhibits human pancreatic tumor growth in nude mice. *Oncogene* **18**:2579-2588.
71. **Xu, L. H., X. Yang, C. A. Bradham, D. A. Brenner, A. S. Baldwin Jr., R. J. Craven, and W. G. Cance.** 2000. The focal adhesion kinase suppresses transformation-associated, anchorage-independent apoptosis in human breast cancer cells. Involvement of Death Receptor-related Signaling Pathways. *J. Biol. Chem.* **275**:30597-30604.
72. **Yamamoto, M., N. Marui, T. Sakai, N. Morii, S. Kozaki, K. Ikai, S. Imamura, and S. Narumiya.** 1993. ADP-ribosylation of the rhoA gene product by botulinum C3 exoenzyme causes Swiss 3T3 cells to accumulate in the G1 phase of the cell cycle. *Oncogene* **8**:1449-1455.
73. **Yang, W., K. Del Villar, J. Urano, and H. Mitsuzawa.** 1997. Advances in the development of farnesyltransferase inhibitors: substrate recognition by protein farnesyltransferase. *J. Cell Biochem. Suppl.* **27**:12-19.
74. **Yonemoto, M., T. Satoh, H. Arakawa, I. Suzuki-Takahashi, Y. Monden, T. Koder, K. Tanaka, T. Aoyama, Y. Iwasawa, T. Kamei, S. Nishimura, and K. Tomimoto.** 1998. J-104,871, a novel farnesyltransferase inhibitor, blocks Ras farnesylation in vivo in a farnesyl pyrophosphate-competitive manner. *Mol. Pharmacol.* **54**:1-7.
75. **Zhang, F. L., and P. J. Casey.** 1996. Protein prenylation: molecular mechanisms and functional consequences. *Annu. Rev. Biochem.* **65**:241-269.

76. **Zhang, F. L., P. Kirschmeier, D. Carr, L. James, R. W. Bond, L. Wang, R. Patton, W. T. Windsor, R. Syto, R. Zhang, and W. R. Bishop.** 1997. Characterization of Ha-ras, N-ras, Ki-Ras4A, and Ki-Ras4B as in vitro substrates for farnesyl protein transferase and geranylgeranyl protein transferase type I. *J. Biol. Chem.* **272**:10232-10239.

APPENDIX A

TABLE 3. Summary of the intermolecular energy between FTase and various ligands

Ligands	FPP	Phosphorylated Arglabin-DMA	FPT Inhibitor II	FTI277	FPT Inhibitor III	FTase Inhibitor II	Arglabin- DMA
Frame1	-61.99	-64.62	-92.71	-82.06	-86.93	-63.61	-45.96
Frame2	-55.26	-64.63	-98.13	-65.36	-79.58	-48.93	-45.45
Frame3	-63.97	-56.78	-91.37	-77.49	-78.42	-58.62	-45.04
Frame4	-72.41	-64.95	-85.42	-68.86	-82.41	-54.61	-39.65
Frame5	-57.63	-64.87	-82.74	-75.04	-81.04	-46.71	-53.86
Frame6	-51.59	-59.53	-85.56	-49.38	-70.68	-65.91	-49.19
Frame7	-62.03	-71.19	-56.14	-60.72	-84.64	-56.76	-54.61
Frame8	-61.45	-57.87	-73.81	-60.33	-71.13	-69.94	-46.93
Frame9	-59.42	-62.25	-71.84	-65.53	-79.31	-53.24	-42.48
Frame10	-62.42	-70.14	-84.15	-54.57	-74.91	-57.43	-46.51
Mean	-60.817	-63.68	-82.19	-65.93	-78.91	-57.57	-46.97

APPENDIX B

TABLE 4. Statistical evaluation of the binding affinity between FTase and various ligands. ANOVA single factor. Probability level: 0.05

Groups	Count	Sum	Average	Variance
FPP	10	-608.17	-60.817	30.92033444
Phosphorylated Arglabin-DMA	10	-636.83	-63.683	22.62002333
FPT Inhibitor II	10	-821.86	-82.186	147.8554711
FTI-277	10	-659.34	-65.934	105.2587156
FPT Inhibitor III	10	-789.03	-78.903	28.78446778
FTase Inhibitor II	10	-575.73	-57.573	53.41153444
Arglabin-DMA	10	-469.68	-46.968	21.30901778

ANOVA						
Source of Variation	SS	df	MS	F	P-value	F crit
Between Groups	8889.07964	6	1481.51327	25.28428888	4.693E-15	2.246409281
Within Groups	3691.43608	63	58.5942235			
Total	12580.51572	69				

VITA

XIAOFEI QIN

EDUCATIONAL BACKGROUND:

Old Dominion University, Norfolk, Virginia 23529

Ph.D., August 2006

Major: Biomedical Sciences

Dissertation on “The cellular mechanism of arglabin-dimethylaminohydrochloride cytotoxicity”.

Capital Institute of Medicine, Beijing, P. R. China

M.D., August 1990

Major: Medicine

PROFESSIONAL EXPERIENCE:

LifeNet, Virginia Beach, Virginia

Research Associate

2001-present

Research field on “tissue engineering using decellularized human tissue scaffold”.

Diabetes Institute of Eastern Virginia Medical School, Norfolk, Virginia

Research Fellow

1994-1996

Research field on “isolation and characterization of novel genes involved in islet neogenesis”.